Advancing Manufacturing Quality Control Capabilities Through The Use Of In-Line High-Density Dimensional Data

Lee Jay Wells

Dissertation submitted to the faculty of the Virginia Polytechnic Institute and State University in partial fulfillment of the requirements for the degree of

Doctor of Philosophy
In
Industrial and Systems Engineering

Jaime A. Camelio, Chair
Ran Jin
Robert H. Sturges
Chris B. Williams

December 4, 2013
Blacksburg, VA

Keywords: Compliant Assembly, High Density Dimensional Data, Inspection Systems, Statistical Process Control, Surface Monitoring, Quality Control

Advancing Manufacturing Quality Control Capabilities Through The Use Of In-Line High-Density Dimensional Data

Lee Jay Wells

ABSTRACT

Through recent advancements in high-density dimensional (HDD) measurement technologies, such as 3D laser scanners, data-sets consisting of an almost complete representation of a manufactured part's geometry can now be obtained. While HDD data measurement devices have traditionally been used in reverse engineering application, they are beginning to be applied as in-line measurement devices. Unfortunately, appropriate quality control (QC) techniques have yet to be developed to take full advantage of this new data-rich environment and for the most part rely on extracting discrete key product characteristics (KPCs) for analysis. In order to maximize the potential of HDD measurement technologies requires a new quality paradigm. Specifically, when presented with HDD data, quality should not only be assessed by discrete KPCs but should consider the entire part being produced, anything less results in valuable data being wasted.

This dissertation addresses the need for adapting current techniques and developing new approaches for the use of HDD data in manufacturing systems to increase overall quality control (QC) capabilities. Specifically, this research effort focuses on the use of HDD data for 1) Developing a framework for self-correcting compliant assembly systems, 2) Using statistical process control to detect process shifts through part surfaces, and 3) Performing automated part inspection for non-feature based faults. The overarching goal of this research is to identify how HDD data can be used within these three research focus areas to increase QC capabilities while following the principles of the aforementioned new quality paradigm.

TABLE OF CONTENTS

ABSTRACT ii
TABLE OF CONTENTS iii
LIST OF FIGURES v
LIST OF TABLES vii
1. Introduction 1
1.1. Motivation and Background 2
1.2. Significance 4
1.3. Research Objectives 6
1.4. Dissertation Outline 7
2. A Bio-Inspired Approach for Self-Correcting Compliant Assembly Systems 9
2.1. Introduction 9
2.2. Adaptive Immunity 12
2.2.1. Active Immunity 13
2.2.2. Artificial Immunity 15
2.2.3. Adaptive Immunity Characteristics 16
2.3. Bio-Inspired Self-Correcting Compliant Assembly System 18
2.3.1. Antigens and Antibodies 18
2.3.2. B Cell Creation 19
2.3.3. Vaccination and B Cell Mutations 23
2.3.4. Antigen Identification 25
2.3.5. B Cell Memory and Mutation 27
2.3.6. B Cell and Antigen Matching 29
2.3.7. B Cell Activation and Decay 31
2.3.8. Class-Switching 32
2.4. Conclusions 34
2.5. References 35
3. Statistical Process Control for Point Clouds using NURBS Surfaces 39
3.1. Literature Review 40
3.2. Proposed Method for Monitoring High-Density Dimensional Data 41
3.2.1. Rationale for using NURBS Surfaces 41
3.2.2. Phase II Monitoring Parameters for NURBS Surfaces 42
3.2.3. Phase II Monitoring Approach using NURBS Surface Representations 47
3.3. Performance Assessment of Proposed SPC Approach 48

3.3.1. Description of Simulation Study 49
3.3.2. Implementation of Proposed SPC Approach 52
3.3.3. Performance for Out-of-Control Conditions 55
3.3.4. Discussion of Results 58
3.3.5. Alternative SPC Approach 60
3.4. Conclusions 64
3.5. References 65
4. Automated Part Inspection Using 3D Point Clouds 67
4.1. Introduction 68
4.2. Literature Review 69
4.3. Challenges and Opportunities for HDD Data in Quality Control 73
4.4. Adaptive Generalized Likelihood Ratio Method 77
4.5. Inspection System Design and Performance Analysis 81
4.5.1. Inspection System Design Case Study 82
4.5.2. Economic-Based Inspection System Design 86
4.6. Conclusions 89
4.7. References 90
5. Contributions and Future Work 94
5.1. Contributions 94
5.1.1. Overall Contributions 94
5.1.2. Self-Correcting Compliant Assembly Systems 96
5.1.3. Statistical Process Control for HDD Data 96
5.1.4. Automated Part Inspection for Non-Feature Based Faults 97
5.2. Future Work 97
5.2.1. Monitoring Process Data as Point Clouds 98
5.2.2. Uncertainty Propagation Modeling Using NURBS Surface Representations 100
5.2.3. Self-Correcting Compliant Assembly Systems 102
5.2.4. Statistical Process Control for HDD Data 103
5.2.5. Automated Part Inspection for Non-Feature Based Faults 103
6. References 105

LIST OF FIGURES

Figure 1.1: Typical Ability of QC Techniques to Reduce Process Variability. 1
Figure 1.2: A Common 3D Laser Scanning System (Triangulation-Based). 3
Figure 1.3: Representation of (a) A CAD Model of a Manufactured Part 6
Figure 2.1: Key B Cell Aspects. 14
Figure 2.2: Finite Element Model Generated from a NURBS Surface for a Nominal Part 21
Figure 2.3: Finite Element Model Generated from a NURBS Surface 22
Figure 2.4: Finite Element Model Generated from a NURBS Surface 23
Figure 2.5: Finite Element Model Generated from a NURBS Surface 25
Figure 2.6: Finite Element Model Generated from a NURBS Surface 25
Figure 2.7: Flowchart Outlining the Entire Process of B Cell Generation. 29
Figure 2.8: Flowchart Outlining the Process of Adding a B Cell to the B Cell Pool. 32
Figure 2.9: Flowchart Outlining the Process of B Cell Activation. 33
Figure 3.1: Nominal Sheet Metal Bracket a) used for Simulation Case Study 49
Figure 3.2: Generated Observation of Deformation Pattern 1: a) Actual and b) Exaggerated. 50
Figure 3.3: Generated Observation of Deformation Pattern 2: a) Actual and b) Exaggerated. 51
Figure 3.4: Generated Observation of Deformation Pattern 3: a) Actual and b) Exaggerated. 52
Figure 3.5: Generated Observation of All Deformation Patterns: a) Actual and b) Exaggerated. 52
Figure 3.6: NURBS Surfaces and their Control Points (Black Spheres) 53
Figure 3.7 SCREE Plots from PCA for Cases (a) 1 and (b) 2. 54
Figure 3.8: Shift Locations, Identified as Red Asterisks with the Nominal Control Point 56
Figure 3.9: Observations of Shifts at Shift Location 3 57
Figure 3.10: NURBS Surface Estimators of Surface Shifts at Location 2 60
Figure 3.11: SCREE Plots from PCA using Alternative Approach for Cases (a) 1 and (b) 2..... 61
Figure 3.12: ARL Comparison of Recommended Monitoring Procedures at Shift Location 1 ... 63
Figure 3.13: ARL Comparison of Recommended Monitoring Procedures at Shift Location 2 ... 64
Figure 3.14: ARL Comparison of Recommended Monitoring Procedures at Shift Location 3 ... 64
Figure 4.1: A Planar Point Cloud with a Surface Flaw in the Lower Left Corner 69
Figure 4.2: A Planar Point Cloud where 1% of the Data Falls Outside Tolerance Limits 73
Figure 4.3: A Planar Point Cloud with a Fault in the Center 74
Figure 4.4: Three Idealized Possible Faults that Could Occur in a Point Cloud 76
Figure 4.5: ROI Seed Generation. 78
Figure 4.6: ROI Seed Size. 78
Figure 4.7: Simulated False Alarm Probabilities Varying ROI Seed Sizes 83

Figure 4.8: Simulated Detection Probabilities 85
Figure 4.9: Expected Inspection System Costs 88
Figure 5.1: Power Consumption during the Turning of a Cylindrical Steel Billet. 98
Figure 5.2: Turning Example 100

LIST OF TABLES

Table 3.1: Control Charting Schemes. 47
Table 3.2: Nominal Part Dimensions (mm). 49
Table 3.3: Mean and Standard Deviation of Monitored Statistics for Cases 1 and 2. 54
Table 3.4: EWMA Design Parameters (*k*) Simulated to Obtain an In-Control ARL of 250. 55
Table 3.5: Actual Maximum Surface Deviations (mm) Caused by Shifts 57
Table 3.6: Out-of-Control ARL Performances for Shift Location 1. 58
Table 3.7: Out-of-Control ARL Performances for Shift Location 2. 58
Table 3.8: Out-of-Control ARL Performances for Shift Location 3. 58
Table 3.9: Mean and Standard Deviation of Monitored Statistics for Cases 1 and 2 61
Table 3.10: EWMA Design Parameters (*k*) Simulated to Obtain an In-Control ARL of 250 61
Table 3.11: Out-of-Control ARL Performances for Shift Location 1 62
Table 3.12: Out-of-Control ARL Performances for Shift Location 2 62
Table 3.13: Out-of-Control ARL Performances for Shift Location 3 62
Table 4.1: Faults Considered in Simulation Study 84
Table 4.2: Potential Inspection Designs for Probability of Detection Criterion. 86
Table 4.3: Detection Performance for Faults 86
Table 4.4: Economic Model Parameters 88
Table 4.5: Detection Probabilities from Optimal Economic Model Design 88

1. Introduction

Since the advent of control charting in the 1920s (Shewhart, 1925), quality control (QC) has been vital in improving the quality of manufactured products. QC can be defined as the quest to eliminate unwanted or harmful variation within a process. In the realm of in-line QC for manufacturing systems, QC is largely dominated by three distinct areas; 1) Engineering process control (EPC) (also referred to as automatic process control), 2) Statistical process control (SPC), and 3) Inspection. While each of these areas aims at reducing variability (therefore increasing quality) their implementations and uses as in-line QC approaches differ drastically. For EPC, inherent system variability is reduced through feedback process adjustments based on the state of the system. In SPC the goal is to detect the presence of assignable causes (sources of non-inherent system variability) so that they can be identified and removed from the system. Finally, while the goal of EPC and SPC is to reduce process variability, inspection ensures an acceptable level of variability by physically removing samples with excess deviations. Depending on the manufacturing system; one, two, or possibly all three of these QC techniques are typically implemented. However, it should be noted that each approach provides a different level of variability reduction, as outlined in Figure 1.1.

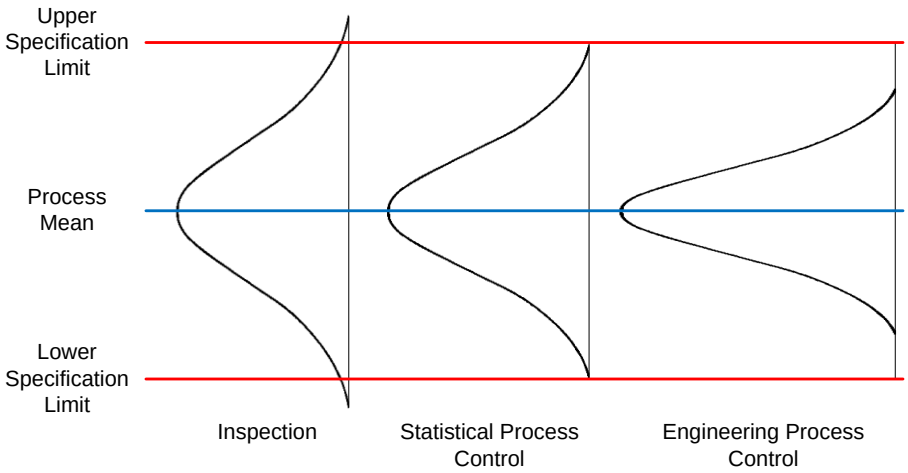

Figure 1.1: Typical Ability of QC Techniques to Reduce Process Variability.

1.1. Motivation and Background

In manufacturing, QC approaches traditionally focus on monitoring a manufactured part's key product characteristics (KPCs), which can be used to assess the majority of a part's quality. In addition, KPCs tend to be physical measures, such as dimensions or locations of features. As discussed by Wells et al. (2012b) the choice of KPCs (and the techniques used to analyze them) is a function of available measurement technologies. For example, consider the assembly of automotive doors, where an inadequate door fit leads to a loss of quality, possibly characterized by excessive door closing effort, increased wind noise, and/or decreased aesthetics. Wu et al. (1994) noted that the quality of a door's fit is a function of dimensional variations in the doors, body openings, and fitting and hanging processes. Quality can also be affected by the general assembly. To assess the fitting quality, practitioners must decide where to measure on the assembly and how to interpret the data. Typically, practitioners select between 15 to 25 sampling points per door, track these points using coordinate measuring machines (CMMs), and then apply SPC methods to assess if the observed vehicle-to-vehicle variation is significant (e.g. Wells et al., 2012a). However, these sampling points may not capture all possible variation sources since only a select number of gaps between the door and the body are measured. Therefore, as measurement technologies advance it becomes vital to develop QC methods that can harness the power these new data-sets provide, in order to fully assess a manufactured product's quality.

Recently there has been a strong focus on the use of high-density dimensional (HDD) data for industrial applications due to their ability to provide not only dimensional information but also information on product geometry, surface defects, surface finish, and numerous other product characteristics that can reflect overall quality. While numerous HDD technologies exist (contract profilometers, optical scanners, ultrasound, white light interferometry, radiography, etc.), this

dissertation focuses mainly on the use of 3D laser scanners (triangulation-based as opposed to time-of-flight).

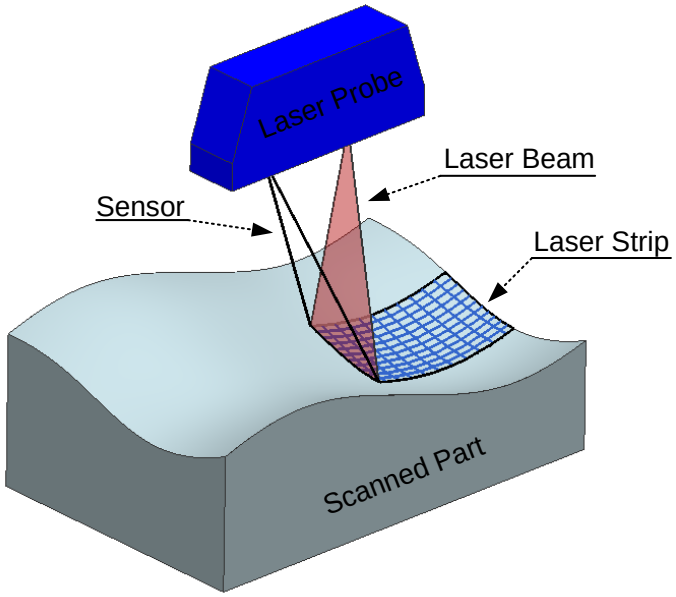

Figure 1.2: A Common 3D Laser Scanning System (Triangulation-Based).

The most common 3D laser scanning systems project a laser stripe onto the sample being measured and the reflected beam is captured by optical sensors (such as cameras), as shown in Figure 1.2. Using image processing techniques and triangulation (Toriwaki and Yoshida, 2009), 3D points on the sample's surface can be acquired. Zussman et al. (1994) highlighted six difficulties associated with using 3D laser scanners for measuring, which can be attributed to their optical sensors and mechanical moving parts. Despite this, 3D scanning technologies represent the future of manufacturing measurement systems as they; 1) Can rapidly record thousands or millions of 3D data points that embody all product features and 2) As discussed by Martinez et al. (2010), 3D laser scanners are a non-contact measurement technique that have faster operational times when compared to current measurement systems, especially when dealing with complex part geometries.

From the respective literature, the research into 3D laser scanners may be divided into three categories. The first research area focuses on how to post-process point clouds into a format acceptable for quality evaluation purposes (Shi et al., 2007; Shi and Xi, 2008; Martínez et al., 2010). The second research area aims to improve the accuracy of 3D scanners by error correction or compensation by contact measurement comparisons; such as a coordinate measuring machine (CMM) (Brajlih et al., 2011; Feng et al., 2001; Isheil et al., 2011; Tamura et al. 1994; Xi et al. 2001) or by developing better scanning plans (Mohib et al., 2009; Shi et al., 2007). The third research area deals with the use of scanning data in manufacturing environments, which can be divided into two categories; reverse engineering and product inspection (Son et al., 2002). This dissertation aims at expanding the applicability of 3D scanners in manufacturing to also include engineering process control, statistical process control, and automated inspection for non-feature based faults.

1.2. Significance

Introducing HDD data as in-line measurements allows for QC approaches to no longer be limited by traditional measurement system capabilities. For instance, by analyzing an entire surface geometry one can detect the occurrence of unexpected fault patterns, i.e. faults that would not normally affect preset CMM measurement points. However, with the opportunity of using HDD data for QC comes new challenges. Specifically, how must current techniques be adapted and/or new approaches be developed for QC in to maximize the potential of HDD data.

It should be noted that the concept of adapting QC methods to account for advancing technologies is not a novel idea. As stated by Box and Woodall (2012):

> *"A primary driving force in the development of statistical science has been the need to adapt and invent theory and methods to handle practical problems faced by scientists and*

other practitioners. Developments in statistical science have also been needed to adapt to the increasing amounts of data available in many applications. Increases in computing power have made the analysis of large sets of data and the use of computationally intensive methods possible."

While this statement is valid, historically, increases in technologies have had only incremental effects on QC strategies and techniques, e.g. the advent of in-line CMMs significantly aided in the transition from univariate to multivariate QC techniques. In contrast, the use of HDD requires a significant leap in how QC is approached and implemented in manufacturing systems. This results from the fact that maximizing the potential of HDD data requires a new QC paradigm where quality is not only assessed by discrete KPCs but considers the entire part being manufactured. In order to illustrate the impact this paradigm shift has on traditional QC strategies, consider the stamped aluminum sheet metal pan in Figure 1.3a. Under the traditional QC paradigm, features or KPC measurements are taken at pre-defined locations, as shown in Figure 1.3b. Here any number of QC approaches can be used to assess the product's quality, including both univariate and multivariate techniques. Under the new QC paradigm, the entire surface (represented as HDD data) is obtained, as shown in Figure 1.3c. Currently there is no effective approach to assess the quality (in terms of QC) for this data-set without performing feature extraction and reverting back to traditional QC strategies.

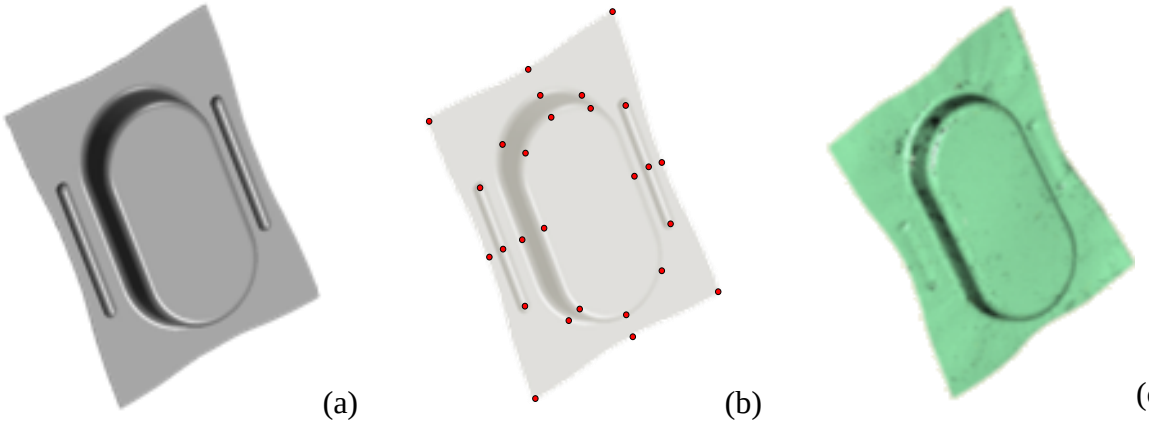

(a) (b) (c)

Figure 1.3: **Representation of (a) A CAD Model of a Manufactured Part, (b) CMM Measurements for Pre-Defined KPCs, and (c) An Actual 3D Laser Scan that Captures all Product Characteristics.**

1.3. Research Objectives

The overarching goal of this research is to adapt current techniques and/or develop new approaches for the use of HDD data in manufacturing systems to increase overall QC capabilities to support the aforementioned paradigm shift. Specifically, this dissertation focuses on how HDD data can be applied to the previously discussed areas of in-line QC for manufacturing systems; 1) Engineering process control, 2) Statistical process control, and 3) Inspection. This will be accomplished through three specific research objectives;

Developing a novel framework for self-correcting compliant assembly systems: Current approaches to part-by-part dimensional error compensation in compliant assembly systems rely on known incoming part error modes, which may be unrealistic in actual assembly environments. Inspired by biological systems, this objective focuses on developing a unique dimensional error-compensation framework for compliant sheet metal assembly processes that acquires immunity to unknown incoming part error modes over time. The resulting autonomous self-correcting compliant assembly system integrates advanced data mining methods, physical models, assembly modeling techniques, HDD measurement technologies, and actuator networks to implement part-by-part dimensional error compensation.

Detecting shifts in manufactured part surfaces: This objective focuses on developing a new approach for statistical process control using HDD point clouds. This approach will transform point clouds into non-uniform rational basis spline (NURBS) surfaces. The control parameters for these NURBS surfaces will be monitored using surface monitoring techniques. Under difference monitoring scenarios the performance of this approach towards the detection of varying shift locations and magnitudes will be analyzed to determine its potential for use as an in-line quality monitoring tool.

P*erforming automated part inspection for non-feature based faults:* The current use of HDD date for part inspection falls into two main categories; 1) Extracting feature parameters, which does not complement the nature of 3D point clouds as it wastes valuable data and 2) An ad-hoc manual process where a visual representation of a point cloud (usually as deviations from nominal) is analyzed; which tends to suffer from slow, inefficient, and inconsistent inspection results. This objective focuses on developing an approach to automate the latter approach to 3D point cloud inspection. This approach will identify the most likely location, size, shape, and magnitude of a potential fault within the point cloud, which transforms the ad-hoc visual inspection approach to a statistically viable automated inspection solution.

1.4. Dissertation Outline

This dissertation is comprised of five chapters. Chapter 2 provides a framework for using HDD data to create a self-correcting compliant assembly systems for unknown or unanticipated fault modes. This chapter originated as a conference paper (Wells and Camelio, 2012) which was extended to its current version and is published in the Journal of Manufacturing Systems (Wells and Camelio, 2013). Chapter 3 describes a new approach for using HDD data-sets to detect process shifts through a surface monitoring technique, which will be submitted to the Journal of Quality

Technology. In Chapter 4 an approach for automated part inspection using HDD data is developed. This chapter originated as a conference paper (Wells et al., 2013) and is currently being extended for submission to the Journal of Manufacturing Science and Engineering. Lastly, Chapter 5 summarizes the contributions made in this dissertation and identifies further avenues for research in the use of HDD data for QC.

2. A Bio-Inspired Approach for Self-Correcting Compliant Assembly Systems

Statistical process control has been popularized in manufacturing as well as various other industries interested in improving product quality and reducing costs. Advances in this field have focused primarily on more efficient ways for diagnosing faults, reducing variation, developing robust design techniques, and increasing sensor capabilities. However, statistical process control cannot address the need for instant variation reduction during assembly operations. This paper presents a unique dimensional error-compensation approach for compliant sheet metal assembly processes. The resulting autonomous self-correcting system integrates rapidly advancing data mining methods, physical models, assembly modeling techniques, high-density dimensional measurement technologies, and actuator networks to implement part-by-part dimensional error compensation. Inspired by biological systems, the proposed engineering process control approach utilizes immunological principles as a means of developing the required mathematical framework behind the self-correcting methodology. The resulting assembly system obtained through this bio-mimicking approach will be used for autonomous monitoring, detection, diagnosis, and control of station and system level faults, contrary to traditional systems that largely rely on final product measurements and expert analysis to eliminate process faults.

2.1. Introduction

Traditionally, two approaches have been implemented to reduce variation and increase productivity in assembly systems: 1) robust design and 2) statistical processes control. Robust design methodologies are generally implemented at the process and product design stages. As an example, simulation models have been developed to evaluate the impact of component tolerances on the quality of an assembled product (Ceglarek et al., 1994). Evaluating variation propagation in an assembly system during design allows for the development of more robust processes and

products. However, assembly systems are complex and it is impractical to design a perfect system that is insensitive to the impact of all process/noise variables. Therefore, quality control systems are placed in production environments to reduce variability and ensure that assembly processes result in high quality products.

Typical quality control approaches rely on control charts to detect abnormal quality conditions or faults. Once a fault is detected, an assembly line is halted while engineers and operators work to determine the source of the problem. A faulty process or component must then be located, analyzed, and repaired/replaced. Current technologies are generally used to monitor final product characteristics, but rely on operator knowledge and expertise for problem compensation. Delays in problem detection and diagnosis result in costly extended production downtimes for manufacturing operations and defective intermediate products.

As sensor and measurement technologies continue to advance, 100% sampling in assembly processes has been achieved in the form of high-density dimensional (HDD) data-sets [Ceglarek and Shi, 1995; Wells et al., 2012a]. This achievement has paved the way for a third approach towards variation reduction, engineering process control (EPC) for active error compensation. These methods rely on continual advancements in programmable tooling, high-density in-line dimensional measurement systems, and advanced variation propagation models to adjust the process on a part-by-part basis.

In machining research, the use of HDD data for EPC has proven quite successful. Coker and Shin (1996) used ultrasonic measurement sensors to estimate and compensate for surface roughness in machining operations. Wang and Huang (2007) proposed a compensation strategy based on equivalent fixture errors to reduce the effect of process errors through the dynamic adjustments of fixture locators. Djurdjanovic and Ni (2007) proposed the use of a state space model

to control variations in multi-station machining applications. Zhou et al. (2012) used HDD data to obtain non-uniform rational basis spline (NURBS) surfaces, which when integrated with a functional morphing routine was used estimate downstream surface deformations in multi-stage machining. It should be noted that the use of EPC in machining to obtain specific product dimensions is often referred to as geometric adaptive control (Koren, 1988).

In EPC for assembly, Mantripragada and Whitney (1999) developed a stage transition model allowing for control theory to be applied to various assembly propagation problems. In their paper, part measurements before assembly were used to calculate control actions to minimize the variation of a product's key characteristics. In addition, it was assumed that the only source of variation in the process was that of the incoming parts. Jin and Ding (2004) developed a design of experiment based engineering process control. In this work, regression models were used with in-line observations of observable noise factors to automatically adjust process control factors to minimize quality loss. Hu and Camelio (2006) suggested that adaptive control could be applied to compliant assemblies through the use of high-fidelity assembly models. Izquierdo et al. (2007) showed that when dealing with rigid sheet metal parts, optimal control action for multi-stage assembly processes can be determined based on optimizing explicit kinematic relationships. Zhong et al. (2010) implemented a feed-forward multistage assembly system controller considering state space modeling errors.

Xie et al. (2012) applied the approach suggested by Hu and Camelio (2006) to compliant sheet metal assemblies. Their paper used expert knowledge of possible dimensional fault patterns in a compliant sheet metal assembly process to develop a collection of pre-determined control actions to perform active error compensation. These control actions were learned in an off-line step, which utilized highly non-linear Finite Element (FE) modeling (that included friction and contact

between parts and tools) coupled with an optimization routine. These pre-determined corrective actions were then implemented as an on-line control strategy based on incoming part measurements. While this method performs well, several challenges still exist; 1) The fault patterns have to be known, which may not be realist, 2) The control strategy cannot learn from the assembly system to identify actual fault patterns, 3) The control strategy cannot adapt to changes in the system, such as; a change in suppliers, a redesigned material handling system, or system degradation, all of which can result in the appearance of new fault patterns, and 4) The method relies on being able to completely capture incoming part errors through a discrete number of pre-defined KPCs, which is not realistic for unanticipated or continuous faults.

Recently, Wells et al. (2011) developed a self-healing framework based upon key insights drawn from the human immunological system. By applying this framework to compliant assembly systems provides the opportunity to overcome the first three aforementioned challenges encountered by the method proposed by Xie et al. (2012). In addition, by incorporating HDD into the framework allows for the fourth challenge to be overcome as well. A brief introduction to adaptive immunity and the key mechanisms that make it successful, as described in Wells et al. (2011), is presented as follows.

2.2. Adaptive Immunity

There are several levels of defense built into the human immunological system. However, for brevity, only a brief introduction to adaptive immunity will be discussed in this paper as it is the driving force behind the proposed self-correcting assembly system. A more thorough discussion into the relationship between the immune system and assembly systems can be found in Wells et al. (2011). Adaptive immunity utilizes pre-existing knowledge of invading organisms (antigens)

to develop responses tailored to maximally eliminate them (Wise and Gordon, 2002) and can be divided into two categories; active and artificial.

2.2.1. Active Immunity

Active immunity results from the development of an antigen specific response. In a general sense, antigens are foreign organisms which pose a threat to the host organism. This response has evolved based on previous encounters with the antigen. Active immunity is the result of the simultaneous implementation of two primary immunological mechanisms; B and T_h Cells.

B Cells are the workhorse behind the active immune system as they provide two crucial functions: antigen recognition and antigen eradication through the production of antibodies. Throughout the course of a day millions of B Cells are continually and pseudo-randomly generated (Stanley, 2002), where each one is capable of dealing with a specific antigen, known as that B Cell's cognate antigen. These B Cells circulate through the blood stream performing continuous antigen surveillance.

Once a B Cell encounters its cognate antigen, it binds to that antigen and awaits an activation signal from a T_h Cell (discussed later in this section). Once activated, the B Cell begins to replicate. The resulting "offspring" can be of two types; plasma cells or memory B Cells. Plasma Cells produce the antibodies to eliminate their cognate antigen. While memory B Cells are inactive versions of their parent B Cell, and remain inactive until they bind to their cognate antigen. This results in an ever increasing population of B Cells that are able to fight off an antigen known to have existed within the host. Interestingly enough, the exact opposite process is also occurring. B Cells that have never been activated will eventually decay and make room for new B Cells to be created.

The successful recognition and eradication of multiple antigens requires diversity among antibodies (Mian et al., 1991). Two immunological processes exist to produce a large diversity of antibodies, namely class-switching and mutation. Different classes of antibodies exist, each of which have unique functions for antigen eradication. In order to take advantage of these different antibody classes, B Cells are able to "switch" which class of antibody they produce during the B Cell replication stage (Market and Papavasiliou, 2003). This results in a robust response to antigens that are known to exist within the host. It should be noted that class-switching is governed by T_h Cells (discussed later in this section). Additionally, during the antigen mass production phase, antigen cells begin to rapidly divide. During this division mutations occur, resulting in a very diverse antibody pool (Diaz and Casali, 2002). These variations within the antibodies result in slight variations on their effectiveness towards fighting the infection. The key B Cell aspects described above are illustrated in Figure 2.1.

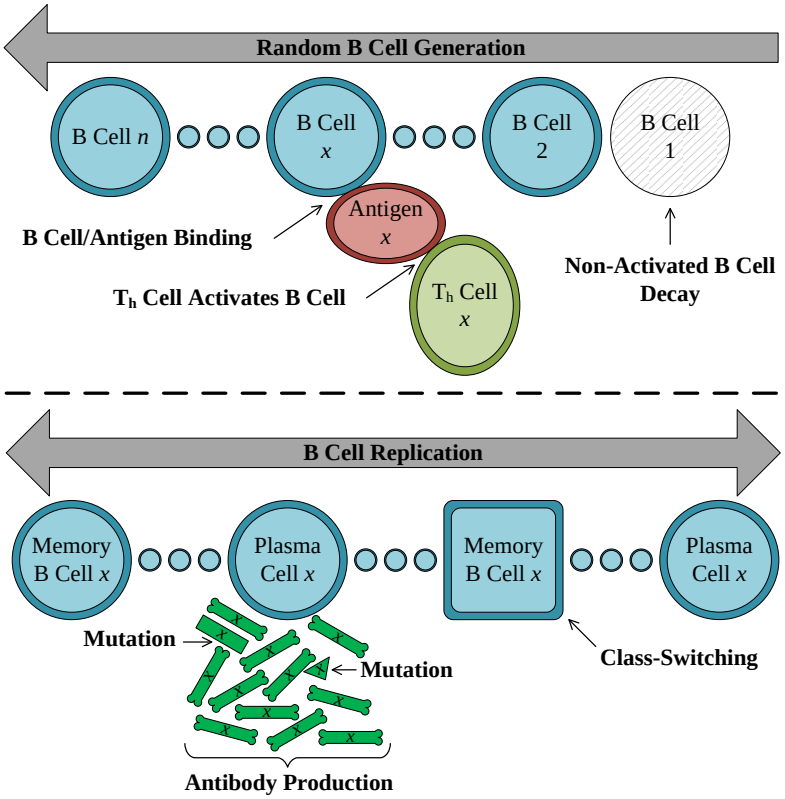

Figure 2.1: Key B Cell Aspects.

While B Cells fight the "war" against invading antigens, T_h Cells orchestrate the "war" effort. Unlike B Cells all T_h Cells start out as equals (naïve T_h Cells). Once a naïve T_h Cell encounters an antigen (which becomes that T_h Cell's cognate antigen), it becomes activated and will begin to replicate. This division results in three types of T_h Cells; Effector, Memory, and Regulatory.

Effector T_h Cells are often considered the driving force of the immune system. In regards to active immunity, Effector T_h Cells do not directly fight the infection, they guide the immune response. When an Effector T_h Cell comes into contact with a B Cell that has bounded to that Effector T_h Cell's cognate antigen, a signal is sent to the B Cell to begin replication. This mechanism is a redundancy check that prevents B Cells from attacking good cells. As discussed earlier, this replication results in the creation of plasma cells (and memory B Cells), which disperse antibodies and fight the antigen. During this replication stage, the Effector T_h Cell also governs the process of class-switching.

Memory T_h Cells lay dormant until they again encounter their cognate antigen. When this occurs they are reactivated and begin to replicate into Effector T_h Cells. Similar to Memory B Cells, Memory T_h Cells result in a large pool of Effector T_h Cells, whose cognate antigens are known to exist within the host.

Regulatory (or Suppressor) T_h Cells maintain balance within the immune system by turning off the immune response. In essence, Regulatory T_h Cells are the antithesis of the Effector T_h Cells, as they limit unnecessary replications of B and T_h Cells once it becomes apparent that the antigen no longer poses a significant threat.

2.2.2. Artificial Immunity

So far it has been assumed that due to the robustness and adaptability of the active immune system all possible antigens can be dealt with. However, due to a lack of memory or a very fierce antigen,

the immune response may be too slow to react before major damage is caused to the host. In these cases, artificial immunity is implemented, where the immunity to a given antigen is obtained from an external source, such as a vaccination.

A vaccination involves exposing individuals to altered or weakened antigens. This technique is mostly used as a prevention method, since vaccines aim to induce immunity without having to experience the actual disease. Vaccines are implemented to prevent a known or newly arising disease from spreading to the remainder of the population, which can be seen in the common practice of vaccinating our young against deadly diseases such as; Hepatitis, Measles, Chickenpox, etc. Once the individual has developed its own antibodies, the memory of how to identify and eradicate the antigen is permanent, basically becoming an element of active immunity.

2.2.3. Adaptive Immunity Characteristics

The previous two subsections highlighted the essential mechanisms that govern adaptive immunity. This subsection identifies the characteristics most vital to the success of the adaptive immune system when these mechanisms are implemented. In addition, the importance of these characteristics towards developing an ideal self-correcting assembly system is explored.

One of the most important characteristics of adaptive immunity is that it is continuously working to become more efficient and robust in detecting and eliminating threats regardless of the host's condition. In fact, for the majority of the time, this process operates without the host being aware that any problem exists. This is made possible by the fact that these two systems (immune and host) operate in parallel and interact only when needed. In an assembly system this behavior is of the utmost importance as the cost associated with waiting for problems to be solved can be devastating. In addition, modern assembly systems are equipped with sensors and measurement

equipment for use in quality control. This provides a wealth of information that could be used by a parallel immune system to further the assembly system's robustness.

The immune system has the ability to fight antigens that fall into two categories; 1) Known - Through the implementation of vaccines the system can defend itself against antigens that are known to exist and 2) Unknown - Through the generation of random B Cells the system can defend itself against antigens that are not known to exist. In addition, due to the nature of cell replication, memory cells, and cell decay, the immune system inherently maintains an optimal ratio of solutions for known and unknown antigens to minimize the use of system resources. It is possible but highly impractical to design/redesign an assembly system to completely account for known faults. Additionally, it is currently not possible/practical to account for unknown faults. Therefore, an effective adaptation of active immune system principles into an assembly system could drastically increase its ability to handle both known and unknown faults.

One of the most unique and effective characteristics of the immune systems relies in its ability to increase antibody diversity through mutations and class-switching. As previously mentioned it is possible to design/redesign an assembly system to defend itself against known faults; however, known faults rarely occur within an actual assembly system. This is due to the fact that faults are continuous. For example, through the use of programmable tooling an assembly system can be designed to perfectly account for a 2˚ flange error on a piece of sheet metal in a joining operation. However, since this is a continuous fault, an exact 2˚ flange error will never happen. With this in mind, it is of the utmost importance for an assembly system to be able to handle a wide array of "mutated" faults. Additionally, complex assembly systems have multiple tools (programmable tooling, machine parameters, etc.) at their disposal to correct faults. Optimization tools coupled with physical system models can be used to determine corrective actions to minimize the effect of

the fault. However, these models tend to be highly non-linear for complex assembly systems, which will not guarantee a global optimum corrective solution. Therefore, it is in the best interest for the assembly system to be able to perform "class-switching", which would allow multiple local optimal solutions (combination and usage of compensation tools) to be implemented.

2.3. Bio-Inspired Self-Correcting Compliant Assembly System

In this section, the previously discussed active immunity principles will be adapted into a mathematical framework for the proposed self-correcting compliant assembly system.

2.3.1. Antigens and Antibodies

In order to start building tools for adaptive immunity in compliant assemblies, one crucial question needs to be answered; What are antigens and antibodies in terms of an assembly system? In a general sense, antigens can be thought of as foreign organisms, which present possible threats to the host. In assembly systems, this equates to any incoming part with errors $(\mathbf{A_g})$ being imparted into the assembly that may result in post-assembly Key Product Characteristic (KPC) deviations $(\mathbf{y})$. Examples of such errors include; fixture position deviations, incoming part errors, deteriorating tooling, welding distortion, etc.

The term antigen is short for antibody generator, which means that the presence of an antigen should initiate an immune response through antibody production, regardless of whether or not any damage has occurred. As discussed in Section 2.2.1 in order for this antibody production to begin, the antibody must first be matched with its cognate B Cell, which is designed to eliminate that antigen. Therefore, a B Cell (in terms of an assembly system) is a pre-defined part with errors $(\mathbf{B})$ that may or may not match an incoming part with errors $(\mathbf{A_g})$. In addition, an assembly system antibody must be a unique corrective action $(\mathbf{A_b})$ designed to compensate for $\mathbf{A_g}$, which is initiated if $\mathbf{B} = \mathbf{A_g}$. Possible correction actions include; adjusting fixture locations, increasing clamping

forces, modifying welding current or voltage, changing spot-welding sequencing, etc. It should be noted that for simplicity, the remainder of this paper only considers the presence of one self-correcting capable assembly station.

2.3.2. B Cell Creation

The proposed self-correcting compliant assembly system relies heavily on the ability to randomly produce pre-defined part errors and subsequently obtain a corrective action. In this approach $\mathbf{A_b}$ is determined through the use of virtual assembly models based upon finite element (FE) analysis. It has been shown that FE models which incorporate friction and contact between parts and tools can produce high fidelity estimates of post-assembly KPC deviations ($\mathbf{y}^*$) as a function of $\mathbf{B}$ for compliant assemblies (Xie et al., 2007). These models can then be used to determine an optimal corrective action ($\mathbf{A_b^*}$) for a given $\mathbf{B}$ by minimizing the weighted sums of squares of $\mathbf{y}^*$, as shown in Eq. (2.1). It should be noted that $\mathbf{y}^*$ is determined after the assembly is released at the end of the process.

$$\begin{aligned} J &= \min_{\mathbf{A_b}} \mathbf{y}^{*\mathrm{T}} \mathbf{Q} \mathbf{y}^* \\ \text{s.t. } &\mathbf{g}(\mathbf{y}^*, \mathbf{A_b}) \leq \mathbf{0}, \end{aligned} \tag{2.1}$$

Here $\mathbf{Q}$ is the weight matrix that captures the relative importance among KPCs and must be a positive definite matrix. The function $\mathbf{g}(\cdot,\cdot)$ contains all the product/process constraints effecting the assembly and the capability to perform corrective actions for the self-correcting capable station, such as; the actuator work space and the degrees of freedom limitations necessary to perform the adjustment. For compliant assemblies, solving Eq. (2.1) requires numerous evaluations of a highly non-linear virtual assembly model, which is computationally exhaustive. In a production environment, solving Eq. (2.1) on a part-by-part basis is not a viable option as the

production time would increase drastically. Luckily this problem can be avoided by imparting adaptive immunity into the assembly system.

The proposed approach will strictly use non-uniform rational basis spline (NURBS) surfaces to develop part geometries. NURBS are widely used in computer aided design (CAD) for the representation of free-form curves and surfaces due to their interesting properties, such as; the ability to handle large surface patches, local controllability (local modification property), lower computational requirements, and the ability to represent analytical forms (Lee, 1999; Kruth and Kerstens, 1997). A NURBS surface is defined as

$$\mathbf{B}(u,v) = \frac{\sum_{i=1}^{n_u}\sum_{j=1}^{n_v} B_{u,i}(u)\cdot B_{v,j}(v)\cdot w_{i,j}\cdot \mathbf{p}_{i,j}}{\sum_{i=1}^{n_u}\sum_{j=1}^{n_v} B_{u,i}(u)\cdot B_{v,j}(v)\cdot w_{i,j}}, \tag{2.2}$$

where **B** is the surface, $\mathbf{B}(u,v)$ is a 1 x 3 vector defining a discrete point on the surface at location (u,v) in a Cartesian coordinate system; n_u and n_v are the number of control points in the u and v directions, respectively; $B_{u,i}(u)$ and $B_{v,j}(v)$ are B-Spline functions in the u and v directions, respectively; and $\mathbf{p}_{i,j}$ and $w_{i,j}$ are a 1 x 3 vector and a scalar defining the coordinates of the control points and their weights, respectively. It should be noted that the B-Spline functions are defined by the order of the defining curves knot sequences. Please refer to Cox (1972) and de Boor (1972) for further details. For syntax simplicity, from this point on it will be assumed that only one compliant part is being added to the self-correcting capable station.

The first step towards generating B Cells requires creating a NURBS surface representation of the nominal part geometry for a given self-correcting capable station. First determine the order of the u and v directions, k_u and k_v, respectively for the surface. This paper suggests using $k_u = k_v = 4$, which will result in cubic curves. In addition, n_u and n_v need to be determined, based on the following two criteria; 1) The number of control points used should provide an exact representation of the nominal surface and 2) The number of control points used provides enough

flexibility to allow a significant amount of randomization amongst the B Cell population, but not too many that could result in wavy or crinkled surfaces. In order to satisfy these criteria, some visual experimentations may be required. Once $k_{\cdot}$ and $n_{\cdot}$ have been chosen (for both directions) nonperiodic knot vectors and the resulting B-Spline functions can be calculated. An example of a nominal part geometry created via a NURBS surface is given in Figure 2.2.

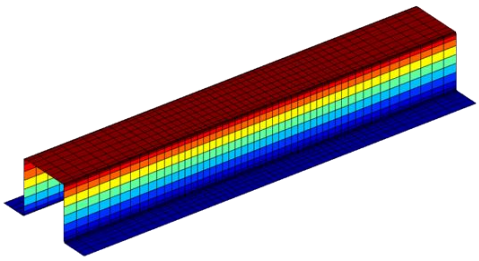

Figure 2.2: Finite Element Model Generated from a NURBS Surface for a Nominal Part Geometry.

For the next step, define $\mathbf{B}_0^* = \left[\mathbf{P}_{\cdot,1}, \cdots, \mathbf{P}_{\cdot,n_v}, w_{\cdot,1}, \cdots, w_{\cdot,n_v}\right]^{\mathrm{T}}$, where $\mathbf{P}_{\cdot,j} = \left[\mathbf{p}_{1,j}, \cdots, \mathbf{p}_{n_u,j}\right]$ and $w_{\cdot,j} = \left[w_{1,j}, \cdots, w_{n_u,j}\right]$. Given that the knot vectors and B-Spline functions have been determined and are now constant, the nominal part surface ($\mathbf{B}_0$) can be summarized from Eq. (2.2) as

$$\mathbf{B}_0 = f(\mathbf{B}_0^*). \tag{2.3}$$

Also, define $\boldsymbol{\delta}$ as a $4 \cdot n_u \cdot n_v$ x 1 random vector, which will be referred to as the B Cell generator. Now a B Cell can be defined as

$$\mathbf{B} = f(\mathbf{B}_0^* + \boldsymbol{\delta}), \tag{2.4}$$

where a small perturbation of the B Cell generator about zero will result in the creation of a random surface based upon the nominal surface. The B Cell generator will be randomly generated sequentially at times $t = 1,2,\cdots$, i.e. $\boldsymbol{\delta}_1, \boldsymbol{\delta}_2, \cdots$. Also, for notation simplicity let $\mathbf{B}_t = f(\mathbf{B}_0^* + \boldsymbol{\delta}_t)$ and $\mathbf{B}_t^* = \mathbf{B}_0^* + \boldsymbol{\delta}_t$.

In order to increase the robustness of the immune system the proposed approach suggests that B Cells be generated from multiple random B Cell types. First define $n_r \geq 1$ as the number of random B Cell types to be implemented. Next for each random B Cell type's B Cell Generator

($\mathbf{R\delta}_i, i = 1, \cdots, n_r$) define its random distribution. Also, set $r\alpha_1 = \cdots = r\alpha_{n_r} = 1/n_r$, and let $\mathbf{r\alpha} = [r\alpha_1, \cdots, r\alpha_{n_r}]$.

To produce a B Cell at time T, randomly generate an independent multinomial observation defined by the event probabilities $\mathbf{r\alpha}$. Let $RX_{i,T}$ be an observation classified in category i at time T where $i = 1, \cdots, n_r$. For each $RX_{i,T} = 1$ generate the B Cell as

$$\mathbf{B}_T = f(\mathbf{B}_0^* + \mathbf{R\delta}_i). \tag{2.5}$$

An example of two B Cells randomly generated from a NURBS surface is given in Figure 2.3a and 2.3b. It should be noted that in this example only one B Cell generator (elements corresponding to control points are normal i.i.d. and elements corresponding to weights are zero) is considered. If additional B Cell generators are used, it is highly recommended to add correlation within the B Cell generator. This will allow for desired characteristics of the nominal geometry to be maintained within the random B Cell, such as; specific planar faces remaining planar or corners remaining convex or concave.

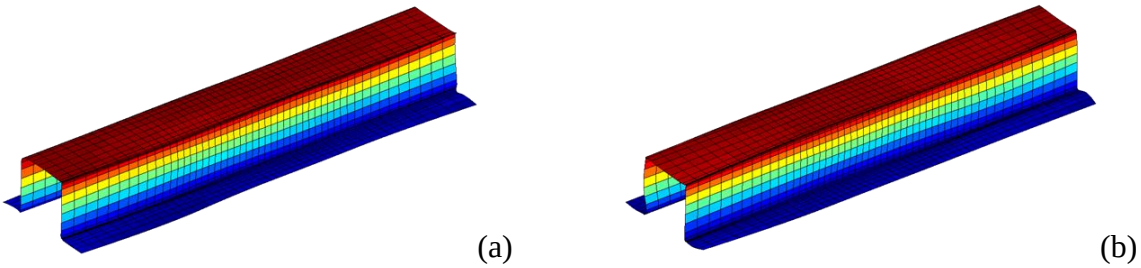

(a) (b)

Figure 2.3: Finite Element Model Generated from a NURBS Surface for Two Random B Cells.

For each $\mathbf{B}_T$ generated, a FE model of the assembly for this geometry is created resulting in the evaluation of Eq. (2.1) to calculate $\mathbf{y}^*(T)$ and $\mathbf{A}_\mathbf{b}^*(T)$. However, in order to reduce the computational effort in evaluating Eq. (2.1), for the initial calculation of $\mathbf{A}_\mathbf{b}^*(T)$ a subset of the actual constraints on the system should be used. Specifically, replace $\mathbf{g}(\cdot,\cdot)$ with $\mathbf{g}^*(\cdot,\cdot)$, where $\mathbf{g}^*(\cdot,\cdot) \leq \mathbf{g}(\cdot,\cdot)$. The implication of this will be discussed later in the paper. To complete the B Cell creation process set $I_T = 0$, to indicate that the T^{th} B Cell has yet to be activated.

It is of the utmost importance to note that the random nature of B Cells could cause impossible surfaces, such as self-intersecting surfaces. However, the occurrence of such a surface is highly unlikely if the distribution of each B Cell generator is realistic. With this is mind $\mathbf{B}_T$ should be analyzed directly after creation to ensure that $\mathbf{B}_T(u,v) \neq \mathbf{B}_T(x,z)$, for all $u \neq x$ and $v \neq z$.

2.3.3. Vaccination and B Cell Mutations

During the initial design of an assembly system, it is often possible to identify known error types that may affect the system. Similar to the vaccination of children, it is vital that a new assembly system be vaccinated for these errors. The first step in implementing the vaccination phase in compliant assemblies is to identify $n_k \geq 0$ incoming known error types in the form of surfaces $(\mathbf{KB}_1, \cdots, \mathbf{KB}_{n_k})$ for the assembly system. These error types can be determined through expert knowledge or a sensitivity analysis, which aids in determining the most critical error types (Hu et al., 2003). Next determine the control points and weights vector ($\mathbf{KB}_i^*$) for each $\mathbf{KB}_i$, that satisfies Eq. (2.3), i.e. $\mathbf{KB}_i = f(\mathbf{KB}_i^*)$, $i = 1, \cdots, n_k$. An example of two vaccines represented as NURBS surfaces for the nominal part shown in Figure 2.2, specifically a flange angle error and a buckling mode is given in Figure 2.4a and 2.4b, respectively. In order to generate the correct proportion of vaccines, rank each known error type i by its estimated frequency or severity as $k\theta_i$ and let $\mathbf{k\theta} = [k\theta_1, \cdots, k\theta_{n_k}] / \|k\theta_1, \cdots, k\theta_{n_k}\|$.

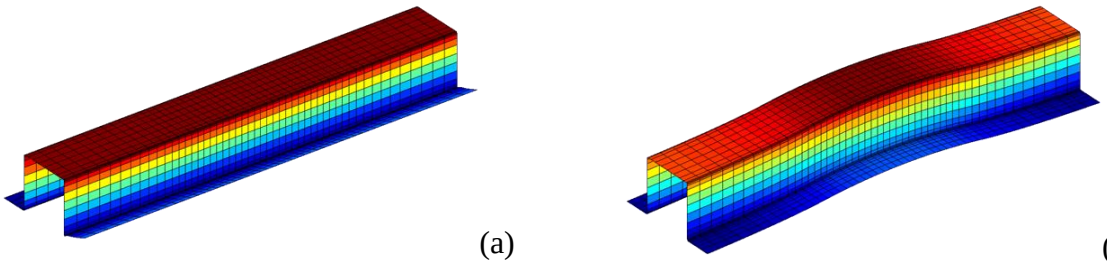

(a) (b)

Figure 2.4: Finite Element Model Generated from a NURBS Surface for a) Flange Error Mode and b) Buckling Error Mode.

As discussed earlier vaccines subject the host to altered or weakened antigens, which results in a similar immune response to actually having been exposed to the real antigens. In this respect, assembly system vaccinations should allow for mutations in the vaccine's B Cells. Therefore, the next step in applying vaccinations is to determine appropriate distributions for a set of B Cell generators for each $\mathbf{KB}_i$. This will allow for the B Cells to mutate and cover a wider range of possible antigens. First define $n_{r,i} \geq 1$ as the number of B Cell generators to use for a known error type i. Next for each B Cell Generator for known error type i ($\mathbf{K\delta}_{i,j}, j = 1, \cdots, n_{r,i}$) define its random distribution and its relative importance ($k\alpha_{i,j}, j = 1, \cdots, n_{r,i}$). In addition, let $\mathbf{k\alpha}_i = [k\alpha_{i,1}, \cdots, k\alpha_{n_{r,i}}]/\|k\alpha_{i,1}, \cdots, k\alpha_{n_{r,i}}\|$.

Define $\beta \in [0,1]$ if $n_k > 0$, 0 otherwise, as the proportion of B Cells to be generated from random B Cell types. For each time T, randomly generate an independent Bernoulli observation (BX_T) defined by the event probability β. For each $BX_T = 1$ generate $\mathbf{B}_T$ from a random B Cell type, outlined earlier. For each $BX_T = 0$ perform the following steps. Randomly generate an independent multinomial observation defined by the event probabilities $\mathbf{k\theta}$. Let $KX_{i,T}$ be an observation classified in category i at time T where $i = 1, \ldots, n_k$. For each $KX_{i,T} = 1$ randomly generate an independent multinomial observation defined by the event probabilities $\mathbf{k\alpha}_i$. Let $KY_{j,T}$ be an observation classified in category j at time T where $j = 1, \cdots, n_{r,i}$. For each $KY_{j,T} = 1$ generate the B Cell as

$$\mathbf{B}_T = f(\mathbf{KB}_i^* + \mathbf{K\delta}_{i,j}). \tag{2.6}$$

An example of two mutated B Cell vaccines generated via a NURBS surface from the known flange error type are given in Figure 2.5. Similarly, two mutated B Cells for the known buckling mode error type is given in Figure 2.6. It should be noted that only one B Cell generator (elements corresponding to control points are normal i.i.d. and elements corresponding to weights are zero)

for each known error type is considered. Similar to the discussion earlier, when implementing multiple B Cell generators for a given vaccine it is highly recommended to add correlation within the B Cell generators.

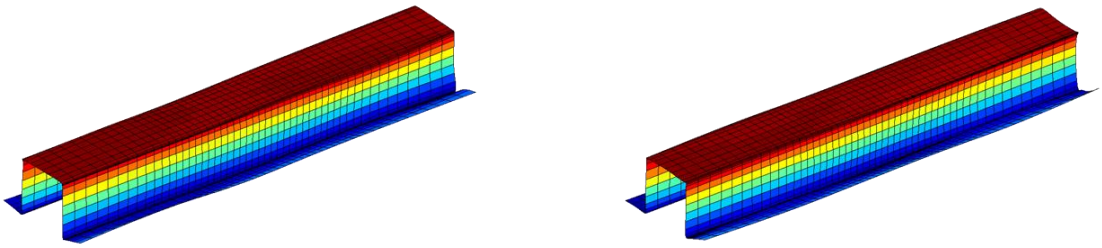

Figure 2.5: Finite Element Model Generated from a NURBS Surface for Two Mutated B Cells for the Flange Error Mode.

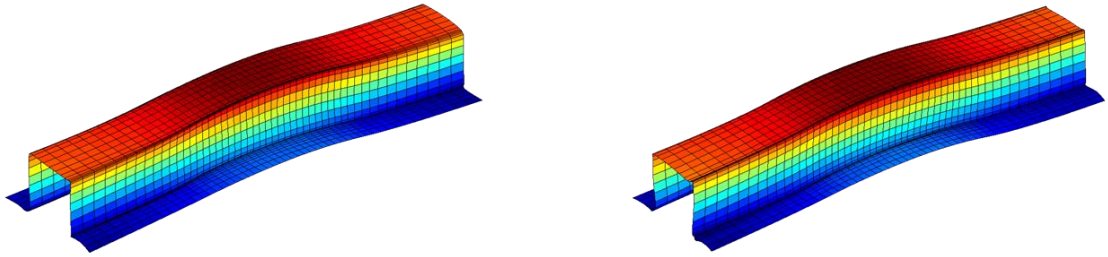

Figure 2.6: Finite Element Model Generated from a NURBS Surface for Two Mutated B Cells for the Buckling Error Mode.

2.3.4. Antigen Identification

An antigen must be identified and eradicated before it causes harm to the system. With respect to an assembly system, this means that each $\mathbf{A_g}$ must be determined and matched with an appropriate $\mathbf{B}$ from the pool of B Cells before the assembly process begins so that the respective $\mathbf{A_b^*}$ can be applied. In order to obtain $\mathbf{A_g}$ this paper suggests the use of in-line HDD measurement devices, such as 3D laser scanners. 3D laser scanners are one of the most state-of-the-art dimensional measurement technologies current being implemented in industry. They can rapidly provide point clouds consisting of millions of data points to represent an entire manufactured parts' surface. Traditionally 3D laser scanners have been used in reverse engineering application, but are beginning to be applied as in-line measurement devices for statistical process control applications (Wells et al., 2012b). It should be noted that more traditional measurement devices, such as optical

coordinate measuring machines (OCMMs) can be used. However, this technology may not provide the resolution needed to accurately capture the surface.

In its raw form the data collected from 3D laser scanners is not appropriate for antigen identification for the following two reasons; 1) Finding a match between the current antigen based on the raw point cloud data and a large pool of B Cells would to be computational impractical and 2) The adaptive immune system must create a memory of the antigen's unique characteristics, which would also prove to be highly computationally impractical as it would require the storage of an entire point cloud. To remedy this problem, this paper suggests that each $\mathbf{A_g}$ be defined as a NURBS surface that best represents the raw point cloud, which can be performed through multiple methods found throughout the literature. However, a majority of these methods are based on simultaneously estimating weights and control points through a least-squares strategy. Such methods require a significant amount of computational effort, which is undesirable for this case. Another approach referred to as lofting or skinning, involves interpolating cross-sectional iso-parametric curves to obtain the NURBS weights and control points, which tend to be more computationally friendly. Recently, Koch (2009) has shown that both of the previously discussed methods produce the exact same results. Therefore, it is suggested that the lofting method be implemented in our approach. The lofting approach requires that the B-Spline functions are known, which is already the case as they were pre-defined by the nominal geometry in the creation of the B Cells. Therefore, each resulting NURBS surface $\mathbf{A_g}$ can be defined with a parameter vector ($\mathbf{A_g^*}$) consisting of weights and control points from Eq. (2.3), i.e. $\mathbf{A_g} = f(\mathbf{A_g^*})$.

It should be noted that this computational effort will be minimal when applied to compliant assemblies. Compliant assemblies typically involve sheet metal parts, which do not require a significantly large resolution to uniquely capture the surface. Moreover small imperfections in the

surface that are not captured will not affect the final assembly. It is recommended that experiments be performed to obtain a scanning resolution to balance the requirement of computational speed and NURBS surface estimation accuracy.

2.3.5. B Cell Memory and Mutation

Through the process of replication, memory B Cells retain knowledge of previous antigen encounters. When an antigen is encountered by a memory B Cell it can replicate itself to become a plasma cell. During this replication, mutations occur, resulting in a slight variation in the B Cell. These mutations cause an increased population of B Cells that are very similar to previously encountered antigens. The proposed approach requires that each encounter with an antigen results in appending the memory matrix

$$\mathbf{A} = [\mathbf{A}_{\mathbf{g}}^{*}(1), \mathbf{A}_{\mathbf{g}}^{*}(2), \cdots, \mathbf{A}_{\mathbf{g}}^{*}(l)], \tag{2.7}$$

where l is the total number of antigens encountered. Once a significant amount of antigens have been encountered ($l > C_p \cdot 4 \cdot n_u \cdot n_v$, where $C_p > 1$), a principal component analysis (PCA) can be performed on **A**. PCA is a dimension reduction technique, where a linear transformation is performed on a set of correlated multivariate variables, resulting in a set of orthogonal variables through eigenvector decomposition. The first step of PCA is to calculate the sample covariance matrix **S** from the memory matrix, followed by solving the eigenvalue decomposition:

$$\mathbf{S} = \mathbf{V}\mathbf{L}\mathbf{V}^{\mathrm{T}}, \tag{2.8}$$

where **L** is a diagonal matrix containing eigenvalues ($\lambda_1 \geq \cdots \geq \lambda_{4 \cdot n_u \cdot n_v} \geq 0$) and **V** is an orthonormal matrix whose columns are eigenvectors. In addition, the quantity

$$\Lambda_i = \frac{\lambda_i}{\lambda_1 + \lambda_2 + \cdots + \lambda_{4 \cdot n_u \cdot n_v}} \tag{2.9}$$

is the proportion of the variability of the original system that can be attributed to the i^{th} principal component. For more details regarding PCA, the reader is referred to Johnson (1998) and Montgomery (2008).

Once the number of encountered antigens has reached a significant number ($l > C_p \cdot 4 \cdot n_u \cdot n_v$), it becomes possible to generate mutations of memory B Cells obtained from a PCA. However, it is still desirable to obtain B Cells from the vaccination and random error types. Let $W(\tau) = e^{-\gamma\tau}$, where $\gamma \in [0, 1]$ is the learning rate for producing B Cells from PCA and τ is the time, where $\tau = 1$ when the value of l at time T_τ becomes greater than $C_p \cdot 4 \cdot n_u \cdot n_v$. At time T, randomly generate an independent Bernoulli observation (MX_T) defined by the event probability $W(T - T_\tau)$. For each $MX_T = 1$ generate $\mathbf{B}_T$ from the procedure outlined in Section 2.3.3. For each $MX_T = 0$ perform the following steps. Randomly generate an independent multinomial observation defined by the event probabilities $\mathbf{\Lambda}$, where $\mathbf{\Lambda} = [\Lambda_{1,}, \cdots, \Lambda_{4 \cdot n_u \cdot n_v}]$. Let $MX_{i,T}$ be an observation classified in category i at time T where $i = 1, \cdots, 4 \cdot n_u \cdot n_v$. For each $MX_{i,T} = 1$ generate the B Cell as

$$\mathbf{B}_T = f(\boldsymbol{\mu} + \mathbf{v}_i \cdot \eta_i), \tag{2.10}$$

where $\eta_i \sim N(0\,, \lambda_i)$, $\mathbf{v}_i$ is the i^{th} column of $\mathbf{V}$, and $\boldsymbol{\mu}$ the $4 \cdot n_u \cdot n_v$ x 1 mean vector of $\mathbf{A}$.

Generating B Cells from memory in this manner is very appealing for several reasons. First, after the system matures the majority of the B Cells that are being generating are reflecting actual error patterns occurring in the system. Second, the system can adapt to changes or drifts in the process. Third, the known error types identified during the vaccination stage could have been completely misguided. Therefore less emphasis should be placed on them in the long run. However, if these error types begin to show up they will still be accounted for through B Cells generated from the PCA. Finally, the majority of the principal component vectors will reflect

statistical noise, which will allow for truly random B Cells to be created furthering the robustness of the system. A flowchart outlining the entire process of B Cell generation is given in Figure 2.7.

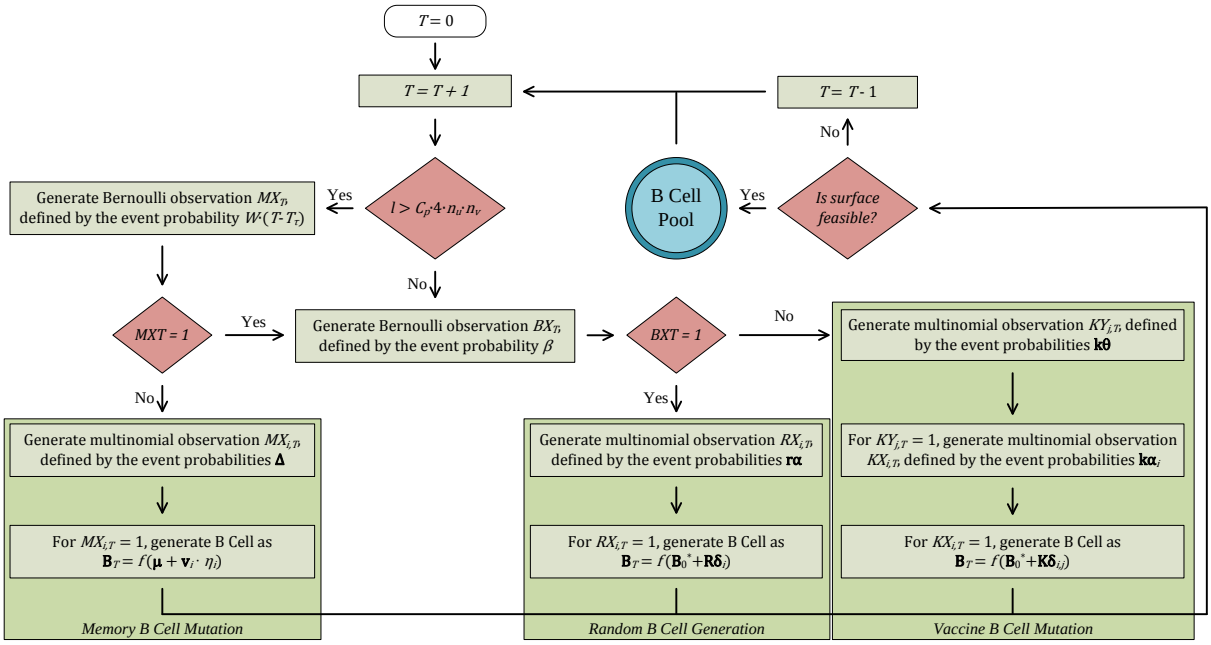

Figure 2.7: Flowchart Outlining the Entire Process of B Cell Generation.

2.3.6. B Cell and Antigen Matching

In the proposed immune system each time an assembly enters a self-correcting capable station it is transformed into a NURBS surfaces $\mathbf{A_g}$. For each $\mathbf{A_g}$ the immune system must be matched with an equivalent **B**. The simplest approach for doing so would be to find the **B** that is most similar to $\mathbf{A_g}$. However, as the immune system matures the large number of candidate B Cells would make this approach highly undesirable, as this matching needs to be as fast as possible. To rectify this problem, this framework will implement a decision tree to find this match. A decision tree is a supervised learning technique that creates a flowchart-like structure for the purpose of data classification. At every internal node within the tree a decision is made on which branch to follow by testing an attribute of the current data set. The final node (leaf or terminal node) contains a class label for the data set. In this case a B Cell's attributes are the elements of its corresponding $\mathbf{B}^*$, while the class labels are based on whether a group of B Cells are highly similar. After the decision

tree is built each $\mathbf{A}_\mathbf{g}^*$ gets classified by the tree. Then its respective $\mathbf{A}_\mathbf{g}$ gets compared to each $\mathbf{B}$ in that class instead of the entire B Cell pool.

Typically decision tree induction (learning) is performed with a training set of data; however since the immune system is continually producing B Cells there is a stream of training data. In order to avoid continually redesigning the decision tree, the proposed framework suggests the use of an incremental method for the induction of the decision tree, namely the ITI algorithm described in Utgoff (1994).

The procedure to generate class labels required for the creation of the decision tree is as follows:

Step 1: Define the criterion ε_d, which is the maximum difference allowable between two B Cells for them to be considered as the same class. Also define the criteria N_d, which is the maximum number of B Cells that are allowed to be in the same class.

Step 2: At time T calculate

$$\varepsilon_{T-j} = \sum_u \sum_v \left(\mathbf{B}_i(u,v) - \mathbf{B}_{T-j}(u,v)\right)^2, \tag{2.11}$$

where, $j = 1, \cdots, T-1$.

Step 3: If any $\varepsilon_{T-j} < \varepsilon_d$ then $\mathbf{B}_t$ gets labelled as the same class as $\mathbf{B}_{T-j}$. If this criterion is met more than once then $\mathbf{B}_T$ gets labelled as the same class as the $\mathbf{B}_{T-j}$ that corresponds to the smallest ε_{T-j}. If the criterion is never met or $T = 1$, $\mathbf{B}_T$ gets labelled as a new class. Also if the addition of $\mathbf{B}_T$ to a class results in the total number of entities for the class exceeding N_d, $\mathbf{B}_T$ is not added and is instead killed (and $T = T - 1$).

When selecting the criteria ε_d and N_d the following considerations should be made; 1) N_d will limit the size of the B Cell pool, 2) N_d will also limit the number candidate B Cells for a given $\mathbf{A}_\mathbf{g}$ to be compared to, and 3) ε_d will affect the overall size of the decision tree. It should be noted that

since the identification of a class for $\mathbf{B}_T$ may result in its death, the classification should be performed before Eq. (2.1) is evaluated for $\mathbf{B}_T$.

As previously stated each $\mathbf{A_g}$ will be classified by the decision tree, based upon attributes $\mathbf{A}_\mathbf{g}^*$. The difference between each B that has the same class label as $\mathbf{A_g}$ is calculated by Eq. (2.12). $\mathbf{A_g}$ is then matched with the **B** that produces the smallest ε_m.

$$\varepsilon_m = \sum_u \sum_v \left(\mathbf{A_g}(u,v) - \mathbf{B}(u,v)\right)^2. \tag{2.12}$$

2.3.7. B Cell Activation and Decay

One of the main tasks of a T_h Cell is to determine whether corrective action $\mathbf{A}_\mathbf{b}^*(t)$ should be implemented for the current antigen when $\mathbf{B}_t = \mathbf{A_g}$ (should the t^{th} B Cell be activated), or in this case when $\mathbf{B}_t \approx \mathbf{A_g}$, where $\mathbf{B}_t$ was the best match identified from the B Cell and antigen matching routine previously discussed. In order to make this decision, define the criterion ε_a which will be the maximum allowable value of the smallest ε_m (ε_m^*) that will result in $\mathbf{A}_\mathbf{b}^*(t)$ being implemented. This criterion performs two functions; 1) It prevents any errors from the classification process resulting in incorrect corrective actions and 2) It ensures that $\mathbf{B}_t \approx \mathbf{A_g}$ within a prescribed tolerance. If this criterion is met ($\varepsilon_m^* < \varepsilon_a$) $\mathbf{A}_\mathbf{b}^*$ is implemented and I_t is set to one, indicating that $\mathbf{B}_t$ has been activated.

Through the process of B Cell activation T_h Cells govern the process of B Cell decay and ultimate death. This is an essential requirement of the proposed approach, as the system resources and efficiency will significantly degrade if the B Cell population is not kept in check. Define N_p as the maximum allowable B Cell population. At each time T, if $T > N_p$ remove $\mathbf{B}_\zeta$, where $\zeta = \min_t \langle t | I_t = 0 \rangle$ and $t = 1, \cdots, T$ from the decision tree. In addition set all $\mathbf{B}_{t-1} = \mathbf{B}_t$, where $\zeta < t \leq T$, followed by setting $T = T - 1$. Here it is assumed that there will always be B Cells that

have never been activated. A flowchart outlining the entire process of adding B Cells to the B Cell pool is given in Figure 2.8.

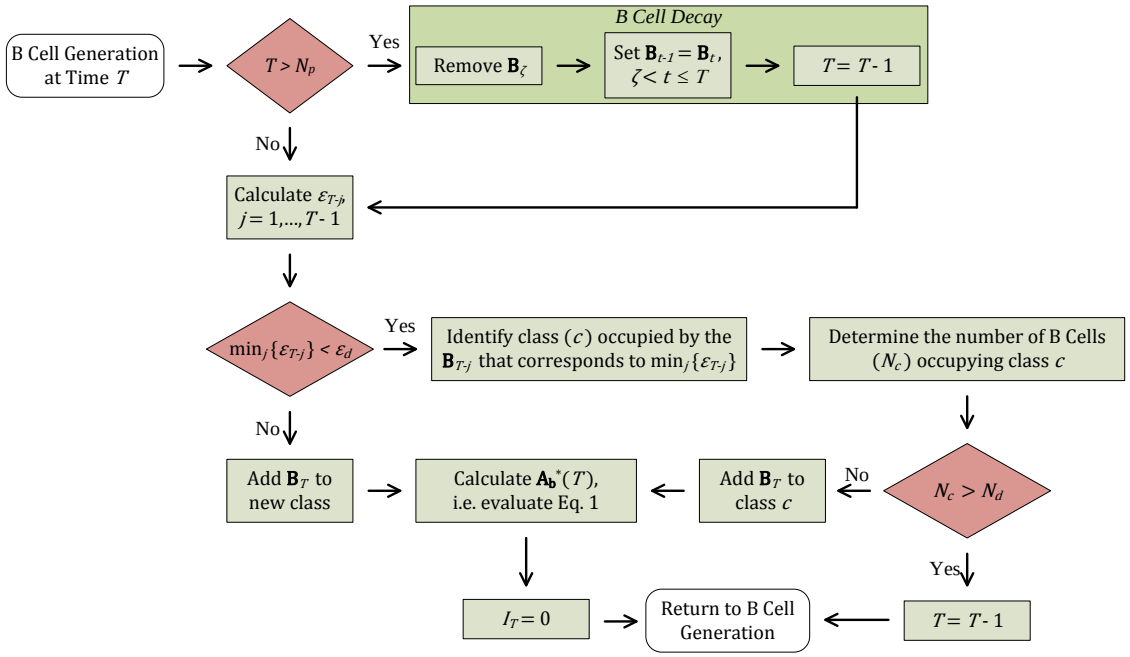

Figure 2.8: Flowchart Outlining the Process of Adding a B Cell to the B Cell Pool.

2.3.8. Class-Switching

In addition to governing the activation and decay of B Cells, T_h Cells also control the process of class-switching. Performing class switching in a compliant assembly system requires the generation of new antibodies or corrective actions for an activated B Cell. If the criterion of $\varepsilon_a < \varepsilon_d$ is met by $\mathbf{B}_t$ and the current $\mathbf{A_g}$, Eq. (2.1) is re-evaluating for $\mathbf{B}_t$. As previously discussed, the initial solution to Eq. (2.1) was implemented using a subset of the actual design space, $\mathbf{g}^*(\cdot,\cdot)$. A new antibody for $\mathbf{B}_t$ can therefore be designed by choosing a different subset of the actual design space. To perform class-switching, define N_c as the number of new antibodies to be generated for $\mathbf{B}_t$. When $\mathbf{B}_t$ is activated, obtain N_c new subsets $(\mathbf{g}_1^*(\cdot,\cdot), \cdots, \mathbf{g}_{N_c}^*(\cdot,\cdot))$ of the original design space. For each $\mathbf{g}_i^*(\cdot,\cdot)$, $i = 1, \cdots, N_c$, re-evaluate Eq. (2.1) to obtain candidate values $\widetilde{\mathbf{A}}_{\mathbf{b}_i}^*(t)$ and $\tilde{\mathbf{y}}_i^*(t)$. Finally set $\mathbf{A}_\mathbf{b}^*(t) = \langle \widetilde{\mathbf{A}}_{\mathbf{b}_i}^*(t) \big| \tilde{\mathbf{y}}_i^*(t) = \min_i \tilde{\mathbf{y}}_i^*(t) \text{ and } \tilde{\mathbf{y}}_i^*(t) < \boldsymbol{y}^*(t) \rangle$.

The reasoning behind implementing class-switching in a self-correcting compliant assembly system is based on the fact that the solution to Eq. (2.1) is not guaranteed to produce a global optimal. It would be possible to use exhaustive search routines to try to obtain a global optimum, however a relatively complex assembly system would make this extremely challenging. With this in mind, it would be highly inefficient to perform exhaustive searches when it is possible that some $\mathbf{A}_\mathbf{b}^*$ may never be applied. In addition these exhaustive searches would slow the process B Cell production, which would result in a loss of overall immunity. The result of implementing class-switching is that the more often a specific antigen is encountered the stronger the antibody becomes that fights it. A flowchart outlining the entire process for activating a B Cell is given in Figure 2.9.

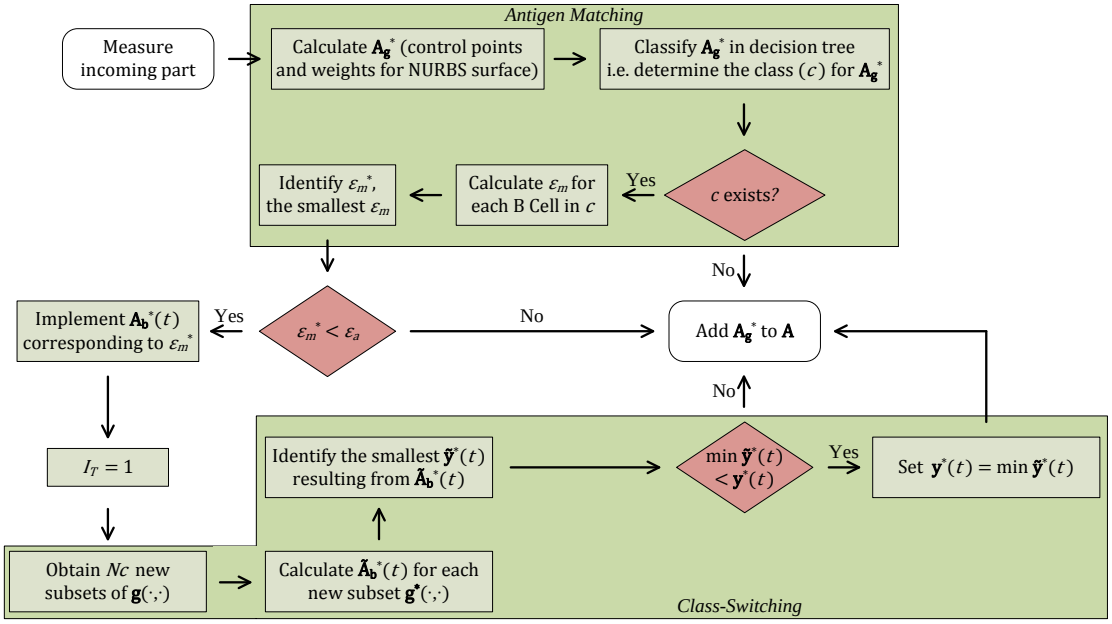

Figure 2.9: Flowchart Outlining the Process of B Cell Activation.

2.4. Conclusions

This paper presents an approach for implementing adaptive immunity into a compliant assembly system. The proposed approach emulates two key immunological tools, namely B and T_h Cells by incorporating advancing data mining methods, physical models, assembly modeling techniques, sensor capabilities, and actuator networks, which results in a system capable of part-by-part error-compensation. This is owed to the fact that the computation burden of the immune system remains separate from the actual assembly system. This separation allows for immunity to be continually developed and refined over time without affecting the assembly system's efficiency.

2.5. References

Ceglarek, D. and Shi, J. (1995), "Dimensional Variation Reduction for Automotive Body Assembly," *Journal of Manufacturing Review*, 8:2, 139-154.

Ceglarek, D., Shi, J., and Wu, S.M. (1994), "A Knowledge-Based Diagnostic Approach for the Launch of the Auto-Body Assembly Process," *Journal of Engineering for Industry*, 116:491–499.

Coker, S.A. and Shin, Y.C. (1996), "In-Process Control of Surface Roughness Due to Tool Wear Using a New Ultrasonic System". *International Journal of Machine Tools and Manufacture*, 36:3, 411-422.

Cox, M.G. (1972), "The Numerical Evaluation of B-Splines," *Journal of the Institute of Mathematics and its Applications*, 15, 99-108.

de Boor, C. (1972), "On Calculating with B-Spline," *Journal of Approximation Theory*, 6, 52-60.

Diaz, M. and Casali, P. (2002), Somatic Immunoglobulin Hypermutation, *Current Opinions in Immunology*, 14:2, 235–240.

Djurdjanovic, D. and Ni, J. (2007), "Online Stochastic Control of Dimensional Quality in Multistation Manufacturing Systems," *Proceedings of the Institution of Mechanical Engineers, Part B: Journal of Engineering Manufacture*, 221:5, 865-880.

Hu, S.J. and Camelio, J. (2006), "Modeling and Control of Compliant Assembly Systems," CIRP Annals - Manufacturing Technology, 55:1, 19-22.

Hu, S.J., Webbink, R., Lee, Y., and Long, Y. (2003), "Robustness Evaluation for Compliant Assembly Systems," *ASME Journal of Mechanical Design*, 125, 262-267.

Izquierdo, L.E., Shi, S., Hu, S.J., and Wampler, C.W. (2007), "Feedforward Control of Multistage Assembly Processes Using Programmable Tooling," *Transactions of NAMRI/SME*, 35, 295-302.

Jin, J. and Ding, H. (2004), "Online Automatic Process Control Using Observable Noise Factors for Discrete-Part Manufacturing," *IIE Transactions*, 36:9, 899-911.

Johnson, D.E. (1998), Applied Multivariate Methods for Data Analysts, Pacific Grove, CA, Duxbury Press.

Koch, K.R. (2009), "Identity of Simultaneous Estimates of Control Points and of Their Estimates by the Lofting Method for NURBS Surface Fitting," *International Journal of Advanced Manufacturing Technology*, 44, 1175-1180.

Koren, Y. (1988). "Adaptive Control Systems for Machining," IEEE American Control Conference, 1161-1167.

Kruth, J.-P. and Kerstens, A. (1997), "Reverse Engineering Modelling of Free-Form Surfaces From Point Clouds Subject to Boundary Conditions," *Journal of Materials Processing Technology*, 76, 120-127.

Lee, K. (1999), Principles of CAD/CAM/CAE Systems, Addison-Wesley.

Mantripragada, R. and Whitney, D.E. (1999), "Modelling and Controlling Variation Propagation in Mechanical Assemblies Using State Transition Models," *IEEE Transactions on Robotics and Automation*, 115, 124-140.

Market, E. and Papavasiliou, F.N. (2003), "V(D)J Recombination and the Evolution of the Adaptive Immune System," *Public Library of Science Biology*, 1:1, 24-27.

Mian, I., Bradwell, A., and Olson, A. (1991), "Structure, Function and Properties of Antibody Binding Sites," *Journal of Molecular Biology*, 217:1, 133–151.

Montgomery, D.C. (2008), Introduction to Statistical Quality Control, Sixth Edition, Hoboken, NJ: Wiley.

Stanley, J. (2002), Essentials of Immunology and Serology, Albany, NY: Thomson Delmar Learning.

Utgoff, P.E. (1994), "An Improved Algorithm for Incremental Induction of Decision Trees," *Proceedings of the Eleventh International Conference on Machine Learning*, 318-325.

Wang, H. and Huang, Q. (2007), "Using Error Equivalence Concept to Automatically Adjust Discrete Manufacturing Processes for Dimensional Variation Reduction," *Transactions-ASME Journal of Manufacturing Science and Engineering*, 129:3, 644-652.

Wells, L.J., Camelio, J.A., and Zapata, G. (2011), "A Bio-Inspired Framework for a Self-Healing Assembly System," *ASME Conference Proceedings*, DOI:10.1115/MSEC2011-50267.

Wells, L.J., Megahed, F.M., Camelio, J.A., and Woodall, W.H. (2012a), "A Framework for Variation Visualization and Understanding in Complex Manufacturing Systems," *Journal of Intelligent Manufacturing*, 23:5, 2025-2036.

Wells, L.J., Megahed, F.M., Niziolek, C.N., Camelio, J.A., and Woodall, W.H. (2012b), "Statistical Process Monitoring Approach for High-Density Point Clouds," *Journal of Intelligent Manufacturing*, 1-13.

Wise, J.D. and Gordon, C.R. (2002), Immunology: A Comprehensive Review, Iowa State University Press.

Xie, K., Izquierdo, L., and Camelio, J.A. (2012), "Part-by-Part Dimensional Error Compensation in Compliant Sheet Metal Assembly Process," *Journal of Manufacturing Systems*, 31:2, 152-161.

Xie, K., Wells, L.J., Camelio, J.A., and Youn, B.D. (2007), "Variation Propagation Analysis on Compliant Assemblies Considering Contact Interaction," *Journal of Manufacturing Science and Engineering*, 129:5, 934-942.

Zhou, L., Wang, H., Berry, C., Weng, X., and Hu, S. (2012), "Functional Morphing in Multistage Manufacturing and Its Applications in High-Definition Metrology-Based Process Control," *Automation Science and Engineering, IEEE Transactions on*, 9:1, 124-136.

Zhong, J., Liu, J., and Shi, J. (2010), "Predictive Control Considering Model Uncertainty for Variation Reduction in Multistage Assembly Processes. *Automation Science and Engineering, IEEE Transactions on*, 7:4, 724-735.

3. Statistical Process Control for Point Clouds using NURBS Surfaces

Statistical process control (SPC) methods have been extensively applied to monitor manufacturing processes to quickly detect and correct out-of-control conditions. The success of SPC tools in detecting process shifts can be primarily attributed to control charts, which were originally developed in the 1920s. As sensor and measurement technologies advance, there is a continual need to adapt and develop new SPC techniques to effectively and efficiently take advantage of these new data-sets. For instance, advanced multivariate and profile monitoring techniques have been developed to account for the increased dimensional data collected from coordinate measuring machines. Currently high-density dimensional (HDD) measurement technologies, such as 3D laser scanners, are being implemented in industry to rapidly collect point clouds consisting of millions of data points to represent an entire manufactured parts' surface. This gives HDD measurements a significant advantage over competing technologies that typically provide tens or hundreds of data points. Consequently, HDD data-sets have the potential to detect unexpected faults, i.e., faults that are not captured by measuring a small number of predefined dimensions of interest. However, in order for this potential to be realized SPC methods capable of handling these data-sets need to be developed. Therefore, this paper presents an approach to performing SPC using high-density point clouds. The proposed approach is based on transforming the high-dimensional point clouds into non-uniform rational basis spline (NURBS) surfaces. The control parameters for these NURBS surfaces will then be monitored using a surface monitoring technique. In this paper point clouds are simulated to determine the performance of the proposed approach under varying fault scenarios.

3.1. Literature Review

Currently, the primary use of HDD data in statistical process control (SPC) relies on performing traditional control charting techniques for extracted feature parameters, which is not an approach specific to HDD data. However, the use of HDD data for SPC can be considered as a form of profile monitoring, which focuses on the relationship between a response and one or more independent/explanatory (location) variables. In this case, instead of observing a single measurement on each product, the practitioner observes "a set of values over a range, when plotted, takes the shape of a curve" (Montgomery, 2008). As noted by Woodall et al. (2004), profiles are often better suited to characterize current manufacturing operations when compared to more traditional SPC techniques; especially for data-intensive processes (Wang and Tsung, 2005), such as those collected by HDD measurement devices.

According to Colosimo et al. (2010) a natural extension of profile monitoring is surface monitoring. In addition, Woodall (2007) suggested that the monitoring of product shapes is a very promising area for profile monitoring research since the shape of manufactured items is usually an important aspect of quality.

While the area of surface monitoring using HDD data is still in its infancy, a few methods have been proposed in the literature. Colosimo et al. (2010) suggested monitoring surfaces through the use of spatial autoregressive regressive models. Their work monitored the turning of simple shapes with CMM data on the order of thousands of measurements per part. Zhou et al. (2012) demonstrated how to monitor a multistage manufacturing process using HDD data and multivariate control charts. Here principal component analysis (PCA) was used to reduce the dimensionality of the data. Wells et al. (2012) proposed a linear profile technique to monitor point clouds through the implementation of Q-Q plots. However, through the act of transforming point

clouds into quantiles, their work loses important spatial data regarding the location of a shift which may delay detection of small sized shifts (here size refers to the amount of physical surface area covered by a fault).

Megahed et al. (2012) suggested a spatiotemporal control charting technique for rapid fault detection in grayscale images. While not specifically being a HDD data problem, the general concept developed by Megahed et al. (2012) could be extended to 3D data. Specifically, images are subtracted from a nominal images allowing for the problem to be generalized towards monitoring deviations from nominal. This generic approach can therefore be extended to 3D data as nominal computer-aided design (CAD) models typically exist for all manufactured products. The basic premise of Megahed et al. (2012) is to identify the regions of interest (ROIs) that maximizes the generalized likelihood ratio (GLR) using current and previous images. If the maximum GLR statistic exceeds a specific control limit the chart signals, and an estimate of the location, size, and change-point of the shift is obtained.

3.2. Proposed Method for Monitoring High-Density Dimensional Data

This section proposes a Phase II SPC method for monitoring HDD data. The statistical bases for this method are described over the next three subsections. First, the rationale behind using NURBS surfaces for the problem of interest is discussed. The second subsection covers the mathematical derivation of the parameters form the NURBS surfaces that will be monitored. The third subsection discusses how these parameters will be monitored for SPC and provides several methods for control chart parameterization.

3.2.1. Rationale for using NURBS Surfaces

The proposed approach for performing SPC on HDD data is an extension of parametric profile monitoring techniques to surfaces. Specifically, this approach estimates 3D point clouds as

NURBS surfaces, where the resulting control points are monitored. The main reason behind the use of NURBS surfaces is their well-known local modification property (Lee, 1999; Kruth and Kerstens, 1997). This property is important in curve design because a curve can be modified locally without changing its global shape. However, if NURBS are estimated from point clouds, the local modification property operates in reverse; basically, local shifts in the point cloud will significantly perturb nearby control points. Therefore, in-control surfaces will result in a definable in-control multivariate distribution of control points. An out-of-control surface, either due to a local or global shift, will then result in a shift in the control point distribution.

Furthermore, given a constant set of B-Spline functions, weights, and scan densities used for the NURBS approximation; control points for each surface observation will reflect the same region of the surface. This will allow for localized part-to-part variation to be understood and will aid in visual shift diagnosis. It must be stressed that detecting a process shift is only the first step in ensuring part quality. Once a shift is detected, it must be eliminated; therefore SPC approached that also provide diagnostic information are invaluable.

3.2.2. Phase II Monitoring Parameters for NURBS Surfaces

Consider an HDD data-set ($\mathbf{S}(\bar{u}_o, \bar{v}_d), o \in 1, \dots, r$ and $d \in 1, \dots, e$) consisting of an r x e grid of points obtained from a HDD measurement device. According to Koch (2009), if the B-Spline functions and the weights are predefined, then the control points for a NURBS surface that best represents the r x e grid of points can be directly calculated through a multivariate linear model (lofting method). For this estimation the mathematical representation of a NURBS surface can be written using homogenous coordinates as

$$\mathbf{B}^w(u,v) = \sum_{i=1}^{n_u} \sum_{j=1}^{n_v} B_{u,i}(u) \cdot B_{v,j}(v) \cdot \mathbf{p}_{i,j}^w, \tag{3.1}$$

where $\mathbf{B}^w$ is the surface, $\mathbf{B}^w(u,v)$ are homogenous coordinates for the surface at location (u,v), n_u and n_v are the number of control points in the u and v directions, $B_{u,i}(u)$ and $B_{v,j}(v)$ are B-Spline functions in the u and v directions, respectively, and $\mathbf{p}_{i,j}^w = \left[w_{i,j}x_{i,j},\ w_{i,j}y_{i,j},\ w_{i,j}z_{i,j},\ w_{i,j}\right]^{\mathrm{T}}$ is the weighted control point vector. It should be noted that the B-Spline functions are defined by the order of the defining curves' knot sequences. Please refer to Cox (1972) and de Boor (1972) for further details.

A NURBS model $\left(\mathbf{B}^w(u,v)\right)$ for the data-set $\mathbf{S}(\bar{u}_o,\bar{v}_d)$ can therefore be written as

$$\sum_{i=1}^{n_u}\sum_{j=1}^{n_v} B_{u,i}(\bar{u}_o)\cdot B_{v,j}(\bar{v}_d)\cdot \mathbf{p}_{i,j}^w = \mathbf{S}(\bar{u}_o,\bar{v}_d) + \mathbf{e}(\bar{u}_o,\bar{v}_d), \tag{3.2}$$

where $\mathbf{e}(\bar{u}_o,\bar{v}_d)$ is the error of the measured coordinates $\mathbf{S}(\bar{u}_o,\bar{v}_d)$. By defining the control points of the isoparametric curves $\mathbf{B}^w(u, v = \text{constant})$ as

$$\mathbf{f}_{i,d} = \sum_{\mathrm{j}=1}^{\mathrm{n_v}} B_{v,j}(\bar{v}_d)\cdot \mathbf{p}_{i,j}^w, \tag{3.3}$$

Eq. (3.2) becomes

$$\sum_{i=1}^{n_u} B_{u,i}(\bar{u}_o)\cdot \mathbf{f}_{i,d} = \mathbf{S}(\bar{u}_o,\bar{v}_d) + \mathbf{e}(\bar{u}_o,\bar{v}_d), \tag{3.4}$$

which can be expressed in matrix notation as

$$\mathbf{B}_u\mathbf{F}_u = \mathbf{S} + \mathbf{E}. \tag{3.5}$$

Here $\mathbf{B}_u$ is the matrix of B-Spline basis functions for the u direction,

$$\mathbf{B}_u = \begin{bmatrix} B_{u,1}(\bar{u}_1) & \cdots & B_{u,n_u}(\bar{u}_1) \\ \vdots & \ddots & \vdots \\ B_{u,1}(\bar{u}_r) & \cdots & B_{u,n_u}(\bar{u}_r) \end{bmatrix}, \tag{3.6}$$

$\mathbf{F}_u$ is the matrix of control points for the isoparametric curves,

$$\mathbf{F}_u = \begin{bmatrix} f_{1,1} & \cdots & f_{1,e} \\ \vdots & \ddots & \vdots \\ f_{n_u,1} & \cdots & f_{n_u,e} \end{bmatrix}, \tag{3.7}$$

S is the matrix of measured points,

$$\mathbf{S} = \begin{bmatrix} \mathbf{s}(\bar{u}_1, \bar{v}_1) & \cdots & \mathbf{s}(\bar{u}_1, \bar{v}_e) \\ \vdots & \ddots & \vdots \\ \mathbf{s}(\bar{u}_r, \bar{v}_1) & \cdots & \mathbf{s}(\bar{u}_r, \bar{v}_e) \end{bmatrix}, \tag{3.8}$$

and **E** is the matrix of errors,

$$\mathbf{E} = \begin{bmatrix} \mathbf{e}(\bar{u}_1, \bar{v}_1) & \cdots & \mathbf{e}(\bar{u}_1, \bar{v}_e) \\ \vdots & \ddots & \vdots \\ \mathbf{e}(\bar{u}_r, \bar{v}_1) & \cdots & \mathbf{e}(\bar{u}_r, \bar{v}_e) \end{bmatrix}. \tag{3.9}$$

From Eq. (3.5) the estimate for $\mathbf{F}_u$ can be calculated as

$$\hat{\mathbf{F}}_u = (\mathbf{B}_u^{\mathrm{T}}\mathbf{B}_u)^{-1}\mathbf{B}_u^{\mathrm{T}}\mathbf{S}. \tag{3.10}$$

Applying this estimate, Eq. (3.3) can be written in matrix form as

$$\mathbf{B}_v\mathbf{P}^{\mathrm{T}} = \hat{\mathbf{F}}_u^{\mathrm{T}} + \mathbf{G}, \tag{3.11}$$

where $\mathbf{B}_v$ is the matrix of B-Spline basis functions for the v direction,

$$\mathbf{B}_v = \begin{bmatrix} B_{v,1}(\bar{v}_1) & \cdots & B_{v,n_v}(\bar{v}_1) \\ \vdots & \ddots & \vdots \\ B_{v,1}(\bar{v}_e) & \cdots & B_{v,n_v}(\bar{v}_e) \end{bmatrix}, \tag{3.12}$$

P is the matrix of control points,

$$\mathbf{P} = \begin{bmatrix} \mathbf{p}_{1,1}^w & \cdots & \mathbf{p}_{1,n_v}^w \\ \vdots & \ddots & \vdots \\ \mathbf{p}_{n_u,1}^w & \cdots & \mathbf{p}_{n_u,n_v}^w \end{bmatrix}, \tag{3.13}$$

and **G** is the matrix of errors from the estimated control points $\hat{\mathbf{F}}_u$,

$$\mathbf{G} = \begin{bmatrix} \mathbf{g}(1,1) & \cdots & \mathbf{g}(n_u, 1) \\ \vdots & \ddots & \vdots \\ \mathbf{g}(1, e) & \cdots & \mathbf{g}(n_u, e) \end{bmatrix}. \tag{3.14}$$

From Eq. (3.11) the estimate for **P** can be calculated as

$$\hat{\mathbf{P}}^{\mathrm{T}} = (\mathbf{B}_v^{\mathrm{T}}\mathbf{B}_v)^{-1}\mathbf{B}_v^{\mathrm{T}}\hat{\mathbf{F}}_u^{\mathrm{T}}. \tag{3.15}$$

The proposed approach will focus on the use of the estimated control points, $\hat{\mathbf{P}}$, as the multivariate surface parameters being monitored in a Phase II control chart. However, it is well

known that multivariate monitoring techniques become impractical for high-dimensional systems (Bersimis et al., 2007), such as a $\widehat{\mathbf{P}}$. In response, this paper suggests performing a dimension reduction operation to efficiently monitor the control points. The proposed approach will use PCA for this dimension reduction. To avoid scaling issues occurring from the varying locations of the control points, $\widehat{\mathbf{P}}$ is replaced with $\widehat{\mathbf{P}}^{*} = \widehat{\mathbf{P}} - \widehat{\mathbf{P}}^{n}$, where $\widehat{\mathbf{P}}^{n}$ is the estimated control points for the nominal geometry being monitored. This PCA will use the historical in-control data-set $\mathbf{X}$,

$$\mathbf{X} = [\mathbf{x}_1, \dots, \mathbf{x}_m], \tag{3.16}$$

where $\mathbf{x}_t = \left[\widehat{\mathbf{p}}_{:,1}^{w^*}, \dots, \widehat{\mathbf{p}}_{:,n_v}^{w^*}\right]^{\mathrm{T}}$ and $\widehat{\mathbf{p}}_{:,j}^{w^*} = \left[\widehat{\mathbf{p}}_{1,j}^{w^*}, \cdots, \widehat{\mathbf{p}}_{n_u,j}^{w^*}\right]$ for the t^{th} observation of

$$\widehat{\mathbf{P}} = \begin{bmatrix} \widehat{\mathbf{p}}_{1,1}^{w^*} & \cdots & \widehat{\mathbf{p}}_{1,n_v}^{w^*} \\ \vdots & \ddots & \vdots \\ \widehat{\mathbf{p}}_{n_u,1}^{w^*} & \cdots & \widehat{\mathbf{p}}_{n_u,n_v}^{w^*} \end{bmatrix}, \tag{3.17}$$

where $\widehat{\mathbf{p}}_{:,:}^{w^*} = \widehat{\mathbf{p}}_{:,:}^{w} - \widehat{\mathbf{p}}_{:,:}^{n}$ and $\widehat{\mathbf{p}}_{:,:}^{n}$ is the estimated control point for the nominal surface geometry.

The first step of PCA is to calculate the sample covariance matrix ($\mathbf{S}$) of $\mathbf{X}$, followed by solving the eigenvalue decomposition:

$$\mathbf{S} = \mathbf{V}\mathbf{L}\mathbf{V}^{\mathrm{T}}, \tag{3.18}$$

where $\mathbf{L}$ is a diagonal matrix containing eigenvalues ($\lambda_1 \geq \cdots \geq \lambda_{3 \cdot n_u \cdot n_v} \geq 0$) and $\mathbf{V}$ is an orthonormal matrix whose columns are eigenvectors. In addition, the quantity

$$\Lambda_i = \frac{\lambda_i}{\lambda_1 + \lambda_2 + \cdots + \lambda_{3 \cdot n_u \cdot n_v}} \tag{3.19}$$

is the proportion of the variability of the original system that can be attributed to the i^{th} principal component. For the dimension reduction, only the first κ ($\kappa \leq 3 \cdot n_u \cdot n_v$) principal components which explain the majority of the system variance will be considered in the proposed monitoring scheme. For more details regarding PCA, the reader is referred to Johnson (1998) and Montgomery (2008).

Using Hotelling's T^2 statistic the i^{th} observed point cloud from the reduced principal component model can be obtained as

$$T_i^2 = \mathbf{z}_i^T \mathbf{L}_\kappa^{-1} \mathbf{z}_i, \tag{3.20}$$

where $\mathbf{z}_i = \mathbf{V}_\kappa^T [\mathbf{x}_i - \overline{\mathbf{X}}]$ and $\mathbf{L}_\kappa$ and $\mathbf{V}_\kappa$ are the eigenvalue and vector matrices containing the first κ PCs, respectively, and $\overline{\mathbf{X}}$ is the mean vector of $\mathbf{X}$.

In addition to obtaining the T^2 statistic, two residual terms for each point cloud observation is obtained. First the sum of squares of the residuals (Q Statistic) obtained from the reduced principal component will be used. The Q Statistic for the i^{th} observation of can be defined as

$$Q_i = (\mathbf{x}_i - \hat{\mathbf{x}}_i)^{\mathrm{T}} (\mathbf{x}_i - \hat{\mathbf{x}}_i), \tag{3.21}$$

where $\hat{\mathbf{x}}_i$ is the estimate of the original observation from the reduced principal component model,

$$\hat{\mathbf{x}}_i = (\overline{\mathbf{X}} + \mathbf{V}_\kappa \mathbf{z}_i). \tag{3.22}$$

The second residual term (R) is the sum or squares of the residuals form the model given in Eq. (3.5), which can be calculated as

$$\hat{\mathbf{E}} = \mathbf{B}_u \hat{\mathbf{P}} \mathbf{B}_v^{\mathrm{T}} - \mathbf{S}. \tag{3.23}$$

The R statistic for the i^{th} observed point cloud (i^{th} observation of $\mathbf{S}$ and $\hat{\mathbf{P}}$) can be calculated as

$$R_i = \sum_{j=1}^{3} \text{trace}\left(\hat{\mathbf{E}}_j^{\mathrm{T}} \hat{\mathbf{E}}_j\right). \tag{3.24}$$

It should be noted that it is not necessary for each observation to have an equal number of measurement points (i.e. the r x e grid can change size from observation to observation). However, if it is possible to constrain each observation to have consistent r x e data-sets the computational effort of the proposed method decreases significantly. Specifically, the terms $(\mathbf{B}_u^{\mathrm{T}} \mathbf{B}_u)^{-1} \mathbf{B}_u^{\mathrm{T}}$ and $(\mathbf{B}_v^T \mathbf{B}_v)^{-1} \mathbf{B}_v^{\mathrm{T}}$ from Eqs. (3.11) and (3.15) are constants and will not have to be calculated for each observation. In addition, regardless of the r x e grid size, $\mathbf{L}_\kappa^{-1}$ (from Eq. (3.20)) will always be a

constant. It should be noted that if the r x e grid size changes from observation to observation Eq. (3.24) should be adjusted to reflect varying data-set sizes.

3.2.3. Phase II Monitoring Approach using NURBS Surface Representations

Once the NURBS surface's monitoring parameters are estimated, their use in the monitoring of Phase II data must be defined. Choosing an adequate monitoring strategy depends on the parameters that have been selected for monitoring and the type of control chart used to monitor each of these parameters. In this paper, simultaneous one-sided EWMA control charts are used to monitor different combinations (monitoring schemes) of statistics based on the NURBS surface estimations, which are summarized in Table 3.1. The reader should note that the general formulation for each of the EWMA control charts used in these cases is given by

$$E_i = rS + (1-r)E_{i-1}$$
$$CL = \mu + k\sigma\sqrt{\frac{r}{2-r}}, \tag{3.25}$$

where E_i is the EWMA statistic for the i^{th} observation, S is the value of the parameter being monitored (i.e. Hotelling's T^2 statistic (T_i^2), Q statistic (Q_i), or the model residuals (R_i)) at observation i, and r is the EWMA smoothing parameter (set at 0.2 in this paper, a typical value). In addition, CL is the one-sided upper control limit for a given EWMA chart, k is an EWMA design parameter, and μ and σ are the in-control mean and standard deviation of the statistic under consideration, respectively. Here, the control chart will signal if its EWMA statistic falls outside its respective control limits. Furthermore, E_0 is taken as zero for all charts.

Table 3.1: Control Charting Schemes.

Scheme	Hotelling's T^2 Statistic	Q statistic	Model residuals (R)
Scheme 1	✓		
Scheme 2	✓	✓	
Scheme 3	✓	✓	✓

EWMA control charts were selected since they have proven to be a simple, yet highly effective method in profile monitoring (Kim et al., 2003; Wang and Tsung, 2005; Mahmoud et al., 2010), of which this research is an extension of. It should be noted that increasing the number of simultaneously monitored parameters (i.e. the number of control charts) does not necessarily lead to an improved quality performance. Increasing the number of charts can result in more false alarms when the process is in-control, while not improving the fault detection capability when the process becomes out-of-control (Montgomery, 2008). The performance of different Phase II control charting procedures is typically evaluated through the use of the average run length (ARL) metric, which is defined as the average number of samples (i.e. scanned part point clouds) taken until a control chart (or group of simultaneous control charts) signals.

3.3. Performance Assessment of Proposed SPC Approach

To determine the performances of the control charting schemes using the proposed SPC approach, points clouds obtained from an HDD measurement device were simulated. The following five subsections describes this simulation study. The first subsection describes the manufactured part under consideration and how the in-control historical point clouds for this part were generated. The second subsection described the implementation of the proposed SPC approach outlined in Section 3.2.2. The third subsection focuses on how the control charting schemes outlined in Table 3.1 are implemented for varying out-of-control conditions. The fourth subsection discusses the results of these simulations via a comparison of the performance of the difference control charting schemes. In the fifth subsection an alternative approach to the proposed monitoring approach is discussed, and its performance is compared with the original SPC approach.

3.3.1. Description of Simulation Study

This simulation study considers the sheet metal bracket illustrated in Figure 3.1a, whose nominal dimensions are listed in Table 3.2. All observations of this sheet metal bracket are generated as a NURBS surface using 756 ($n_u = 36, n_v = 21$) control points, whose locations are identified in Figure 3.1b as black circles. The order for the u and v directions, k_u and k_v, are both set to 4 (cubic curves) and non-periodic knot vectors were used to determine $B_{u,i}(u)$ and $B_{v,j}(v)$. It should be noted that this geometry is significantly over-defined with this large number of control points. This is intentional as it allows for a variety of errors to be added to the geometry by simply perturbing control point locations.

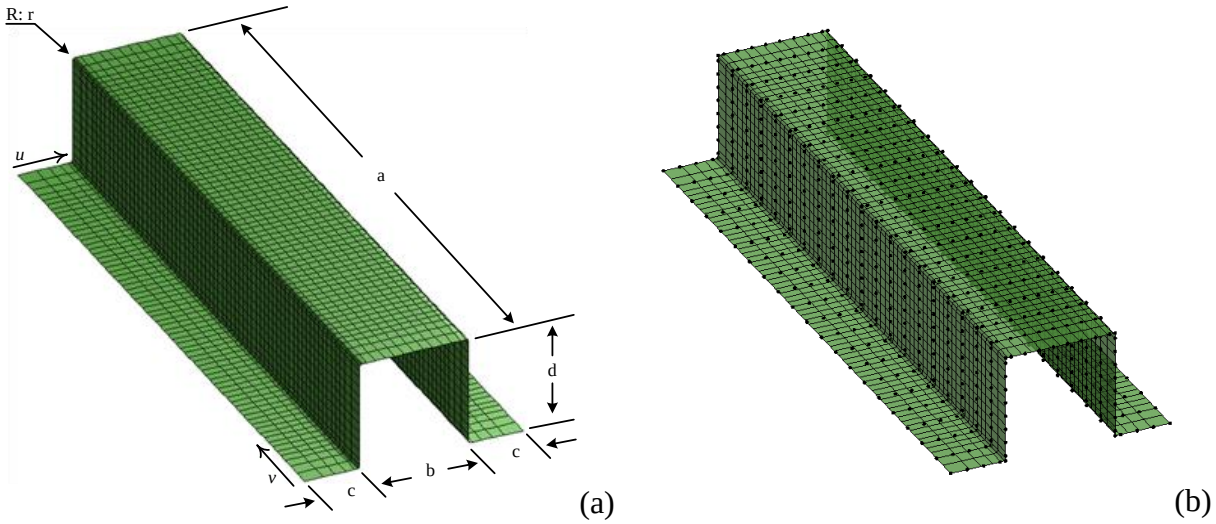

Figure 3.1: Nominal Sheet Metal Bracket a) used for Simulation Case Study and b) with Locations of Control Points.

Table 3.2: Nominal Part Dimensions (mm).

a	b	c	d	r
285.75	50.8	25.4	50.8	1

Each in-control sheet metal bracket is simulated to have three inherent deformation patterns;

Deformation Pattern 1: Earing Along the Edges.

Deformation Pattern 2: Wavy Surface

Deformation Pattern 3: Bend Error in the Left Flange (as Viewed in Figure 3.1).

Deformation pattern 1 affects only the control points that define edges. For each of these control points, the directional components that are normal to its respective edge and in the *u*-*v* plane are independent normal distributions with mean zero and standard deviation of 0.005 mm. A NURBS surface generated with only deformation pattern 1 is illustrated in Figure 3.2a. An exaggerated version of this deformation pattern is also given in Figure 3.2b.

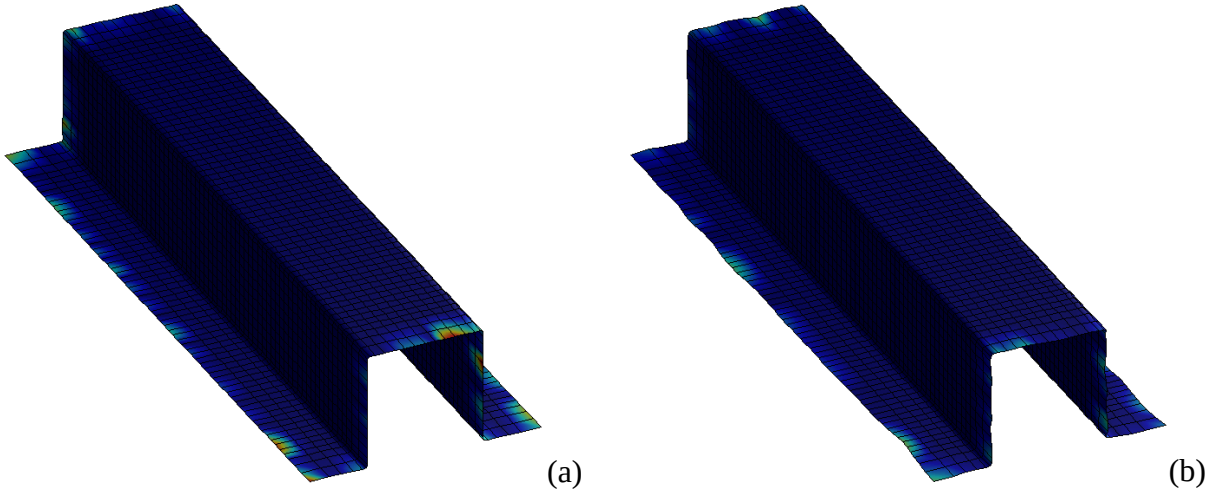

(a) (b)

Figure 3.2: Generated Observation of Deformation Pattern 1: a) Actual and b) Exaggerated.

Deformation pattern 2 affects all of the control points in the model, except those affected by deformation pattern 3 (discussed in next paragraph). For each of these control points, the directional components that are normal to the NURBS surface follow independent normal distribution with mean zero and standard deviation of 0.005 mm. A NURBS surface generated with only deformation pattern 2 is illustrated in Figure 3.2a. An exaggerated version of this deformation pattern is also given in Figure 3.3b.

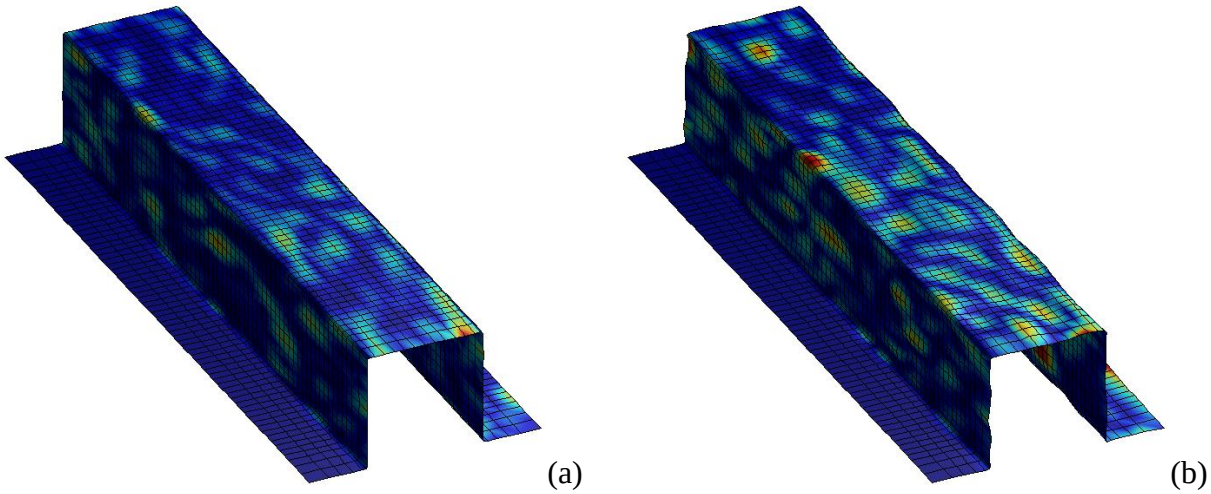

(a) (b)

Figure 3.3: Generated Observation of Deformation Pattern 2: a) Actual and b) Exaggerated.

Deformation pattern 3 affects only the control points that define the left flange of the bracket. For these control points, the directional components that are normal to the NURBS surface, referred to as *N*, follow a multivariate normal distribution with a zero mean vector. From left to right the *N* variables in the first row (u=constant) have a standard deviation of 0.05 mm, the second row have a standard deviation of 0.035 mm, the third row have a standard deviation of 0.02 mm, and for the fourth and final row have a standard deviation of 0.005 mm. The correlation coefficient for pairs of *N* variables that are on the same row is 1, and all other pairs of *N* variables have a correlation coefficient of 0.9. A NURBS surface generated with only deformation pattern 3 is illustrated in Figure 3.4a. An exaggerated version of this deformation pattern is also given in Figure 3.4b.

Each in-control part in generated to include all three deformation patterns. An example of such an observation is illustrated in Figure 3.5a. An exaggerated version of all deformation patterns is also given in Figure 3.5b. For each observed NURBS surface, a point cloud (**S**) containing 3366 measurements is obtained by evaluating theses NURBS surfaces as a 51 x 66 ($r = 51, e = 66$) grid of uniformly spaced sample points.

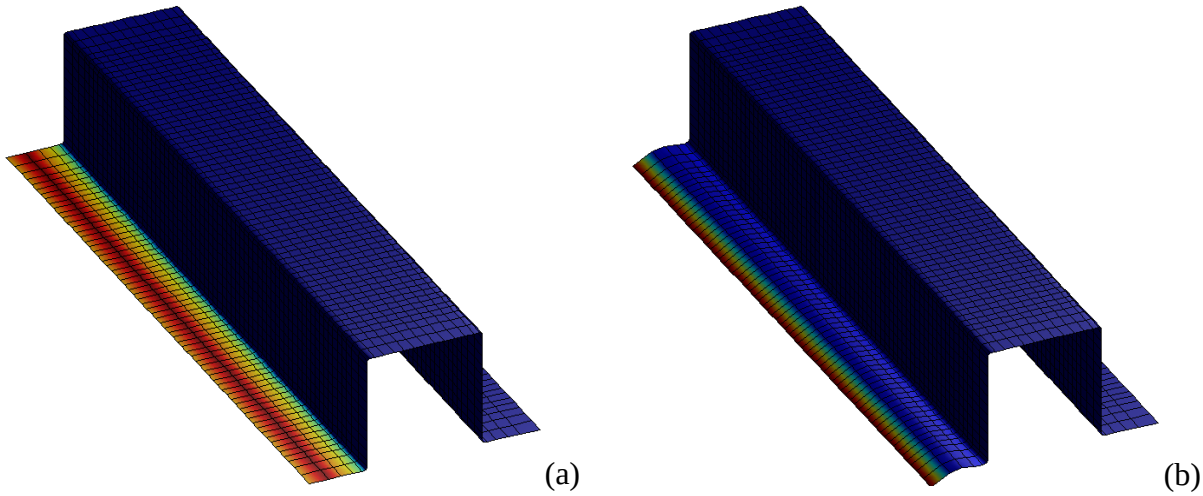

(a) (b)

Figure 3.4: Generated Observation of Deformation Pattern 3: a) Actual and b) Exaggerated.

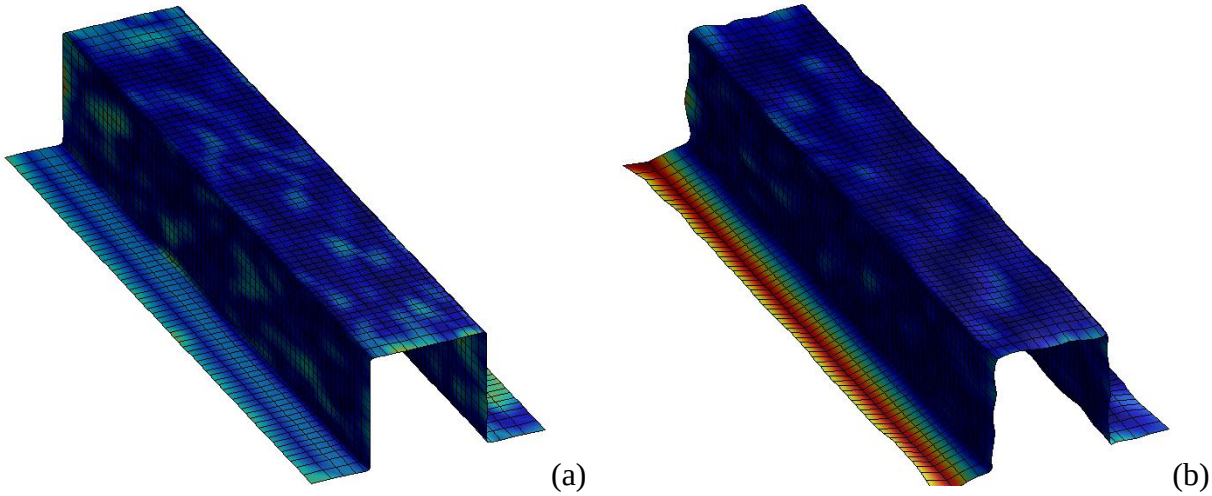

(a) (b)

Figure 3.5: Generated Observation of All Deformation Patterns: a) Actual and b) Exaggerated.

3.3.2. Implementation of Proposed SPC Approach

For this case study, two approaches in the implementation of the proposed SPC approach are considered; 1) Monitoring a NURBS surface that is over-defined (i.e. the estimated NURBS surface contains more control points than necessary to represent the nominal geometry) and 2) Monitoring a NURBS surface that is under-defined (i.e. the estimated NURBS surface contains fewer control points than necessary to represent the nominal geometry). The reason over-defined NURBS surface estimators are considered is the fact that they have additional "freedom" to accurately represent non-nominal surfaces, i.e. surfaces with shifts. This ability will significantly

aid in shift detection. Unfortunately, due to complex geometries, the use of over-defined NURBS surface estimators may result large dimension problems. In this scenario, the use of under-defined NURBS surfaces may be used instead, which is the reason for including them in this performance study.

For the over-defined case (Case 1), NURBS surfaces are estimated from each observation of **S** using 496 ($n_u = 31, n_v = 16$) control points. Similarly the under-defined case (Case 2) uses 66 ($n_u = 11, n_v = 5$) control points. The resulting NURBS surfaces and their control points (black circles) estimated from the nominal part geometry for the over-defined and under-defined cases are illustrated in Figure 3.6a and Figure 3.6b, respectively.

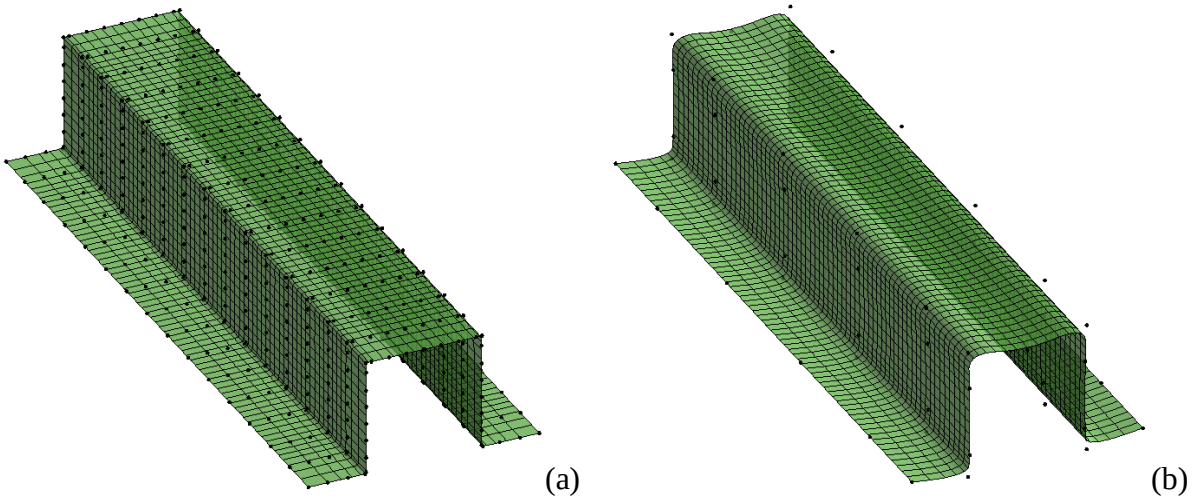

(a) (b)

Figure 3.6: NURBS Surfaces and their Control Points (Black Spheres) Estimated from the Nominal Part Geometry for the (a) Over-Defined and (b) Under-Defined Cases.

In order to obtain the mean and standard deviations (required by Eq. (3.25)) of the parameters to be monitored (T^2, Q, and R), 10,000 historical in-control observations of **S** were generated. The mean and standard deviation of R can be directly calculated from the historical observations, while the means and standard deviations of T^2 and Q require the development of principal component models. The historical observations were also used to generate the historical control point data-sets (Eq. (3.16)) required for the PCA for both Cases 1 and 2. From the PCA, the first three and

first principal components were identified as significant for Cases 1 and 2, respectively. The SCREE plots used to make these decisions for Case 1 and 2 are given in Figure 3.7a and Figure 3.7b, respectively. Using these reduced principal component models, the means and standard deviations for T^2 and Q were determined, and are given in Table 3.3.

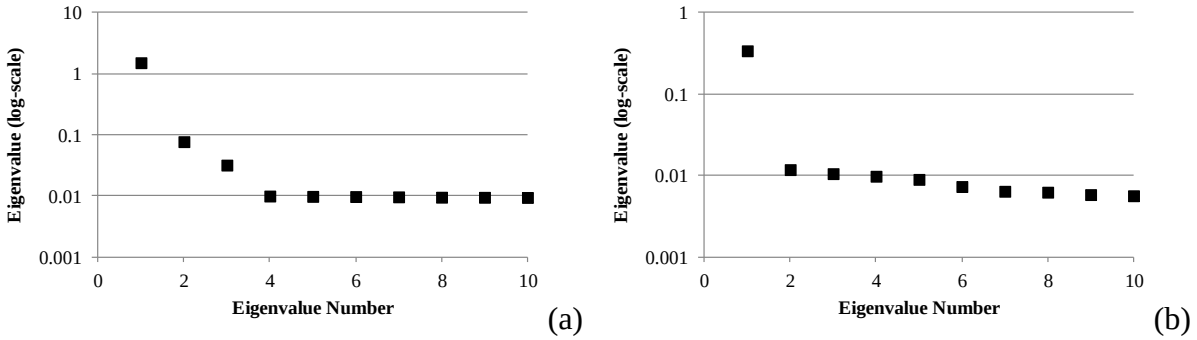

Figure 3.7 SCREE Plots from PCA for Cases (a) 1 and (b) 2.

Table 3.3: Mean and Standard Deviation of Monitored Statistics for Cases 1 and 2.

	T^2		Q		R	
	μ	σ	μ	σ	μ	σ
Case 1	3.0000	2.4601	2.7248	0.17310	86.942	0.22040
Case 2	0.99990	1.4114	0.22336	0.043756	4918.8	17.970

To complete the designs for the control charting schemes (Table 3.1) for Cases 1 and 2, required determining the EWMA parameters k for each statistic in each scheme. The control charts used in this paper are all designed to have an in-control ARL (ARL_0) of approximately 250, which allows for the control charts' out-of-control performances to be directly comparable. Simulations of the EWMA statistics are used to determine the correct k values for each control charting scheme. It must be noted for simultaneous control charts, k values are initially determined assuming independent control charts and are then refined to obtain correct values for simultaneous charting. This approach is quite common for simulation based ARL_0 calculations (e.g. Wells et al., 2012; Ryan et al., 2011). The simulations used to calculate k values and all subsequent ARL simulations

are performed using 1,000 replications. Table 3.4 provides the k values and their resulting ARL_0 values from simulations.

Table 3.4: EWMA Design Parameters (k) Simulated to Obtain an In-Control ARL of 250.

	Case 1			Case 2		
	Scheme 1	Scheme 2	Scheme 3	Scheme 1	Scheme 2	Scheme 3
k_{T^2}	1.9530	2.3022	2.4986	2.3043	2.7671	3.0313
k_Q		1.8231	2.0235		1.9581	2.0099
k_R			1.8452			2.0510
ARL_0	249.10	249.68	249.99	252.02	249.97	249.96

3.3.3. Performance for Out-of-Control Conditions

The performance of the proposed SPC approach is analyzed for its ability to detect stationary "dent" like shifts in the bracket's surface. For these shifts, a control point used to define the original geometry is shifted in the normal direction of the surface. In this analysis three shift locations are considered; Shift Location 1: The right flange located extremely close to a nominal control point for Case 1 and significantly far from any nominal control point for Case 2, Shift Location 2: The top of the bracket located significantly far from any nominal control point for either Cases 1 or 2, and Shift Location 3: The left flange located significantly far from any nominal control point for either Cases 1 or 2. These three shift locations are illustrated in Figure 3.8.

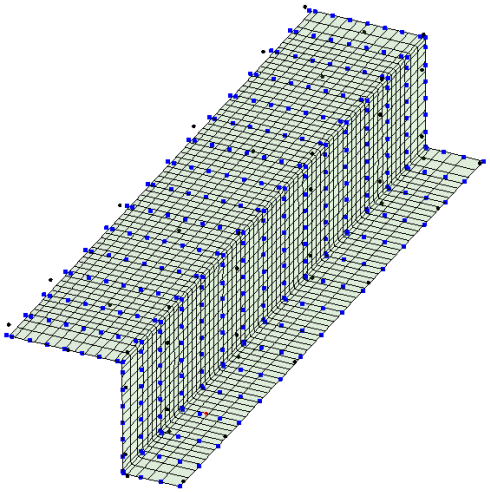

(a)

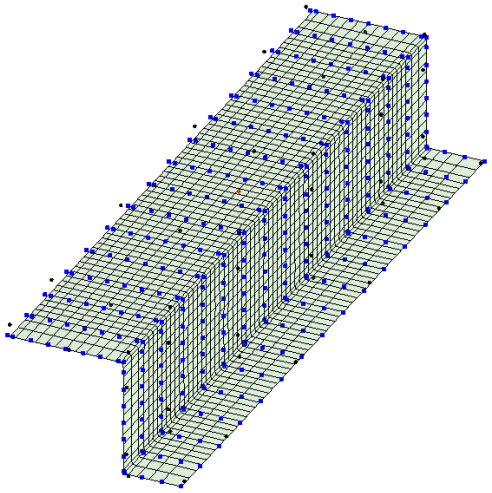

(b)

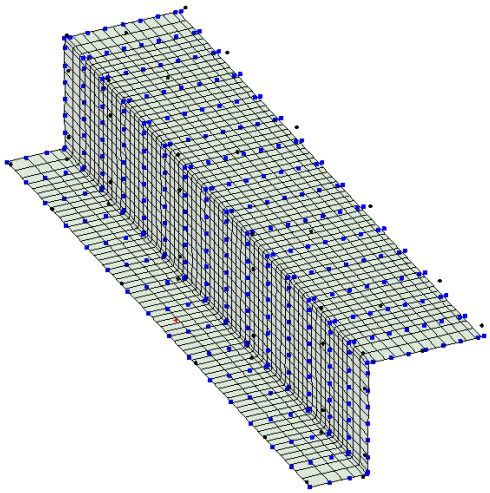

(c)

Figure 3.8: Shift Locations, Identified as Red Asterisks with the Nominal Control Point Estimates for Cases 1 and 2 Given as Blue Squares and Black Circles, Respectively for Shifts (a) 1, (b) 2, and (c) 3.

For every shift location, six magnitudes (δ=5, 2, 1, 0.5, 0.25, 0.1 mm) of the shift are considered. Observations of these shifts have been illustrated for Shift Location 3 in Figure 3.9. It must be noted that due to the nature of NURBS surfaces, control point shift magnitudes to not directly equate to the size of the surface shift. The actual maximum surface deviations caused by the considered shift magnitudes on the nominal surface are given in Table 3.5. As can be seen the maximum deviation cause by these shifts are significantly less than the shift itself.

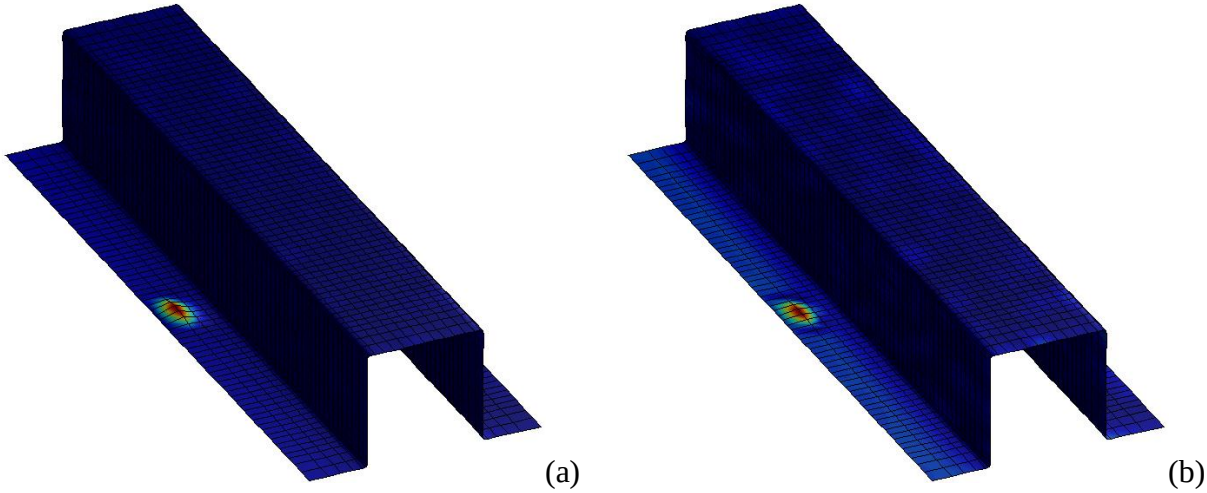

(a) (b)

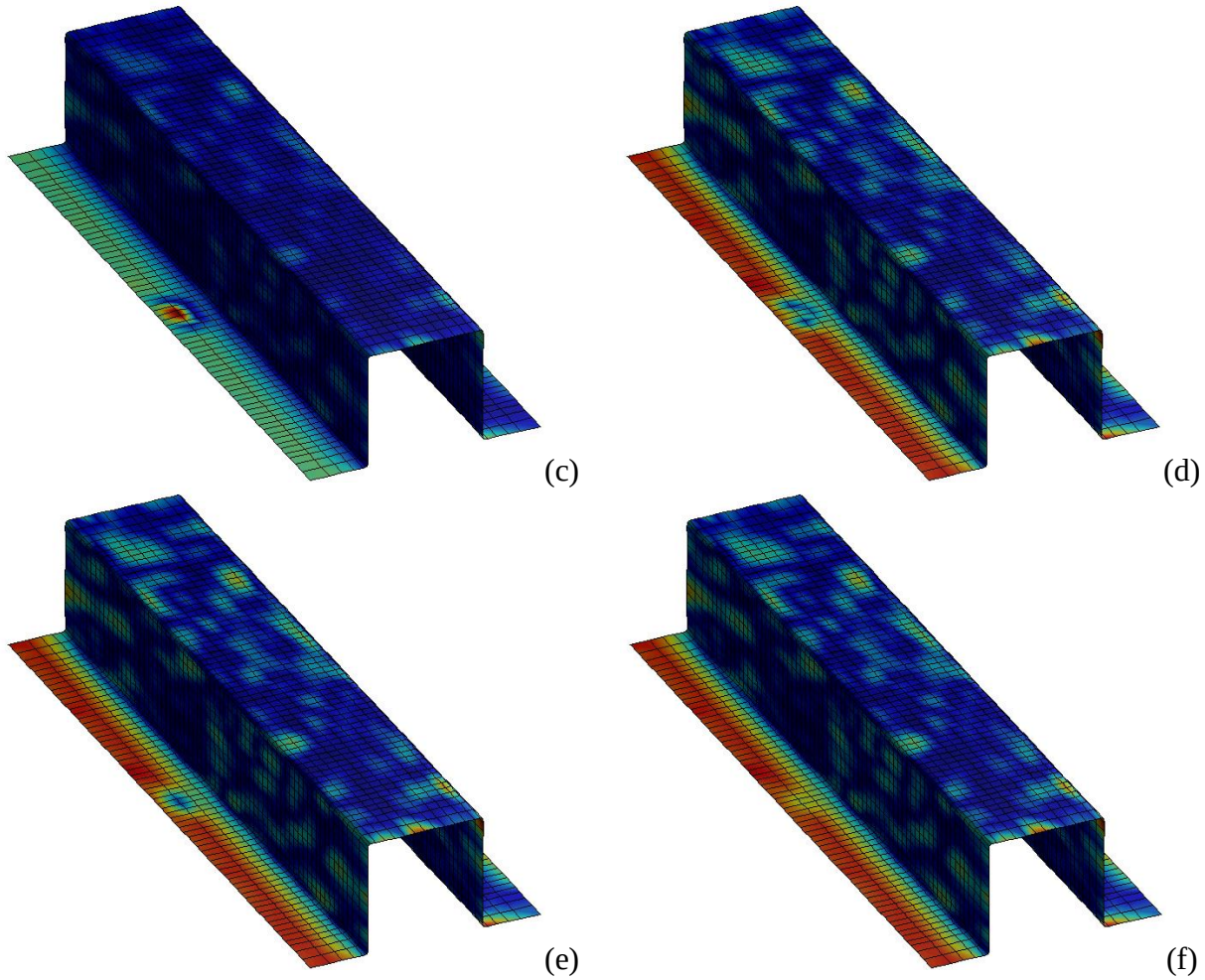

Figure 3.9: Observations of Shifts at Shift Location 3, for Shift Magnitudes δ = (a) 5, (b) 2, (c) 1, (d) 0.5, (e) 0.25, and (f) 0.1 mm.

Table 3.5: Actual Maximum Surface Deviations (mm) Caused by Shifts on the Nominal Surface.

	Shift Magnitude (mm)					
	5	2	1	0.5	0.25	0.1
Shift Location 1	2.7387	1.0955	0.54776	0.27388	0.13694	0.054776
Shift Location 2	2.6610	1.0644	0.53220	0.26610	0.13305	0.053220
Shift Location 3	2.4278	0.97113	0.48557	0.24278	0.12139	0.048557

For each simulation, 1,000 replications were used to determine out-of-control ARL performances. For these simulations a zero-state ARL analysis was performed, which assumes that the shift has occurred before the first control chart sample is collected. The results of these simulations for all six shift magnitudes, both cases, and all three control charting schemes are given in Table 3.6 to Table 3.8 for Shift Location 1 to Shift Location 3, respectively. In these tables, the

best ARL performances for each case are identified by a bold-face font. Since only 1,000 replications were performed, ARL estimates will have slightly elevated standard errors. For this reason multiple ARL performances may have bold-face font.

Table 3.6: Out-of-Control ARL Performances for Shift Location 1.

	Case 1			Case 2		
Shift (δ)	Scheme 1	Scheme 2	Scheme 3	Scheme 1	Scheme 2	Scheme 3
5	225.67	**1.0000**	**1.0000**	255.94	**1.0000**	**1.0000**
2	233.59	**3.6800**	**3.7600**	247.49	**3.1020**	**3.1360**
1	237.64	**8.2200**	**8.3600**	254.94	**8.7390**	**8.7800**
0.5	248.55	**19.300**	20.440	260.31	**34.230**	36.327
0.25	236.65	**73.500**	109.52	256.16	140.45	**130.24**
0.1	258.25	**144.22**	214.72	269.47	222.72	**216.58**

Table 3.7: Out-of-Control ARL Performances for Shift Location 2.

	Case 1			Case 2		
Shift (δ)	Scheme 1	Scheme 2	Scheme 3	Scheme 1	Scheme 2	Scheme 3
5	223.00	**1.1050**	**1.1390**	251.93	**3.8740**	**3.8660**
2	238.67	**4.9100**	**4.9350**	261.20	**16.954**	**17.256**
1	237.06	**10.648**	**10.950**	257.74	**87.598**	95.810
0.5	249.89	**28.648**	32.220	259.76	**189.27**	225.42
0.25	236.53	**116.09**	137.88	254.11	**230.15**	253.08
0.1	257.82	**218.61**	245.21	266.50	**236.09**	257.89

Table 3.8: Out-of-Control ARL Performances for Shift Location 3.

	Case 1			Case 2		
Shift (δ)	Scheme 1	Scheme 2	Scheme 3	Scheme 1	Scheme 2	Scheme 3
5	2.9590	**1.0000**	**1.0000**	190.42	**4.7700**	**4.8020**
2	19.198	**4.0150**	**4.0500**	245.19	**24.952**	**25.727**
1	79.787	**9.6950**	**9.8350**	259.36	117.08	**105.65**
0.5	165.76	**23.864**	27.332	258.11	210.68	**194.55**
0.25	221.79	**104.67**	126.57	265.43	244.57	**235.17**
0.1	258.59	**209.37**	224.04	263.83	250.88	**243.25**

3.3.4. Discussion of Results

The results of the ARL performances show quite interesting results. The most obvious result is that T^2 should never be monitored alone. Another result of note is the fact that control charting Scheme 2 in Case 1 performed uniformly better than all other monitoring scenarios (except for

Schemes 2 and 3 in Case 2 for Shift Location 1, where it barely underperformed). More interesting is the fact that in Case 2, Scheme 2 did not perform uniformly better than Scheme 3. For Shift Location 2, Scheme 2 performed uniformly better than Scheme 3; but for Shift Locations 1 and 3, Scheme 2 performed better than Scheme 3 for larger shifts but worse than Scheme 3 for smaller shifts.

These observations lead to one specific question, whether to simultaneously monitor T^2 and Q; or to simultaneously monitor T^2, Q, and R. For Case 2, when Scheme 3 outperforms Scheme 2 the performance difference is minimal. However, when Scheme 2 outperforms Scheme 3 the performance difference is much more significant. In addition, given the fact that Scheme 2 always outperforms Scheme 3 for Case 1, it would seem that the best option is to always implement Scheme 2. Therefore, this paper recommends simultaneously monitoring T^2 and Q regardless of whether an over or under-defined NURBS surface is used for estimation (to detect dent-like shifts).

Another significant observation is the fact that for Shift Location 2, Case 1 performed significantly better than Case 2, despite the fact that neither NURBS surface estimator had control points close to the shift. On the other hand, for Shift Location 1, Case 1 has a control point located directly at the shift and Case 2 did not. While Case 1 still performed better than Case 2, it was not as drastic as with Shift Location 2. This seems a little counter-intuitive since at Shift Location 1, Case 1 has a control point at the shift's exactly location.

It turns out that a control point's proximity to a shift is not the deciding factor in the ability of the proposed SPC approach to detect shifts in the surface. More important than control point location is the freedom of control points to represent the geometry of the shift rather than the nominal part geometry. Consider the cross-sectional view ($v =$ constant) for each surface shift at Shift Location 2 given in Figure 3.10a and Figure 3.10b for Case 1 and Case 2, respectively. In

these figures the solid lines represents the shift geometry and the dotted lines represent the NURBS surface estimate of the geometry. Here Case 2 is rather insensitive to shifts (compared to Case 1) at this location, which is due to the fact that the control points are needed to represent the global part geometry and lack the "freedom" to represent a localized surface shift.

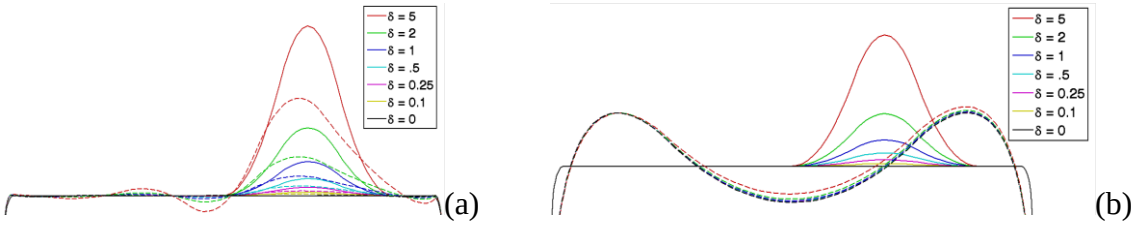

Figure 3.10: NURBS Surface Estimators of Surface Shifts at Location 2 for (a) Case 1 and (b) Case 2.

This conclusion suggests that under-defined NURBS surface estimators should not be used for monitoring. However, for complex parts this may be unavoidable as the high-dimensionality of an over-defined NURBS surface could be infeasible to monitor. In this paper, an alternative approach to reduce the dimensions of an over-defined NURBS surface is considered, which is described in the next section.

3.3.5. Alternative SPC Approach

In this alternative approach the magnitude of control point deviations from nominal are used instead of component deviations. Specifically, $\hat{\mathbf{p}}_{:,:}^{\boldsymbol{w}^*}$ in Eq. (3.17) is replaced by $\hat{\mathbf{p}}_{:,:}^{\boldsymbol{w}^*} = \left\|\hat{\mathbf{p}}_{:,:}^{\boldsymbol{w}} - \hat{\mathbf{p}}_{:,:}^{\boldsymbol{n}}\right\|$. The in-control design and out-of-control implementation of the alternative monitoring approach are performed exactly as the original set of simulations. From the PCA, the first three and first principal components were identified as significant for Cases 1 and 2, respectively. The SCREE plots used to make these decisions for Case 1 and 2 are given in Figure 3.11a and Figure 3.11b, respectively. Using these reduced principal component models, the means and standard deviations for T^2 and Q were determined, and are given in Table 3.9. This table also includes the

mean and standard deviation or R, which remains unchanged from the original approach. Finally, Table 3.10 provides the k values and their resulting ARL_0 values from simulations.

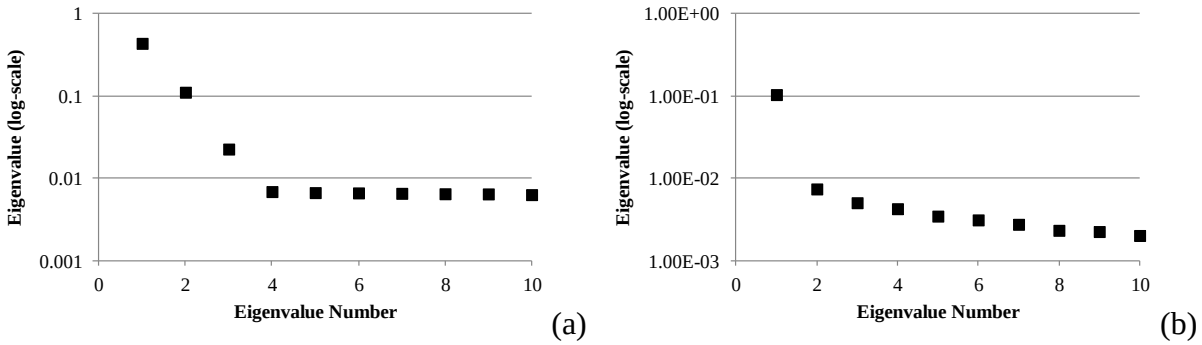

Figure 3.11: SCREE Plots from PCA using Alternative Approach for Cases (a) 1 and (b) 2.

Table 3.9: Mean and Standard Deviation of Monitored Statistics for Cases 1 and 2 using Alternative Approach.

	T^2		Q		R	
	μ	σ	μ	σ	μ	σ
Case 1	2.9997	2.9981	1.2498	0.093357	86.942	0.22040
Case 2	0.99990	1.8599	0.079560	0.020647	4918.8	17.970

Table 3.10: EWMA Design Parameters (k) Simulated to Obtain an In-Control ARL of 250 for Alternative Approach.

	Case 1			Case 2		
	Scheme 1	Scheme 2	Scheme 3	Scheme 1	Scheme 2	Scheme 3
k_{T^2}	2.2681	2.7585	3.0670	2.6484	3.2164	3.6844
k_Q		1.8840	1.9281		2.2051	2.1237
k_R			1.9711			2.0999
ARL_0	249.58	248.20	250.19	250.79	249.88	249.75

As with the original approach, zero-state out-of-control ARL simulations were performed. The results of these simulations for all six shift magnitudes, both cases, and all three control charting schemes are given in Table 3.6 to Table 3.8 for Shift Location 1 to Shift Location 3, respectively. In these tables, the best ARL performances for each case are identified by a bold-face font.

Table 3.11: Out-of-Control ARL Performances for Shift Location 1 for Alternative Monitoring Approach.

	Case 1			Case 2		
Shift (δ)	Scheme 1	Scheme 2	Scheme 3	Scheme 1	Scheme 2	Scheme 3
5	250.22	**1.0000**	**1.0000**	248.64	**1.0000**	**1.0000**
2	259.26	**2.5070**	**2.5470**	250.81	**3.3050**	**3.2760**
1	253.67	**7.0390**	**7.0270**	252.16	28.116	**25.652**
0.5	258.58	**23.417**	**23.408**	260.68	206.00	**132.72**
0.25	246.51	**176.46**	**179.69**	237.33	245.51	**209.32**
0.1	272.47	**250.01**	**250.67**	263.78	269.64	**234.88**

Table 3.12: Out-of-Control ARL Performances for Shift Location 2 for Alternative Monitoring Approach.

	Case 1			Case 2		
Shift (δ)	Scheme 1	Scheme 2	Scheme 3	Scheme 1	Scheme 2	Scheme 3
5	242.83	**1.0000**	**1.0000**	256.58	**4.1320**	**4.1000**
2	245.63	**3.1480**	**3.1310**	243.57	69.677	**58.648**
1	252.21	**8.4570**	**8.5220**	257.61	229.96	**216.06**
0.5	258.11	**23.595**	24.044	249.44	**274.02**	**276.89**
0.25	250.43	**106.79**	109.55	247.42	**275.26**	**268.06**
0.1	263.96	**211.92**	213.07	254.76	**256.28**	**262.98**

Table 3.13: Out-of-Control ARL Performances for Shift Location 3 for Alternative Monitoring Approach.

	Case 1			Case 2		
Shift (δ)	Scheme 1	Scheme 2	Scheme 3	Scheme 1	Scheme 2	Scheme 3
5	2.4000	**1.0030**	**1.0070**	336.94	**4.4720**	**4.3910**
2	103.12	**3.9540**	**3.9590**	296.72	**20.936**	**19.867**
1	401.33	**9.5910**	**9.7560**	279.54	137.17	**102.54**
0.5	385.21	**20.809**	21.220	254.51	236.32	**190.77**
0.25	309.57	**74.920**	81.019	257.95	264.09	**238.05**
0.1	283.73	212.92	**199.28**	251.86	**250.11**	**245.06**

While some of the results for the alternative approach are similar to the original approach, others are quite different. Firstly, in the alternative approach T^2 should still never be monitored alone as with the original approach. This result is even more significant with the alternative approach, as monitoring only T^2 can actually decrease the performance of method (e.g. several ARL values for Shift Location 3 are well above the in-control ARL of 250). Another equivalent result of note is the fact that control charting Scheme 2 in Case 1 performed uniformly better than all other monitoring scenarios (except for Scheme 3 in Case 2 for Shift Location 3). The major

difference between the two approaches is that in the alternative approach, regardless of whether the NURBS surface estimator is under or over-defined, simultaneously monitoring T^2, Q, and R is either significantly better than or at least on par with simultaneously monitoring T^2 and Q. Therefore, this paper recommends simultaneously monitoring T^2, Q, and R for the alternative approach, as opposed to the recommendation of simultaneously monitoring T^2 and Q for the original approach (to detect dent-like shifts).

This conclusion leads to the question of whether to use the original approach with control charting scheme 2 or the alternative approach with control charting scheme 3. ARL comparisons of these two possible monitoring strategies are given in Figure 3.12 to Figure 3.14 for Shift Location 1 to Shift Location 3, respectively. From these comparisons, neither strategy uniformly outperforms the other. However, when the original approach outperforms the alternative approach the gain in performance is much more than when the alternative approach outperforms the original. Therefore, this paper suggests that the original approach using monitoring scheme 2 be employed to detect dent-like shifts. In addition, if it becomes necessary to reduce the dimensionality of the problem, the alternative approach using monitoring scheme 3 is still a viable option.

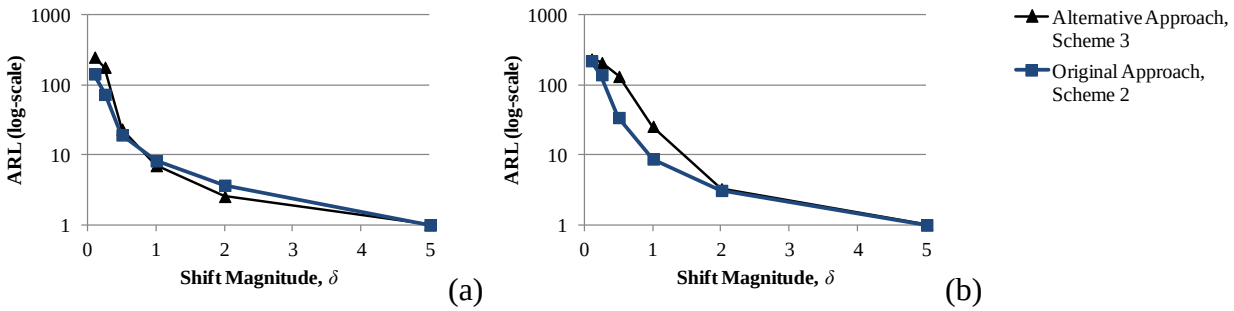

Figure 3.12: ARL Comparison of Recommended Monitoring Procedures at Shift Location 1 for (a) Case 1 and (b) Case 2.

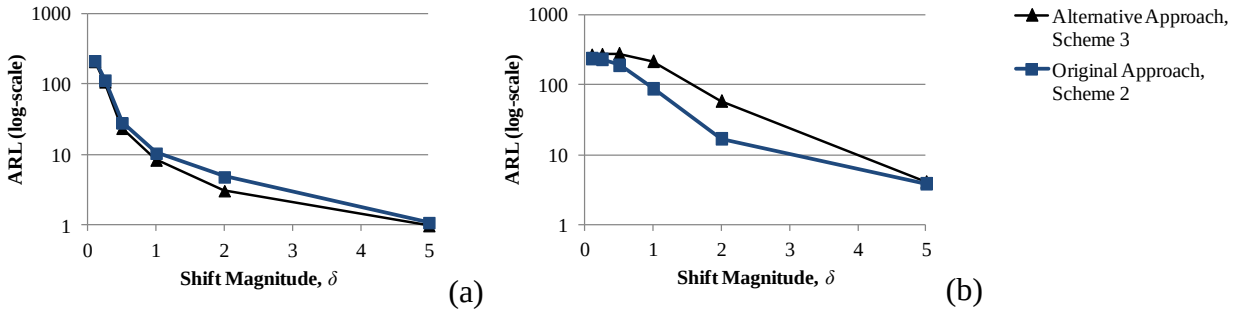

Figure 3.13: ARL Comparison of Recommended Monitoring Procedures at Shift Location 2 for (a) Case 1 and (b) Case 2.

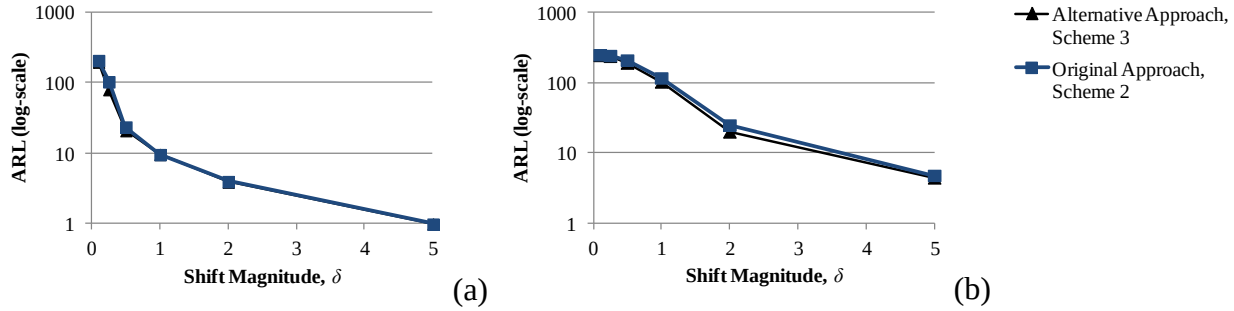

Figure 3.14: ARL Comparison of Recommended Monitoring Procedures at Shift Location 3 for (a) Case 1 and (b) Case 2.

3.4. Conclusions

The method proposed in this paper introduces a new approach for the use of HDD data in SPC. This method can be applied to any mass production manufacturing process where an entire product's dimensional characteristics are of key importance to ensuring a high quality part. The most important practical benefit from this paper is that the proposed methodology can be used to detect shifts that affect a part's geometry, regardless of its relationship to key features or production characteristics. The "dent" like faults examined in this paper could have easily gone undetected with traditional measurement devices (e.g. CMMs) that require the specification of a limited number of measurement locations.

3.5. References

Bersimis, S., Psarakis, S., and Panaretos, J. (2007), “Multivariate Statistical Process Control Charts: An Overview,” *Quality and Reliability Engineering International*, 23:5, 517-543.

Colosimo, B.M., Mammarella, F., and Petro, S. (2010), "Quality Control of Manufactured Surfaces," *Frontiers of Statistical Quality Control*, 9, 55-70.

Cox, M.G. (1972), "The Numerical Evaluation of B-Splines," *Journal of the Institute of Mathematics and its Applications*, 15, 99-108.

de Boor, C. (1972), "On Calculating with B-Splines," *Journal of Approximation Theory*, 6, 52-60.

Johnson, D.E. (1998), Applied Multivariate Methods for Data Analysts, Duxbury Press.

Kim, K., Mahmoud, M.A., and Woodall, W.H. (2003), "On the Monitoring of Linear Profiles," *Journal of Quality Technology*, 35:3, 317-328.

Koch, K.R. (2009), "Identity of Simultaneous Estimates of Control Points and of Their Estimates by the Lofting Method for NURBS Surface Fitting," *International Journal of Advanced Manufacturing Technology*, 44, 1175-1180.

Kruth, J.-P. and Kerstens, A. (1997), "Reverse Engineering Modeling of Free-Form Surfaces From Point Clouds Subject to Boundary Conditions," *Journal of Materials Processing Technology*, 76, 120-127.

Lee, K. (1999), Principles of CAD/CAM/CAE Systems, Addison-Wesley.

Mahmoud, M.A., Morgan, J.P., and Woodall, W.H. (2010), "The Monitoring of Simple Linear Regression Profiles with Two Observations per Sample," *Journal of Applied Statistics*, 37:8, 1249-1263.

Megahed, F.M., Wells, L.J., Camelio, J.A., and Woodall, W.H. (2012), "A Spatiotemporal Method for the Monitoring of Image Data," *Quality and Reliability Engineering International*, 28:8, 967-980.

Montgomery, D.C. (2008), Introduction to Statistical Quality Control, Sixth Edition, Hoboken, NJ: Wiley.

Ryan, A.G., Wells, L.J., and Woodall, W.H. (2011), "Methods for Monitoring Multiple Proportions when Inspecting Continuously," *Journal of Quality Technology*, 43:3, 237-248.

Wang, K. and Tsung, F. (2005), "Using Profile Monitoring Techniques for a Data-Rich Environment with Huge Sample Size," *Quality and Reliability Engineering International*, 21:7, 677-688.

Wells, L.J., Megahed, F.M., Niziolek, C.B., Camelio, J.A., and Woodall, W.H. (2012), "Statistical Process Monitoring Approach for High-Density Point Clouds," *Journal of Intelligent Manufacturing*, 1-13.

Woodall, W.H., Spitzner, D.J., Montgomery, D.C., and Gupta, S. (2004), "Using Control Charts to Monitor Process and Product Quality Profiles," *Journal of Quality Technology*, 36:3, 309-320.

Woodall, W.H. (2007), "Current Research on Profile Monitoring," Produção, 17:3, 420-425.

Zhou, L., Wang, H., Berry, C., Weng, X., and Hu, S. (2012), "Functional Morphing in Multistage Manufacturing and Its Applications in High-Definition Metrology-Based Process Control," *Automation Science and Engineering, IEEE Transactions on*, 9:1, 124-136.

4. Automated Part Inspection Using 3D Point Clouds

Ever advancing sensor and measurement technologies continually provide new opportunities for knowledge discovery and quality control (QC) strategies for complex manufacturing systems. One such state-of-the-art measurement technology currently being implemented in industry are 3D laser scanners, which can rapidly provide millions of data points to represent an entire manufactured part's surface. This gives 3D laser scanners a significant advantage over competing technologies that typically provide tens or hundreds of data points. Consequently, data collected from 3D laser scanners have a great potential to be used for inspecting parts for surface and feature abnormalities. The current use of 3D point clouds for part inspection falls into two main categories; 1) Extracting feature parameters, which does not complement the nature of 3D point clouds as it wastes valuable data and 2) An ad-hoc manual process where a visual representation of a point cloud (usually as deviations from nominal) is analyzed, which tends to suffer from slow, inefficient, and inconsistent inspection results. Therefore this paper proposes an approach to automate the latter approach to 3D point cloud inspection. The proposed approach uses a newly developed adaptive generalized likelihood ratio (AGLR) technique to identify the most likely size, shape, and magnitude of a potential fault within the point cloud, which transforms the ad-hoc visual inspection approach to a statistically viable automated inspection solution. In order to aid practitioners in designing and implementing an AGLR-based inspection process, this paper also reports the performance of the AGLR with respect to the probability of detecting specific size and magnitude faults in addition to the probability of a false alarms.

4.1. Introduction

Traditional quality control (QC) focuses on monitoring and/or inspecting a manufactured part's key product characteristics (KPCs), which can be used to assess the majority of a part's quality. In addition, KPCs tend to be physical measures, such as dimensions or locations of features. As discussed by Wells et al. (2012b) the choice of KPCs (and the techniques used to analyze them) is a function of available measurement technologies. For instance, the advent of in-line coordinate measurement machines (CMMs) has led to a significant increase in the number of KPCs being collected and furthered the use of multivariate methods for QC.

Advanced measurement technologies, such as 3D scanners and digital images, can collect millions of data points (referred herein as high-density dimensional (HDD) data) that can almost entirely reflect a manufacture part's geometry. Unfortunately, QC techniques have yet to be adapted to take full advantage of this new data-rich environment and for the most part rely on extracting discrete KPCs. In order to maximize the potential of HDD data collection technologies requires a new quality paradigm. Specifically, when presented with HDD data, quality should be assessed not by discrete KPCs alone but should consider the entire part being produced, anything less results in valuable data being wasted.

Specifically this paper addresses the issue of applying this new paradigm to automated part inspection using 3D point clouds obtained using laser scanning technology. As previously discussed current QC techniques extract feature parameters from a point cloud, which can be easily automated with commercially available software. An alternative ad-hoc approach for inspecting 3D point clouds exists where the entire point cloud is used to detect the presence of abnormalities (both feature and non-feature based), which is a highly manual process where a visual representation of a point cloud (usually as deviations from nominal displayed as a color map) is

analyzed. For example, consider the planar point cloud (represented as deviations from a nominal computer aided design (CAD) geometry) given in Figure 4.1a, where a surface flaw exists in the lower left corner. In order to consistently and accurately identify abnormalities of this nature requires zooming in and visually scanning the entire point cloud, as shown in Figure 4.1b. While this approach is significantly time consuming and costly it fits with the new paradigm that the entire part is used to assess quality. Therefore, this paper proposes an approach to automate this 3D point clouds inspection process. This approach uses a newly developed adaptive generalized likelihood ratio (AGLR) technique to identify the most likely location, size, shape, and magnitude of a potential fault within the point cloud; which transforms the ad-hoc inspection approach to a statistically viable inspection solution.

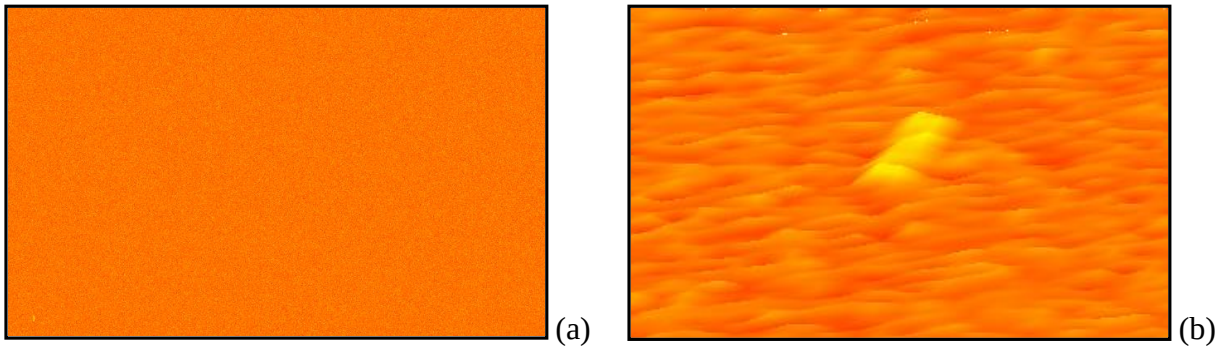
(a) (b)

Figure 4.1: A Planar Point Cloud with a Surface Flaw in the Lower Left Corner (a) Viewed as the Entire Point Cloud and (b) Zoomed in View of the Surface Flaw.

4.2. Literature Review

Recently there has been a strong focus on the use of high-density dimensional (HDD) data, obtained from technologies such as 3D scanners and digital images, for industrial applications due to their ability to provide not only dimensional information but also information on product geometry, surface defects, surface finish, and numerous other product characteristics that can reflect overall quality. From the respective literature on this topic, 3D scanning research may be categorized into three categories. The first research area focuses on how to post-process point clouds into a format acceptable for quality evaluation purposes (Shi et al., 2006; Shi and Xi, 2008;

Martínez et al., 2010). The second research area aims to improve the accuracy of 3D scanners by error correction or compensation by contact measurement comparisons; such as coordinate measuring machine (CMM) (Fenga et al., 2001; Brajlih et al., 2011; Isheil et al., 2011) or by developing better scanning plans (Shi et al., 2007; Mohib et al., 2009). The third research area deals with the use of scanning data in manufacturing environments, which can be divided into two categories: reverse engineering and product inspection (Son et al., 2002). In reverse engineering applications, manufactured parts are transformed into CAD models using scanning systems (Hsiao and Chuang, 2003; Mohaghegh et al., 2007).

The use of 3D laser scanners for product inspection typically involves categorizing products as either “good” or "bad" based on deviations of the scanned part from the nominal CAD model (Wells et al., 2012b). The current use of 3D point clouds for product inspection falls into two main categories. The first category focuses on extracting geometrical and dimensional feature parameters (Li and Gu, 2004; Martínez et al., 2010; Ravishankar et al., 2010; Brajlih et al., 2011), which does not complement the nature of 3D point clouds as it wastes valuable data. The other category aims to utilize laser scanners’ ability to provide an entire depiction of the surface of a manufactured part in order to capture unspecified faults (e.g. defects on surfaces, such as cracks, corrosion, lighting strikes on a product).

The current common approach to make use of point clouds to detect unspecified faults is an ad-hoc manual process where a visual representation of a point cloud, usually as deviations from nominal, is analyzed (Prieto et al., 1998; Li and Gu, 2004; Morel et al., 2005). It should be noted, that this inspection approach suffers from slow, inefficient, and inconsistent inspection results because it depends on human inspectors. Human inspectors experience fatigue and distraction, which can result in highly inconsistent inspection results among operators (Megahed et al., 2011).

In addition, this approach fails completely when a large number of inspections are required, limiting the ability of this approach to be used in 100% inspection. Moreover, the human eye cannot detect faults smaller than the noise in the obtained point cloud and cannot account for the spatial relationships between successive samples. Consequently, product inspection for detecting unspecified faults must be automated in order to 1) Avoid the manual visual inspection limitations, 2) Formalize the methods of inspection human expertise in order to make them robust and systematic, and 3) Exploit the full potential of point cloud data.

While there has been little to no research in automated inspection for 3D point clouds, there is however a strong research effort in using digital images for automated process monitoring and inspection. As reported by Megahed et al. (2011), image-based control charting techniques are typically used to detect faults that occur spatially instead of detecting changes in an image over time. In order to detect these spatial faults, a moving window approach is used to progressively scan different regions over the entire image. The moving window size is based on the target defect size to be detected and a statistic is calculated for every single window where a "spatial" control chart is used for detecting the targeted defects. This inspection technique is used in several applications such as oil seal inspection (Jiang and Jiang, 1998), inspection of the uniformity of high-grade LCD monitors (Jiang et al., 2005), and the inspection of woven fabrics (Tunák et al., 2009).

Another QC approach for images is to divide an image into regions of interest (ROIs), determined according to the targeted fault types, where for each ROI a spatial statistic is calculated to detect the presence of a fault (Megahed et al., 2012). The ROI is a reduced zone of the image where the main processing work will be applied in order to save the computing time of the analysis by avoiding the treatments of the normal parts of the image. Moreover, the use of ROIs handles

the shortcomings of global inspection approaches by avoiding treatments for irrelevant regions of the image, which can negatively influence the output results (Nacereddine et al., 2005).

Nacereddine et al. (2005) developed processing algorithms to automatically detect weld defects in radiographic images based on both local and global approaches. In these approaches ROIs are pre-selected at locations most likely to contain a defect and then applied one or more passes of a median filter. Wang et al. (2011) also proposed an automated crack detection algorithm for aircraft wing inspection using ROI minimization and an enhanced Canny edge detection algorithm. The edge detection operator is used to detect crack edges in the ROI by looking for local maxima of the gradient of the image which is calculated using the derivative of a Gaussian filter. After that, the local gradient and edge direction are computed at each point. An edge point is defined to be a point whose strength is locally maxima in the direction of the gradient.

Megahed et al. (2012) suggested a spatiotemporal control charting technique which allows for rapid fault detection in grayscale images. In this work, a Phase II spatiotemporal control charting technique was developed using a generalized likelihood ratio (GLR) statistic. First the image is divided into pre-defined ROIs, determined according to the type of faults to be detected. For each observation (image) the maximum GLR is calculated for each ROI including data collected from previous observations. If the GLR statistic exceeds a specific control limit the chart signals, and an estimate of the location, size, and change-point of the shift is obtained. The adaptive generalized likelihood ratio (AGLR) technique proposed later in this paper is developed as an extension of this spatiotemporal approach for part inspection using 3D point clouds.

4.3. Challenges and Opportunities for HDD Data in Quality Control

This section discusses the main challenges and opportunities associated with using HDD data for the purpose of automated quality control; specifically this section will address 1) Maintaining spatial relationships within the point cloud, 2) Accounting for varying size, shape, location and magnitude of possible point cloud abnormalities, and 3) Developing an approach that can encompass the task of both inspection and monitoring,.

According to Wells et al. (2012a) maintaining spatial relationships between 3D measurements is of the utmost importance when trying to understand, interpret, and use 3D data for QC purposes. This assertion becomes even more valid when dealing with 3D data-sets from HDD data sources. For instance, consider the two simulated planar 3D point clouds given in Figure 4.2, where each point cloud consists of one million deviation from nominal measurements. In both of these point clouds an arbitrary fault tolerance limit is applied to the data, where any data point exceeding the limit is displayed as red and any point that does not exceed the tolerance limit is displayed as yellow. In addition, both of these simulated point clouds have 1% of the data fall outside of the tolerance limit.

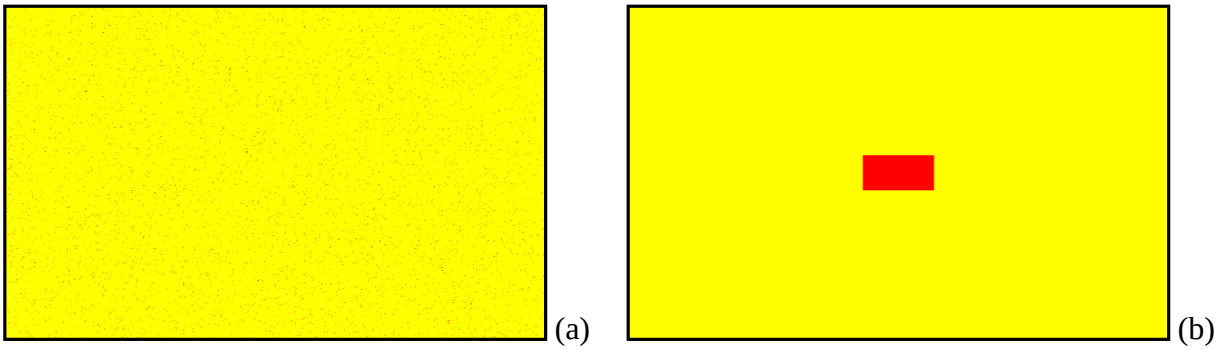

(a) (b)

Figure 4.2: A Planar Point Cloud where 1% of the Data Falls Outside Tolerance Limits Due to (a) Noisy Data and (b) The Existence of a Fault.

If the spatial relationships within the point clouds are not considered when analyzing these two data-sets the resulting conclusion would be the same for both cases, a fault exists. However, it can be clearly seen that the point cloud in Figure 4.2a does not have a fault, but instead suffers from

noisy data. This is an unavoidable characteristic when using HDD data since the probability of outlying samples increases significantly with large data-sets. If the spatial relationships within the point clouds are considered, the resulting conclusion is that only the point cloud shown in Figure 4.2b actually contains a fault.

In addition, considering spatial correlations enhances the ability of a QC system to detect small deviations in the point cloud. This can be thought of as the spatial equivalent to how exponential weighted moving average (EWMA) and cumulative sum (CUSUM) control charts exploit temporal correlations to detect small shifts. For instance, consider the simulated planar 3D point clouds given in Figure 4.3a, which consists of one million deviation from nominal measurements. The majority of this point cloud has no faults and merely suffers from noisy data. In the center of this point cloud, a fault exists whose magnitude is significantly smaller than the noise, making it nearly impossible to detect visually. However, if one was to take into consideration the correlation within the data, the defect is quite easy to see, as shown in Figure 4.3b.

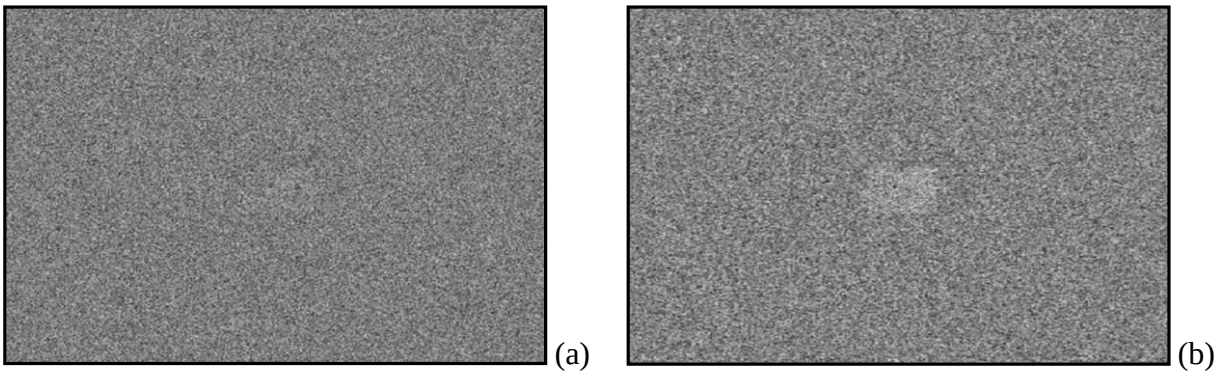
(a) (b)

Figure 4.3: A Planar Point Cloud with a Fault in the Center (a) Before and (b) After Implementing a Filter.

In this figure a simple averaging filter (each point is represented as the average of that point and its surrounding points) was implemented for the data in Figure 4.3a. The AGLR technique outlined in the next section is specifically designed to take advantage of spatial correlations to increase its ability to detect small shifts, thusly increasing its capabilities further than the currently ad-hoc approach.

Beyond taking into account spatial relationships within HDD data, it is also vital that an inspection or monitoring scheme for HDD data be able to account for the fact that faults can occur in varying sizes, shapes, locations and magnitudes. In this paper, the size of a fault refers to the amount of area covered by the fault; while a fault's magnitude refers to the severity of the measurement (e.g. the magnitude of a fault in a digital image would be measured by its pixel value and the magnitude of a fault in a point cloud would be measured by its deviation from nominal). As discussed earlier, traditional QC revolves around KPCs or product features, which can generally be quantified as a single measurement that either increases or decreases. This allows for inspection tolerances and monitoring control limits to be easily defined, which is not the case when dealing with HDD data. For instance, consider the three idealized possible faults that could occur in a point cloud measuring deviations from nominal, illustrated in Figure 4.4. The data within the point clouds that define these faults differ drastically; however the automated inspection process should be able to detect all three.

From the previous literature review two general approaches were identified to accomplish automated fault detection with image data; namely moving window and ROI based methods. While these methods work well to detect specific fault types, they do not work as well to detect a wide range of faults, such as those illustrated in Figure 4.4. This tends to occur when windows or ROIs differ drastically in the size and shape of the fault they are trying to detect. If the window or ROI is significantly smaller than the fault there may not be enough data to support the conclusion that a fault is present. Consider a very small window entirely inside of the oval shaped fault given in Figure 4.4. Since the oval shaped fault has a small magnitude and the window can only observe a small section of the fault it may be impossible to detect the fault. Conversely if the window is significantly larger than the fault, the data that supports the presence of a fault may be

overshadowed by the data that does not come from a fault. Consider a very large window that completely encompasses the hair-line fault given in Figure 4.4. Despite the fact that the fault magnitude is large, the data that comes from the fault is hidden by the large amount of data that does not come from the fault. The adaptive generalized likelihood ratio (AGLR) technique proposed in this paper attempts to overcome these drawbacks to using window and ROI based approach by adaptively selecting data most likely to contain a fault.

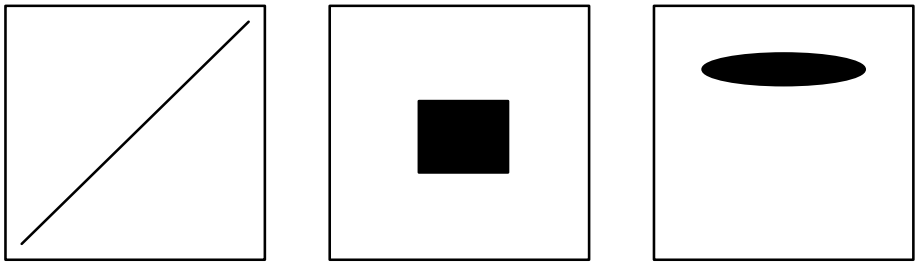

Figure 4.4: Three Idealized Possible Faults that Could Occur in a Point Cloud Measuring Deviations from Nominal.

Finally, in order for a QC framework to be truly useful in a manufacturing system the basic principle behind it should be able to handle the task of both inspection and monitoring. The previously discussed ad-hoc visual approach to inspection is useful for inspection but completely fails if applied to process monitoring. Firstly, due to the time consuming nature of visual inspection, samples are too infrequent to be useful in a monitoring framework. Second, there is no way to obtain a quantifiable statistic to implement monitoring using completely visual inspection. In order to employ a useful monitoring scheme requires a quantifiable measure that can be observed. In addition, building temporal correlations between samples requires that any used measurement must contain information on the size, shape, location, and magnitude of a fault in order to maximize the potential to signal. While the QC approach proposed in this paper is specifically designed to perform part inspection, it can be extended to the field of monitoring.

4.4. Adaptive Generalized Likelihood Ratio Method

The adaptive generalized likelihood ratio (AGLR) method proposed in this paper is an adaptation of the spatiotemporal control charting approach developed to detect process shifts in grayscale images developed by Megahed et al. (2012). In this work pre-defined ROIs are developed to cover a wide range of possible fault locations and sizes in an image. For each new image, the maximum generalized likelihood ratio (GLR) is calculated for each ROI including data collected from previous images. The main drawback of this approach is that its ability to detect faults is highly dependent on the size and shape of the pre-defined ROIs. The AGLR method attempts to overcome this disadvantage by selectively "growing" an ROI to maximally cover a possible fault.

The remainder of this section will cover the steps of the AGLR method, specifically; 1) Transforming 3D point clouds into 2D matrices, 2) Initializing the AGLR method, and 3) ROI growth for maximum fault coverage.

Megahed et al. (2012) developed their spatiotemporal control charting approach to monitor grayscale images. Therefore, the first step of the AGLR method is to transform the data structure of a 3D point cloud into that of a grayscale image. This not only allows the AGLR approach to be implemented, but also generalizes the problem of dealing with 3D point clouds as 2D data structures. In essence a grayscale image is merely a 2D matrix where each element corresponds to a pixel intensity. In order to transform a 3D point cloud into a 2D matrix the measurements obtained from a laser scanner (or comparable HDD measurement device) are acquired as a grid of $r \times e$ points, as discussed by Koch (2009), where the total number of points on the grid is R. The spacing between these grid points will be considered as the maximum resolution of the measurement technology, R_s. This grid of measurement points is then compared to the nominal CAD model, which can be easily implemented in a variety of commercially available software

packages. This comparison results in a $r \times e$ grid of 3D deviations from nominal. Taking the Euclidian norm for each point in this grid results in a 2D matrix of deviations from nominal.

Instead of relying on pre-defined ROIs for the inspection process, the AGLR approach allows for ROI growth to maximize fault coverage. This is done by first dividing the 2D matrix of deviations into "ROI seeds" as illustrated in Figure 4.5. The size of the ROI seeds, R_r, is defined by the number of measurement points an ROI seed contains, as illustrated in Figure 4.6. It should be noted that R_r will later be used as a design parameter for the inspection technique, discussed in the next section. For the AGLR algorithm, these seeds will determine where to initiate the growth of the ROI. Similar to the work of Megahed et al. (2012), the AGLR approach focuses on the ROI seed that has the maximum GLR, which would suggest the most likely location for a fault to exist.

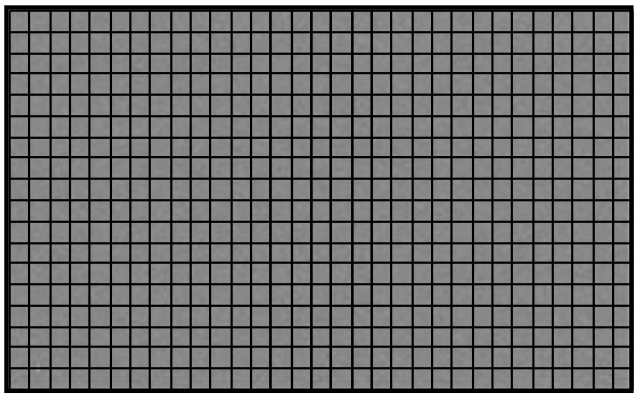

Figure 4.5: ROI Seed Generation.

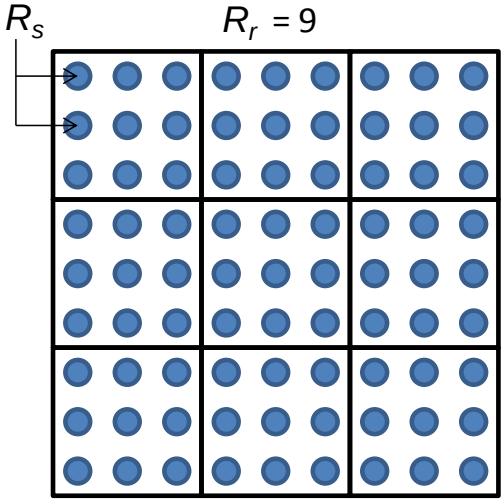

Figure 4.6: ROI Seed Size.

The goal of the AGLR method is to detect the presence of a fault within a point cloud that can be captured as a deviation from nominal. For a part that contains no faults, each sample point in the 2D matrix can be assumed to be i.i.d and follow a normal distribution with a mean of zero and a standard deviation of ε (i.e. the only noise present within the system comes from the measurement device and is therefore known). The resulting likelihood function at ROI seed $S_{i,j}$ (the ROI seed occupying the i^{th} row and j^{th} column of the ROI seed grid) under a no fault condition is

$$L(\mu = 0|\mathbf{X}_{i,j}) = \left(\frac{1}{\sqrt{2\pi}\varepsilon}\right)^{R_r} \exp\left(\frac{-1}{2\varepsilon^2}\sum_{k=1}^{R_r}\left(\mathbf{X}_{i,j}(k)\right)^2\right), \tag{4.1}$$

where $\mathbf{X}_{i,j}$ is a vector containing all deviation measurements in $S_{i,j}$.

It is assumed that the presence of a fault causes an unknown mean shift, μ_1, in the deviations from nominal. The resulting likelihood function at $S_{i,j}$ that is completely encompassed by this fault is

$$L(\mu = \mu_1|\mathbf{X}_{i,j}) = \left(\frac{1}{\sqrt{2\pi}\varepsilon}\right)^{R_r} \exp\left(\frac{-1}{2\varepsilon^2}\sum_{k=1}^{R_r}\left(\mathbf{X}_{i,j}(k) - \mu_1\right)^2\right). \tag{4.2}$$

The resulting log likelihood ratio for $S_{i,j}$ becomes

$$\mathrm{LR}_{i,j} = \frac{R_r}{2\varepsilon^2}\mu_1^2. \tag{4.3}$$

For the GLR, there is no assumed value for μ_1 (i.e. the fault magnitude is unknown), and instead is estimated by $\mathbf{X}_{i,j}$ as

$$\hat{\mu}_1 = \frac{1}{R_r}\sum_{k=1}^{R_r}\mathbf{X}_{i,j}(k), \tag{4.4}$$

resulting in the GLR for $S_{i,j}$ to be

$$\mathrm{GLR}_{i,j} = \frac{1}{2\varepsilon^2 R_r}\left(\sum_{k=1}^{R_r} \mathbf{X}_{i,j}(k)\right)^2. \tag{4.5}$$

The interpretation of the GLR statistic is fairly straightforward. The larger the GLR statistic becomes, the more likely that the data comes from a distribution other than the noise of the measurement device, i.e. the data is no longer normally distributed with a mean of zero. In order to use the GLR statistic to detect small faults (size and magnitude), it becomes advantageous to determine and use the area within the 2D matrix that results in the largest GLR possible. This is performed by adaptively growing the ROI starting with the $S_{i,j}$ that corresponds to the largest GLR.

For each sample being inspected, Eq. (4.5) is evaluated to obtain the GLR for each ROI seed. The initial GLR value of the ROI to be grown (referred to as simply the ROI) is the GLR value of the ROI seed that corresponds to the largest GLR, GLR*. The basic premise of the ROI growth process is to assess whether an adjacent test ROI seed, S_T, will increase GLR*, or more specifically if

$$\mathrm{GLR}^* < \frac{(Z+Y)^2}{2\varepsilon^2 R_r m}, \tag{4.6}$$

where Z is the sum of all data points within the ROI, Y is the sum of all of the data point within S_T, and m in the number of ROI seeds that constitute the ROI. If this inequality is true, then S_T is added to the ROI, i.e.

$$\mathrm{GLR}^* = \frac{(Z+Y)^2}{2\varepsilon^2 R_r m}; \tag{4.7}$$

if this inequality in not true then the growth process for that direction stops and a new growth direction is initiated. This process continues until either no S_T increases GLR* or the AGLR

Go/No-Go threshold, h, has been exceeded (a fault is identified). It should be noted that the use and design of h will be discussed in the next section.

The ROI growth strategy used in our paper is a fairly straightforward two phase process. Phase I (Horizontal Growth): Starting with the ROI seed (S_{i^*,j^*}) that produces the largest GLR, the first ROI test seed is S_{i^*,j^*+1}, the second is S_{i^*,j^*+2}, etc. This growth continues until either of two termination criteria are met, namely; Eq. (4.6) is false or a boundary in the 2D matrix has been reached. The growth then continues S_{i^*,j^*-1}, S_{i^*,j^*-2}, etc., once again until termination. Phase II (Vertical Growth): Repeat Phase I at S_{i^*+1,j^*}, then at S_{i^*+2,j^*}, etc. until termination. Finally repeat Phase I at S_{i^*-1,j^*}, then at S_{i^*-2,j^*}, etc. until termination. It should be reiterated that the entire growth process stops whenever GLR* exceeds h, since there is no reason to continue to grow an ROI once a fault has been identified.

It should be noted that the AGLR approach is very computationally efficient. This is due to the assumptions that data absent of faults are i.i.d. normal with a mean of zero, and that faults are modeled as a pure mean shift. As seen in Eq. (4.6), the ROI growth process only requires keeping the sum data from each ROI seed. This means that after the initial calculation of each $\mathrm{GLR}_{i,j}$ the original scan data for $S_{i,j}$ is no longer needed and can be removed from system memory. In addition, the efficiency of the proposed algorithm is trivial when considering the time required to obtain the measurements.

4.5. Inspection System Design and Performance Analysis

The design of the AGLR inspection system requires defining performance criteria for the maximum allowable probability of false alarms, P_F, and minimum probabilities of detecting specific fault sizes (F_S) and specific fault magnitudes (F_M), $P_D(F_S, F_M)$. In general, P_F and $P_D(F_S, F_M)$ are proportional, as the probability of false alarms increases so does the probability of

detection (100% probability of false alarms is also 100% probability of detection). As P_F decreases from 100% the ability to detect small faults begins to diminish as they become indistinguishable from system noise. Therefore, the basic premise of designing the system is to determine how much to sacrifice $P_D(F_S, F_M)$ for small shifts (size and magnitude) in order to obtain an acceptable P_F.

In the previous section, two design parameters for the AGLR method were identified, the size of the ROI seeds, R_r, and the Go/No-Go threshold, h. These two design parameters must be determined in tandem to achieve (or come close to achieving) a desired system performance as P_F and $P_D(F_S, F_M)$ depend on a non-linear relationship between R_r and h. For instance, if it is desirable to detect small sized faults one could use a small R_r. However a smaller R_r increases P_F, which is never desirable. This could be counteracted by increasing h which would make it more difficult to detect a small sized fault, especially if that fault has a small magnitude. For the purpose of system design, it should be noted that a decrease in R_r increases the computational requirements for the AGLR approach as the number of ROI seeds will increase.

In order to accurately design the AGLR inspection system requires understanding the relationships between P_F, $P_D(F_S, F_M)$, R_r, and h. In addition, it is advantageous to generalize these relationships to be applicable to any measurement system, i.e. the relationships are independent of the resolution, R_s, and noise, ε, of the measurement system. With this in mind, for the remainder of this paper the units for F_S will be R_s and the units for h and F_M will be ε.

4.5.1. Inspection System Design Case Study

This sub-section describes a case study for designing an inspection system to detect square shaped faults for a manufactured part consisting of $R = 10{,}000$ deviation measurements $\left(r = e = \sqrt{R}\right)$. Given the complex nature of the AGLR approach, obtaining analytical results for

P_F and $P_D(F_S, F_M)$ is computationally infeasible. Therefore simulated data is used to evaluate P_F and $P_D(F_S, F_M)$ for this case study.

The simulated data used in this paper is based directly on the assumptions used to develop the AGLR method. Each simulated case contains 1,000 replications and each replication is composed of a random planar point cloud consisting of 10,000 deviation measurements. In addition, for a given fault size and magnitude, every replication allows for the fault to be located in a random position.

For this case study six specific ROI seed sizes $R_r = [4, 16, 25, 100, 400, 625]$, which all result in a completely filled ROI seed grid, are considered. The resulting false alarm probabilities for these ROI seed sizes using the AGLR approach are given in Figure 4.7 as solid lines. In addition, the false alarm rates with no ROI growth (referred to herein as the GLR approach) are also given in Figure 4.7 as dotted lines. As can be seen the AGLR method results in increased false alarm rates for equal inspection system design parameters, which is expected. It should be noted that this should not detract from the use of the AGLR approach, since; 1) The tails of the distributions are not significantly different, which is most likely where the final design will be located and 2) The ability of the inspection system to detect faults has yet to be analyzed.

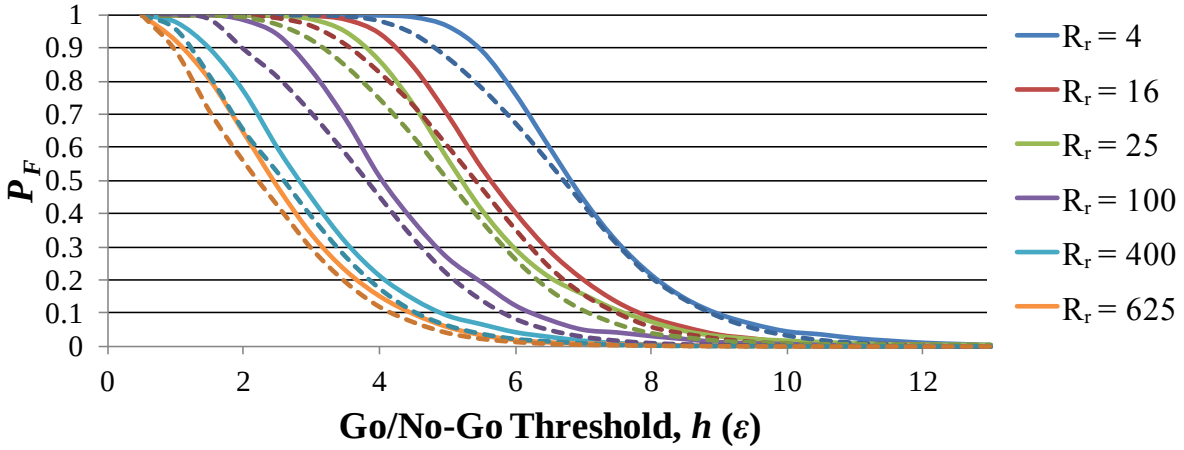

Figure 4.7: Simulated False Alarm Probabilities Varying ROI Seed Sizes and Go/No-Go Thresholds for AGLR Method (Solid Lines) and GLR Method (Dotted Lines).

For this fictitious case study nine different faults ($F_1 - F_9$) are known to exist with the system, which are summarized in Table 4.1. The simulated probabilities of detecting these faults using the AGLR approach are given in Figure 4.8 as solid lines. In addition, the probabilities of detection using the GLR approach are also given in Figure 4.8 as dotted lines. In this figure, the benefits of the AGLR method are quite obvious. For instance, in Figure 4.8g there is a significant performance gain using the AGLR method for an ROI resolution of 4 with large Go/No-Go thresholds. Furthermore in Figure 4.7 at higher Go/No-Go thresholds for an ROI resolution of 4, there is only a minimal increase in false alarm rates for the AGLR approach.

Table 4.1: Faults Considered in Simulation Study

		Fault Magnitude (ε)		
		2	5	10
Fault Size (R_s^2)	4	F_1	F_2	F_3
	9	F_4	F_5	F_6
	16	F_7	F_8	F_9

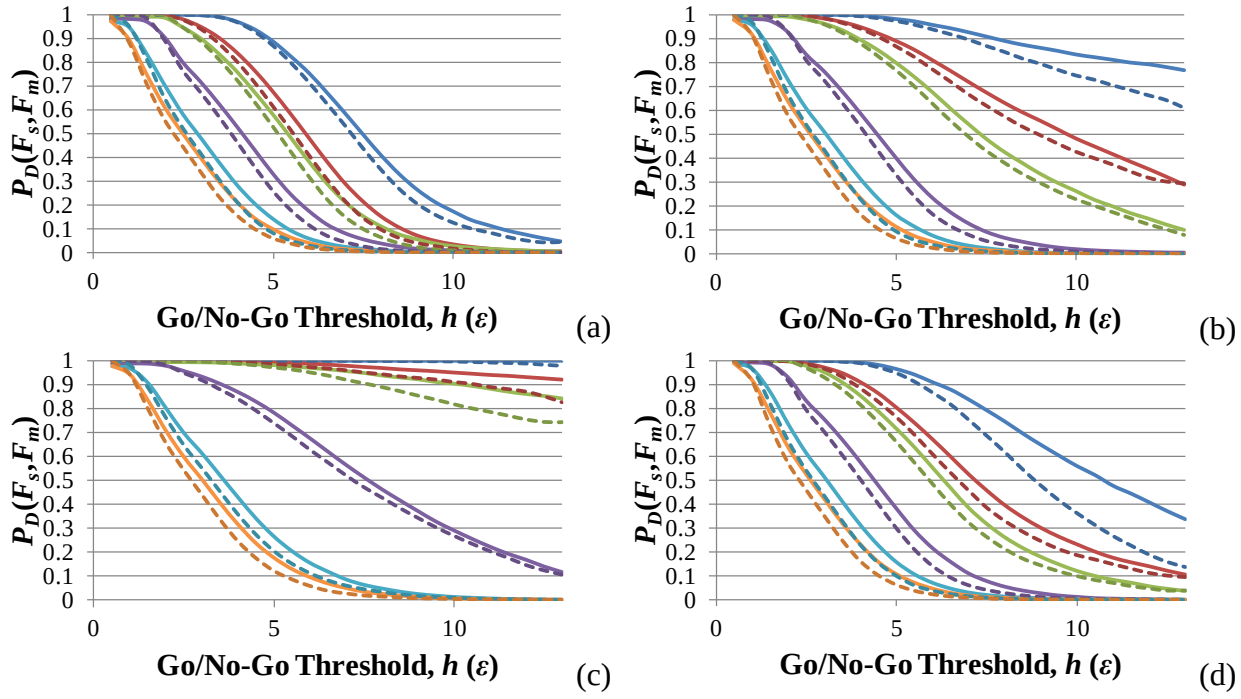

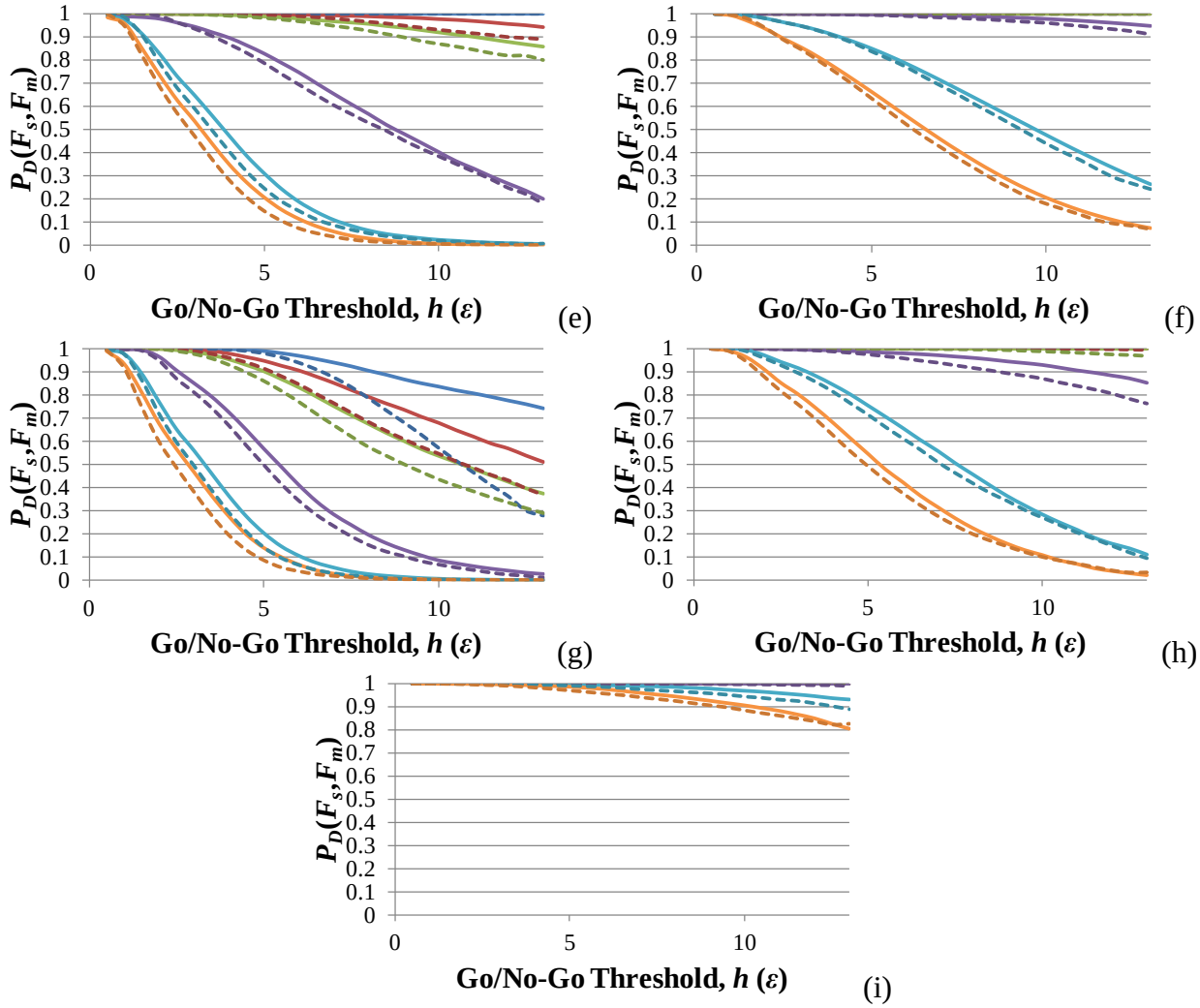

Figure 4.8: Simulated Detection Probabilities for Fault (a) F_1, (b) F_2, (c) F_3, (d) F_4, (e) F_5, (f) F_6, (g) F_7, (h) F_8, and (i) F_9 for AGLR Method (Solid Lines) and GLR Method (Dotted Lines). It Must be Noted That These Figure use the Same Legend as Figure 4.7.

For this case study consider the following inspection system criteria: 1) Correctly detect all faults that has a magnitude greater than or equal to 5ε and a size greater than or equal to $9R_s^2$ at least 90% of the time and 2) Have a false alarm rate less than 10%. In designing an AGLR-based inspection system, Figure 4.8e gives several options for the first criterion, which are given in Table 4.2. Evaluating Figure 4.7 at these possible design locations gives the resulting false alarm probabilities, also given in Table 4.2. From this analysis, an acceptable inspection system could be: $h = 10.75$ and $R_r = 25$; resulting in $P_D(F_S > 5\varepsilon\,, F_M > 9R_s^2) \approx 90\%$ and $P_F \approx 0\%$, which satisfies the design criteria.

Table 4.2: Potential Inspection Designs for Probability of Detection Criterion.

h	1.25	1.5	4	10.75
R_r	625	400	100	25
P_F (%)	86	89.8	51	0

While this inspection system design satisfies the criteria, it does not guarantee specific performance levels for faults having magnitudes less than 5ε or sizes less than $9R_s^2$, such as $F_1 - F_4$ and F_7. This can become a serious problem when dealing with faults that are very large in magnitude but small in size (such as a deep surface scratch) or vice versa. Thusly, the final step in this design is to evaluate the probabilities of detection for these faults, which are given in Table 4.3. As can be seen, the detection probabilities for faults not considered in the original design criteria are relatively low. If the faults with low detection probabilities are deemed inconsequential for the given system the design should be accepted. However, if these faults significantly impact the system at hand, the inspection system design should be re-evaluated by; 1) Analyzing alternative designs that meet the design specifications, 2) Determining more realistic performance criteria, 3) Developing multiple detection probabilities for varying fault magnitudes and sizes, 4) Exploring different measurement system alternatives, and 5) Implementing an economic-based inspection system design, which is discussed in the following section.

Table 4.3: Detection Performance for Faults not Considered During Inspection System Design.

	F_1	F_2	F_3	F_4	F_7
P_D (%)	1.556	21.15	88.76	8.939	49.44

4.5.2. Economic-Based Inspection System Design

Due to unrealistic design criteria, the resulting inspection system designed in the previous sub-section was incapable of detecting faults known to exist within the system. This problem occurred because the design criteria was only concerned with detecting faults with magnitudes greater than or equal to 5ε and a size greater than or equal to $9R_s^2$. An alternative approach to design an AGLR

inspection system is to not focus on specific design criteria, but to minimize the cost (with respect to false alarms and missed detections) of the inspection system.

Such an approach would be very similar to the economic modeling methods used in control charts (Lorenzen and Vance, 1986; Woodall, 1986.). It should be noted that applying an economic model is no trivial task, as it requires obtaining costs for false alarms and missed detections for varying fault size and magnitude combinations. In addition, one would also have to estimate the distribution of healthy and faulty parts as well as the joint distribution of fault sizes and magnitudes. However, if these parameters can be accurately estimated, economic-based models can be quite useful in determining optimal inspection system designs.

For continuous fault size and magnitude distributions, the expected cost of an inspection system can be formulated as

$$\mathrm{E}[C] = \iint f_{\mathrm{F_s},\mathrm{F_m}}(F_s, F_m) * \left(1 - P_D(F_S, F_M)\right) * C(F_s, F_m) dF_s dF_m, \tag{4.8}$$

where $f_{\mathrm{F_s},\mathrm{F_m}}(\cdot,\cdot)$ is the joint PDF of F_s and F_m and $C(\cdot,\cdot)$ is the missed detection cost function. It should be noted that for the continuous case the concept of false alarms no longer applies as a defect-free part is not physically possible. For discrete faults, such as the case study presented in this paper, the expected cost can be formulated as

$$\mathrm{E}[C] = C_{FA} * P_F * P_0 + (1 - P_0) \sum_i P(i|\mathrm{F}) * \left(1 - P_D(i)\right) * C(i), \tag{4.9}$$

where C_{FA} is cost of a false alarm, P_0 is the probability of a defect-free part, $P(i|\mathrm{F})$ is the probability of fault i conditioned on the presence of a defect, $P_D(i)$ is the probability of detection fault i, and $C(i)$ is the cost of not detecting fault i. For the case study described in the previous sub-section $C_{FA} = 0.1$, $P_0 = 0.5$, and the remainder of the economic model parameters are given in Table 4.4

Table 4.4: Economic Model Parameters

	i								
	1	2	3	4	5	6	7	8	9
$P(i\|\mathrm{F})$	0.4047	0.2023	0.04047	0.2024	0.1012	0.004047	0.04047	0.004047	0.0004047
$C(i)$	0.05	0.1	0.2	0.1	0.4	0.3	0.2	0.3	0.5

The resulting expected costs using the AGLR approach for the six ROI seed sizes with varying Go/No-Go thresholds are given in Figure 4.9 as solid lines. In addition, the expected costs using the GLR approach are also given in Figure 4.9 as dotted lines. The most important observation from this figure is the fact that the cost of any inspection system design using the AGLR approach is equal to or less than the cost of any inspection system design using the GLR approach (for this example). Further analysis of these results indicates the inspection system with the lowest design cost occurs at the parameter values: $h = 10$ and $R_r = 4$. The resulting probabilities of detection for this design are listed in Table 4.5, where the false alarm rate is 4.4%.

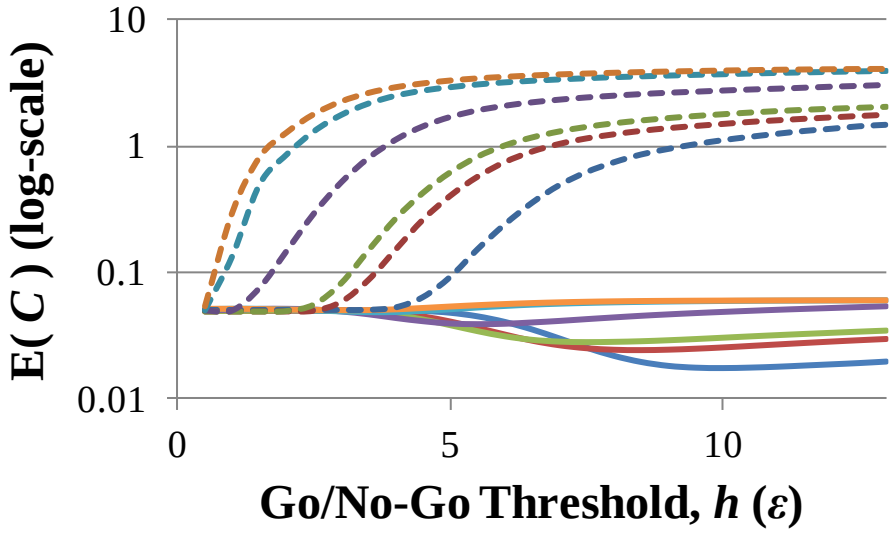

Figure 4.9: Expected Inspection System Costs for AGLR Method (Solid Lines) and GLR Method (Dotted Lines).It Must be Noted That These Figure use the Same Legend as Figure 4.7. for AGLR Method (Solid Lines) and GLR Method (Dotted Lines).

Table 4.5: Detection Probabilities from Optimal Economic Model Design

	i								
$P_D(i)$	1	2	3	4	5	6	7	8	9
	0.1737	0.8320	1.000	0.5599	1.000	1.000	0.8353	1.000	1.000

4.6. Conclusions

The automated inspection of 3D point clouds is a novel research area with significant potential. The proposed approach uses a newly developed adaptive generalized likelihood ratio (AGLR) technique to identify the most likely location, size, shape, and magnitude of a potential fault within a point cloud, which transforms the current ad-hoc visual inspection approach to a statistically viable automated inspection solution. The proposed AGLR method attempts to overcome the main drawback of the current ROI based methods by selectively "growing" an ROI to maximally cover a possible fault. The drawback in the current method is that its ability to detect faults is highly dependent on the size and shape of the pre-defined ROIs. In order to aid practitioners in designing and implementing an AGLR-based inspection process, this paper also reports the performance of the AGLR with respect to the probability of detecting specific size and magnitude faults in addition to false alarm rates.

4.7. References

Brajlih, T., Tasic, T., Drstvensek, I., Valentan, B., Hadzistevic, M., Pogacar, V., Balic, J., and Acko, B. (2011), "Possibilities of Using Three-Dimensional Optical Scanning in Complex Geometrical Inspection," *Journal of Mechanical Engineering*, 57:11, 826-833.

Fenga, H., Liua, Y., and Xib, F. (2001), "Analysis of Digitizing Errors of a Laser Scanning System," *Journal of the International Societies for Precision Engineering and Nanotechnology*, 25, 185–191.

Hsiao, S.-W. and Chuang, J.-C. (2003), "A Reverse Engineering Based Approach for Product Form Design," *Design Studies*, 24:2, 155-171.

Isheil, A., Gonnet, P., Joannic, D., and Fontaine, F. (2011), "Systematic Error Correction of a 3D Laser Scanning Measurement Device," *Optics and Lasers in Engineering*, 49, 16–24.

Jiang, B.C. and Jiang, S.J. (1998), "Machine Vision Based Inspection of Oil Seals," *Journal of Manufacturing Systems*, 17, 159-166.

Jiang, B.C., Wang, C.-C., and Liu, H.-C. (2005), "Liquid Crystal Display Surface Uniformity Defect Inspection Using Analysis of Variance and Exponentially Weighted Moving Average Techniques," *International Journal of Production Research*, 43, 67-80.

Koch, K.R. (2009), "Identity of Simultaneous Estimates of Control Points and of Their Estimates by the Lofting Method for NURBS Surface Fitting," *International Journal of Advanced Manufacturing Technology*, 44, 1175-1180.

Li, Y. and Gu, P. (2004), "Free-Form Surface Inspection Techniques State of the Art Review," *Computer-Aided Design*, 36, 1395–1417.

Lorenzen, T.J. and Vance, L.C. (1986). "The Economic Design of Control Charts: A Unified Approach," *Technometrics*, 28, 3-10.

Martínez, S., Cuesta, E., Barreiro, J., and Álvarez, B. (2010), "Analysis of Laser Scanning and Strategies for Dimensional and Geometrical Control," *International Journal of Advanced Manufacturing Technology*, 621-629.

Megahed, F.M., Wells, L.J., Camelio, J.A., and Woodall, W.H. (2012), "A Spatiotemporal Method for the Monitoring of Image Data," *Quality and Reliability Engineering International*, 28:8, 967-980.

Megahed, F., Woodall, W., and Camelio, J. (2011), "A Review and Perspective on Control Charting with Image Data," *Journal of Quality Technology*, 43:2, 83-98.

Mohaghegh, K., Sadeghi, M., and Abdullah, A. (2007), "Reverse Engineering of Turbine Blades Based on Design Intent," *International Journal of Advanced Manufacturing Technology*, 32, 1009–1020.

Mohib, A., Azab, A., and ElMaraghy, H. (2009), "Feature-Based Hybrid Inspection Planning: A Mathematical Programming Approach," *International Journal of Computer Integrated Manufacturing*, 22:1, 13–29.

Morel, O., Meriaudeau, F., Stolz, C., and Gorria, P. (2005), "Polarization Imaging Applied to 3D Reconstruction of Specular Metallic Surfaces," *Electronic Imaging*, 178-186.

Nacereddine, N., Zelmat, M., Belaïfa, S. S., and Tridi, M. (2005), "Weld Defect Detection in Industrial Radiography Based Digital Image Processing," *Transactions on Engineering Computing and Technology*, 2, 145-148.

Prieto, F., Boulanger, P., Redarce, H.T., and Lepage, R. (1998), "Visual System for the Fast Automated Inspection of 3D Parts," *International Journal of CAD/CAM Computer Graphic*, 13:4, 1-17.

Ravishankar, S., Dutt, H., and Gurumoorthy, B. (2010), "Automated Inspection of Aircraft Parts Using a Modified ICP Algorithm," *International Journal of Advanced Manufacturing Technology*, 46, 227–236.

Reinhart, G. and Tekouo, W. (2009), "Automatic Programming of Robot-Mounted 3D Optical Scanning Devices to Easily Measure Parts in High-Variant Assembly," *CIRP Annals - Manufacturing Technology*, 58, 25–28.

Shi, Q. and Xi, N. (2008). "Automated Data Processing for a Rapid 3D Surface Inspection System," *2008 IEEE International Conference on Robotics and Automation*, 3939-3944.

Shi, Q., Xi, N., Chen, Y., and Sheng, W. (2006). "Registration of Point Clouds for 3D Shape Inspection," *Proceedings of the 2006 IEEE/RSJ - International Conference on Intelligent Robots and Systems*, 235-240.

Shi, Q., Xi, N., and Spagnuluo, C. (2007), "A Feedback Design to a CAD-Guided Area Sensor Planning System for Automated 3D Shape Inspection," *Computer-Aided Design & Applications*, 4, 209-218.

Son, S., Park, H., and Lee, K. (2002), "Automated Laser Scanning System for Reverse Engineering and Inspection," *International Journal of Machine Tools & Manufactur*e, 42, 889–897.

Tunák, M., Linka, A., and Volf, P. (2009), "Automatic Assessing and Monitoring of Weaving Density," *Fibers and Polymers*, 10:6, 830-836.

Wang, X., Wong, B.S., Tan, C., and Tui, C.G. (2011), "Automated Crack Detection for Digital Radiography Aircraft Wing Inspection," *Research in Nondestructive Evaluation*, 22:2, 105-127.

Wells, L.J., Megahed, F.M., Niziolek, C.B., Camelio, J.A., and Woodall, W.H. (2012a), "Statistical Process Monitoring Approach for High-Density Point Clouds," *Journal of Intelligent Manufacturing*, 1-13.

Wells, L.J., Megahed, F.M., Camelio, J.A., and Woodall, W.H. (2012b), "A Framework for Variation Visualization and Understanding in Complex Manufacturing Systems," *Journal of Intelligent Manufacturing*, 23:5, 2025-2036.

Woodall, W.H. (1986), "Weaknesses of the Economic Design of Control Charts," *Technometrics*, 28:4, 408-409.

5. Contributions and Future Work

This chapter summarizes the contributions made in this dissertation and identifies further avenues for research in the use of HDD data for QC.

5.1. Contributions

The quality control tools presented in this dissertation provide the foundation for increasing the applicability of HDD data as in-line measurement systems. This foundation is built off of specific overall contributions made throughout this dissertation.

5.1.1. Overall Contributions

The first overall contribution of this dissertation is the emphasis on the quality control paradigm shift, when presented with HDD data, quality should not be assessed by discrete KPCs alone, but should consider the entire part being produced, anything less results in valuable data being wasted. Through the adherence to this paradigm, new ways to consider the use of HDD data in engineering process control, statistical process control, and inspection have been introduced. This increases the applicability of HDD technologies from being thought of as merely reverse engineering tools to being a valid on-line measurement systems. This increased applicability will drive HDD measurement system OEMs to develop faster and more accurate systems suitable for in-line use. Additionally, I strongly believe that the work presented in this dissertation will be a starting point for further research into how to most efficiently take advantage of this HDD data not only in QC but for manufacturing in general, which is a necessity, as HDD is without doubt the future of manufacturing measurement systems.

The second overall expected contribution of this dissertation is the emphasis on establishing a strong link between CAD and HDD data. In order to produce high quality products, an ideal manufacturing system must be insensitive to and/or be able to accurately and efficiently predict,

detect, control, and ultimately reduce the effects of incoming part errors. The continued progression of computer aided engineering techniques has led to the development of advanced methods for uncertainty propagation analysis, active error compensation, and statistical process control. When integrated into the design and implementation of a manufacturing system, these state-of-the-art approaches bring the aforementioned ideal manufacturing system one step closer to realization.

Typically in CAD, manufactured component geometries are created based upon specific features. In order to facilitate design changes, these features are often parameterized in a CAD environment. The previously mentioned design and analysis techniques typically use these parameters as the basis for creating part deviations that reflect possible incoming part errors. However, using these parameters severely restricts the set of geometric states for manufactured components, such as any plastic deformations that occur in the part from material handling.

The evolution of HDD data will inevitably result in the quality of a manufactured part to no longer be quantified through the use of individual features and discrete measurement points, but by the entire part's geometry. Therefore, the continued use of design and analysis techniques based upon the use of CAD model parameters will result in a severe disconnect between how quality is assessed and how manufacturing systems are designed and analyzed to improve quality. The proposed NURBS based methods described in Chapters 2 and 3 will aid in overcoming this disconnection, where the focus is not on specific features but rather the entire surface (which becomes the feature).

In addition to overall contribution of this dissertation, Chapters 2 through 4 make distinct contributions to their respective research areas, which are discussed in the following three subsections, respectively.

5.1.2. Self-Correcting Compliant Assembly Systems

The main contribution of this research area is the concept that despite the fact that some incoming part errors may be unknown or unanticipated it may be possible to account for and correct them. Due to high computational costs, determining appropriate corrective actions for highly non-linear assemblies in-line is not an option. The proposed approach described in Chapter 2 overcomes this problem by implementing assembly system immunity, which can handle known, unknown, or developing incoming part error types.

The success of the proposed immune system comes from the second contribution of this research area, which is that the immune system operates in parallel to the assembly system. More specifically, the immune system is continually increasing its immunity capabilities to possible incoming part errors regardless of the state of the assembly system itself. This allows for a continual increase in immunity robustness during the times where the assembly system is not under attack (experiencing incoming part errors).

5.1.3. Statistical Process Control for HDD Data

In this area, the major contribution is the development of a technique to monitor HDD data. Currently, only one technique has been published in the QC literature to handle HDD in a quality monitoring system (Wells et al., 2012b). This approach uses Q-Q plots to significantly reduce the dimensionality of the problem. Unfortunately the aggregation nature of these plots results in the loss of important spatial information. This loss of information not only makes the approach less sensitive to shifts, but also impedes shift diagnosis. This is a strong contribution due to the fact that creating awareness of the applicability of HDD in process monitoring and diagnosis will hopefully promote other researchers to investigate this problem. In addition, the proposed method will provide an adequate baseline for other researchers to compare their methods against.

5.1.4. Automated Part Inspection for Non-Feature Based Faults

The main contribution of this research area revolves around the notion that even though HDD data often represents 3D data, it can be transformed into a 2D space without data loss. Given that any engineering product can be represented as a surface by a function of two iso-parametric curves, means that any surface to be represented in 2D space. This not only allows for easier analysis, but can also generalizes all point clouds to a common structure. In addition, this opens the door for the use of established image processing techniques for HDD data.

The second contribution of this research area has to do with the development of the AGLR approach itself. Previous ROI or moving window approaches tend to fail when the fault of interest is small compared to the ROI (or inspection window) or when the magnitude of the fault is small and the ROI or window only covers part of the fault. To account for these drawbacks, the AGLR approach adaptively grows an ROI to 1) Only include data that supports the presence of a fault and 2) Maximize the amount of data included to support the presence of a fault. Such an adaptive approach can also be useful outside of HDD data in areas such as digital imaging, for both inspection and process monitoring.

5.2. Future Work

The approaches developed within this dissertation have provided further avenues for research in the use of HDD data for QC. Discussed in the following two subsection are new areas of work that came about as a byproduct of the research performed in this dissertation, namely; 1) Monitoring process data as point clouds and 2) Uncertainty propagation modeling using NURBS surface representations.

5.2.1. Monitoring Process Data as Point Clouds

Recall from Chapter 3 that a set of measured coordinates $\mathbf{S}(\bar{u}_o, \bar{v}_d)$ from an r x e grid of points can be used to estimate a NURBS surface that best represents a physical part. While NURBS surfaces are traditionally used as a CAD tool to represent geometry, the mathematical representation is not restricted to only coordinate measurements. In fact, $\mathbf{B}^w(\cdot,\cdot)$, from Eq. (3.1), can be a 1 x n vector defining any number of discrete measurable quantities on a surface.

Future research in this area will consider in-line process measurements as additional "coordinates" for NURBS surface representations. To illustrate this concept consider the time-series power consumption data taken from a lathe that turned down a cylindrical billet of steel given in Figure 5.1. As can be seen there is something odd occurring during this process. For further investigation a NURBS surface representation of this data is constructed. Given a constant sampling frequency, cutting feed, cutting speed, and diameter of the work-piece; an r x e grid of measurement points for the power can be constructed, as seen in Figure 5.2a.

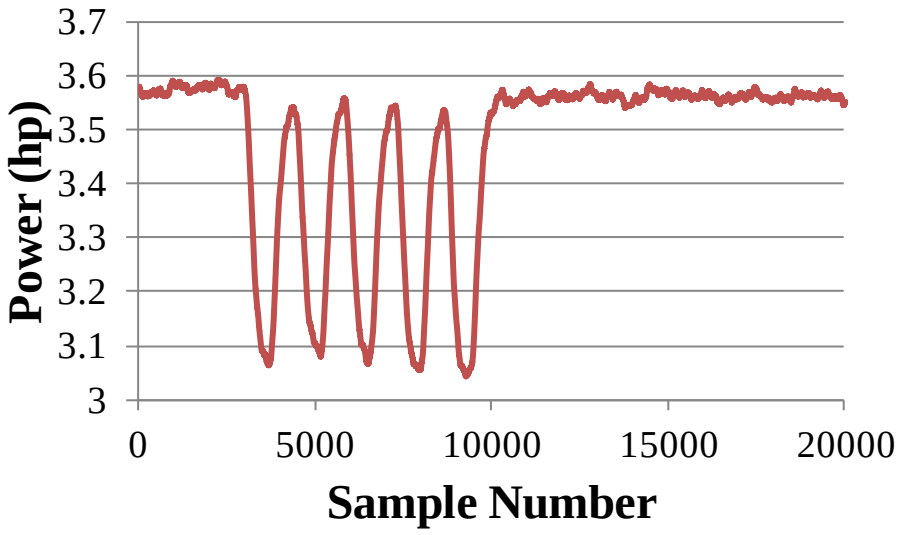

Figure 5.1: Power Consumption during the Turning of a Cylindrical Steel Billet.

For each point on this grid, measurements for the three Cartesian coordinates and power are collected to form the data-set **S**. It should be noted that the part being machined was not measured

and nominal post-machining coordinates are used to form **S**. Using **S** the lofting procedure outline in Chapter 3 was implemented for a NURBS surface with 500 ($n_u = 10, n_v = 50$) control points with 3rd order ($k_u = k_v = 4$) B-Splines. The resulting NURBS surface estimation of this data is given in Figure 5.2b. In this figure, the Cartesian coordinates are displayed as a 3D surface while the fourth dimension of the NURBS surface (power) is given as a color map. As can be seen, the behavior of the time-series data given in Figure 5.1 is represented in the NURBS surface as five equal width repeating stripes around the cylinder's circumference. The reason for the occurrence of these stripes becomes evident when considering the actual geometry of the part (pre-machining), which is given in Figure 5.2c. Here it can be seen that five grooves existed on the cylinder (pre-machining) resulting in the five repeated stripes in the NURBS surface representation shown in Figure 5.2b.

The purpose of this example is to show how process data can easily be modeled through a NURBS surface. This unique modeling approach allows dimensional data and processes data to co-exist in one simple model. Furthermore, additional time-series data sources can be added to the NURBS surface without significantly increasing the complexity of the model. I foresee this approach as having potential not only in statistical process control but also in the areas of adaptive machining, tool-life prediction, and process understanding.

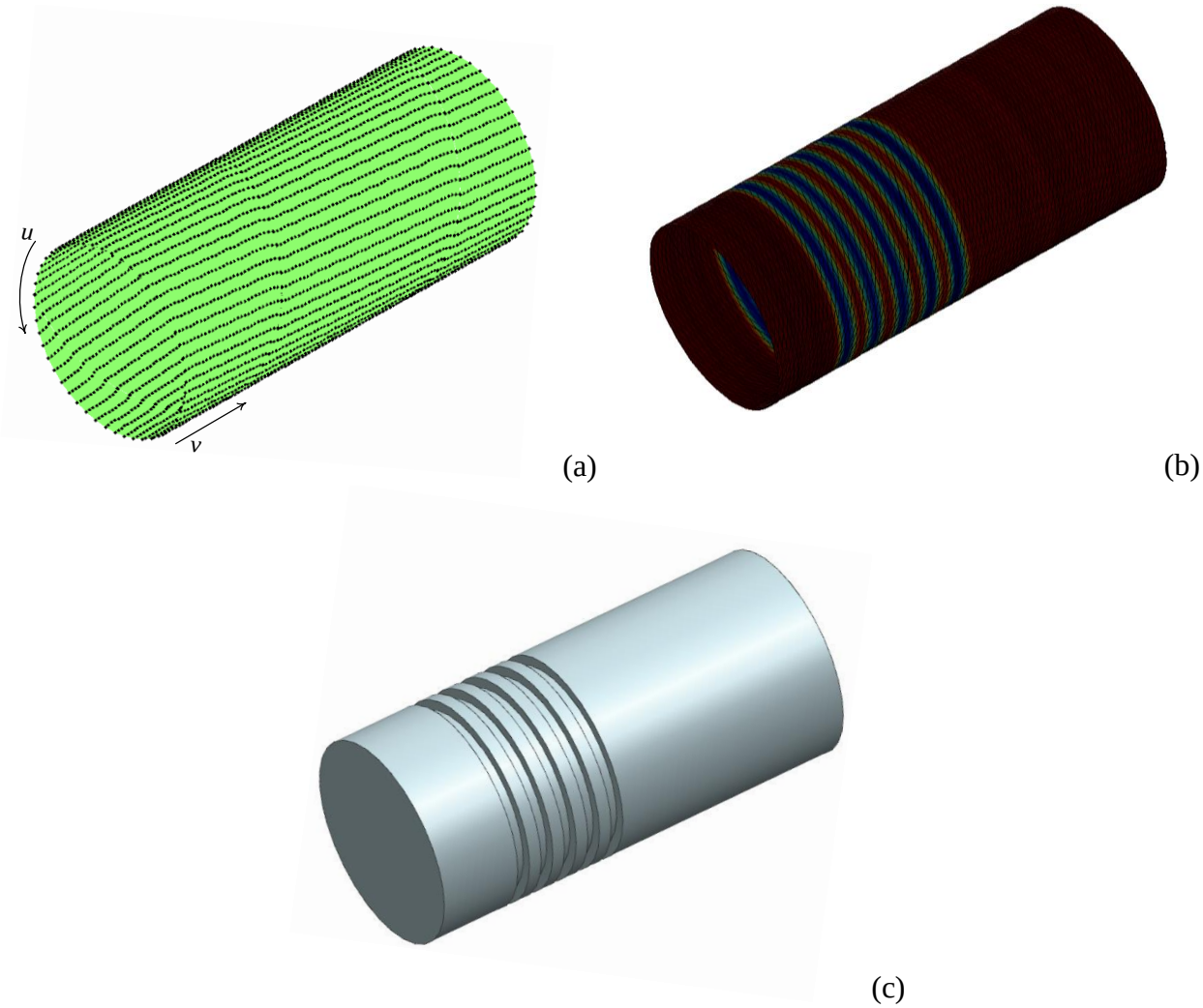

Figure 5.2: Turning Example Illustrating (a) An $r\ x\ e$ Grid of Measurement Locations for Lathe Power, (b) A NURBS Representation of Dimensional Coordinates and Power, and (c) A CAD Model of Pre-Machined Part.

5.2.2. Uncertainty Propagation Modeling Using NURBS Surface Representations

In order to determine the overall quality of a product, one must assess the final product dimensional variation from nominal, which is often caused by individual component variations in an assembly system. This requires being able to develop a relationship between incoming part errors and final product variations. A common approach to developing this relationship is through the use of uncertainty propagation models, such as the method described by Liu and Hu, (1997). In their method, the assembly process is broken into the following four steps, which are analyzed through the finite element method:

1. *Parts are located by the fixtures.*
2. *Clamps push the parts against the locators.*
3. *Weld guns join the parts.*
4. *Weld guns and clamps are released, and the part experiences spring-back.*

Through this method, the deviations of the assembly $\mathbf{V}_a$ is related to the deviation of the incoming parts$\mathbf{V}_i$ as $\mathbf{V}_a = \mathbf{S}\mathbf{V}_i$, where the sensitivity matrix $\mathbf{S}$ is determined using the method of influence coefficients (MIC). The major drawback of this approach is that $\mathbf{V}_i$ and $\mathbf{V}_a$ are vectors of features or discrete measurement points on the assembly. This limits the ability to represent assembly geometries accurately and uniquely while also reducing the validity of the analysis for downstream assembly station models.

In order to avoid this issue, future work will aim at revising the approach described by Liu and Hu (1997), where NURBS surface parameters are used instead of discrete points on the surface. Specifically the goal would be to determine a new sensitivity matrix $\mathbf{S}^*$ for which

$$\boldsymbol{\delta}_a = \mathbf{S}^* \boldsymbol{\delta}_i, \tag{5.1}$$

where $\boldsymbol{\delta}_a$ and $\boldsymbol{\delta}_i$ are the assembly and incoming part deviations represented as NURBS surface perturbation vectors (described in Chapter 2 as B Cell generators), respectively. Due to the local modification property of NURBS surfaces and using the same assumptions as Liu and Hu (1997), deviations from nominal are small and the materials remains in the linear range, the two formulations should give similar results. However, when using the NURBS formulation, the geometry of the assembly is maintained. It should be noted that $\boldsymbol{\delta}_a$ can be easily obtained through the results of the finite element method by letting the nodes (post-assembly) be the r x e grid of points used to estimate a NURBS surface, as described in Chapter 3.

Traditionally the results of an uncertainty propagation model are used for robust design and tolerance allocation. As discussed by Hu et al. (2003), $\mathbf{S}$ (or $\mathbf{S}^*$) can be used to determine how sensitive the system is with respect to incoming part variations and the ability of the system to either suppress or amplify these variations. These results can then be used to analyze the robustness of a system under different design alternatives.

While the use of $\mathbf{S}^*$ is directly applicable to robust design it is not valid for tolerance allocation. The reason for this is that $\mathbf{S}^*$ describes the relationship between NURBS surface control points, which currently have no physical interpretation in tolerance design. The simple solution to this problem is to evaluate the function $\mathbf{V} = h(\boldsymbol{\delta})$ that relates a NURBS surface perturbation vector to a vector of specific features or points used for the tolerance analysis. A further research area to explore involves reconsidering how tolerances are perceived and allocated. The evolution towards the use of in-line HDD data will inevitably lead to part quality being assessed by its entire geometry. This would suggest that in the future, tolerances will be applied across an entire part's surface. With this in mind, $\boldsymbol{\delta}$ can be used directly in tolerance analysis as it contains all of the information regarding a part's surface. However, the importance of feature tolerances should never be completely neglected as they are crucial for mating parts during assembly.

In addition to identifying new areas of research, the areas addressed in Chapters 2 through 4 offer a wide range of future research possibilities, which are discussed in the following three subsections, respectively.

5.2.3. Self-Correcting Compliant Assembly Systems

While the mathematically framework for a self-correcting compliant assembly system was developed in Chapter 2, the actual implementation will rely on three crucial aspects. Firstly, for the immune system to perform efficiency requires a sophisticated relational database to keep track

of the B Cells and their current status within the system. Secondly, a highly robust finite element model (in terms of mesh generation, constraints, contact interactions, etc.) must be generated for the assembly system to account for the randomness allowed within the B Cell pool. Thirdly, an assembly system test-bed with appropriate HDD measurement devices and actuator networks needs to be developed and implemented with the proposed self-correcting assembly system approach to verify its ability to autonomously correct for unknown or unanticipated incoming part errors.

5.2.4. Statistical Process Control for HDD Data

Chapter 3 outlined the process for using NURBS surfaces for monitoring shifts using HDD data. While the performance of the proposed method was analyzed for several shift magnitudes and locations, only one specific shift type and surface geometry was considered. In order to implement this approach in any quality control system requires further investigation into its ability to detect a wider range of shift types. In addition, the performance of the proposed method needs to be compared to previously proposed SPC approaches for HDD data such as the Q-Q plot approach proposed by Wells et al. (2012b).

5.2.5. Automated Part Inspection for Non-Feature Based Faults

The future work in this area revolves around verifying the AGLR method through real-life case studies. For these case studies, a large population of both "healthy" and "faults" parts with known fault sizes and magnitudes will need to be measured with a high accuracy, high resolution computer controlled HDD measurement device. Measurement noises and resolutions can be artificially generated for further verification studies. Moreover, since the AGLR method is an adaptation of the spatiotemporal control charting approach proposed by Megahed et al. (2012), performance can only be guaranteed under the presence of a single fault. This results in unknown performance levels

of the AGLR method when multiple faults exist. Lastly, the assumption of i.i.d. noise will not hold true for real-life measurement scenarios. However, the AGLR approach can be altered to consider spatially varying noise distributions, which is an area of further investigation.

6. References

Box, G.E. and Woodall, W.H. (2012), "Innovation, Quality Engineering, and Statistics," *Quality Engineering*, 24:11, 20-29.

Brajlih, T., Tasic, T., Drstvensek, I., Valentan, B., Hadzistevic, M., Pogacar, V., Balic, J., and Acko, B. (2011), "Possibilities of Using Three-Dimensional Optical Scanning in Complex Geometrical Inspection," *Journal of Mechanical Engineering*, 57:11, 826-833.

Feng, H.-Y., Liu, Y., and Xi, F. (2001), "Analysis of Digitizing Errors of a Laser Scanning System," *Precision Engineering*, 25, 185-191.

Hu, S.J., Webbink, R., Lee, J., and Long, Y. (2003), "Robustness Evaluation for Compliant Assembly Systems," *ASME Journal for Mechanical Design*, 125, 262-267.

Isheil, A., Gonnet, J.P., Joannic, D., and Fontaine, J.F. (2011), "Systematic Error Correction of a 3D Laser Scanning Measurement Device," *Optics and Lasers in Engineering*, 49:1, 16-24.

Liu, S.C. and Hu, S.J. (1997), "Variation Simulation for Deformable Sheet Metal Assemblies Using Finite Element Methods," *ASME Journal of Manufacturing Science and Engineering*, 119:3, 368-374.

Martínez, S., Cuesta, E., Barreiro, J., and Álvarez, B. (2010), "Analysis of Laser Scanning and Strategies for Dimensional and Geometrical Control," *International Journal of Advanced Manufacturing Technology*, 46:5, 621-629.

Mohib, A., Azab, A., and Elmaragy, H. (2009), "Feature-Based Hybrid Inspection Planning: A Mathematical Programming Approach," *The International Journal of Computer Integrated Manufacturing*, 22:1, 13-29.

Shewhart, W.A. (1925), "The Application of Statistics as an Aid in Maintaining Quality of a Manufactured Product," *Journal of the American Statistical Association*, 20, 546-548.

Shi, Q. and Xi, N. (2008), "Automated Data Processing for a Rapid 3D Surface Inspection System," *IEEE Conference on Robotics and Automation*, 3939-3944.

Shi, Q., Xi, N., and Spagnuluo, C. (2007), "A Feedback Design to a CAD-Guided Area Sensor Planning System for Automated 3D Shape Inspection," *Computer-Aided Design and Applications*, 4, 209-218.

Son, S., Park, H., and Lee, K.H. (2002), "Automated Laser Scanning System for Reverse Engineering and Inspection," *International Journal of Machine Tools and Manufacture*, 42:8, 889-897.

Tamura, S., Kim, E.-K., Close, R., and Sato, Y. (1994), "Error Correction in Laser Scanner Three-Dimensional Measurement by Two-Axis Model and Coarse-Fine Parameter Search," *Pattern Recognition*, 27:3, 331-338.

Toriwaki, J. and Yoshida H. (2009), Fundamentals of Three-Dimensional Digital Image Processing, Springer.

Wells, L.J. and Camelio, J.A. (2012), "A Bio-Inspired Approach for Self-Correcting Compliant Assembly Systems," *4th CIRP Conference on Assembly Technologies and Systems*, Ann Arbor, MI.

Wells, L.J. and Camelio, J.A. (2013), "A Bio-Inspired Approach for Self-Correcting Compliant Assembly Systems," *Journal of Manufacturing Systems, Special Issue on Assembly Technologies and Systems (In Press).*

Wells, L.J., Megahed, F.M., Camelio, J.A., and Woodall, W.H. (2012a), "A Framework for Variation Visualization and Understanding in Complex Manufacturing Systems," *Journal of Intelligent Manufacturing*, 23:5, 2025-2036.

Wells, L.J., Megahed, F.M., Niziolek, C.B., Camelio, J.A., and Woodall, W.H. (2012b), "Statistical Process Monitoring Approach for High-Density Point Clouds," *Journal of Intelligent Manufacturing*, 1-13.

Wells, L.J., Shafae, M.S., and Camelio, J.A. (2013), "Automated Part Inspection Using 3D Point Clouds," *Proceedings of the ASME International Manufacturing Science and Engineering Conference*, June 10-14, Madison, WI.

Wu, S.-K., Hu, J., and Wu, S.M. (1994), "A Fault Identification and Classification Scheme for an Automobile Door Assembly Process," *The International Journal of Flexible Manufacturing Systems*, 6, 261-285.

Xi, F., Liu, Y., and Feng, H.-Y. (2001), "Error Compensation for Three-Dimensional Line Laser Scanning Data," *The International Journal of Advanced Manufacturing Technology*, 18, 211-216.

Zussman, E., Schuler, H., and Seliger, G. (1994), "Analysis of the Geometrical Feature Detectability Constraints for Laser-Scanner Sensor Planning," *The International Journal of Advanced Manufacturing Technology*, 9, 56–64.